Photocopy and Use Authorization

In presenting this thesis in partial fulfillment of the requirements for an advanced degree at Idaho State University, I agree that the library shall make it freely available for inspection. I further state that permission for extensive copying of my thesis for scholarly purposes may be granted by the Dean of the Graduate School, Dean of my academic division, or by the University Librarian. It is understood that any copying or publication of this thesis for financial gain shall not be allowed without my written permission.

Signature _____

Date _____

Bone-Targeted Delivery of Novokinin, an Angiotensin II Type 2 Receptor Agonist, for Improved Pharmacokinetics and Therapeutic Effects

by

Arina Ranjit

A dissertation

submitted in partial fulfillment

of the requirements for the degree of

Doctor of Philosophy in the Department of Biomedical and Pharmaceutical Sciences

Idaho State University

May 2023

Committee Approval

To the Graduate Faculty:

The members of the committee appointed to examine the thesis of Arina Ranjit find it satisfactory and recommend that it be accepted.

Dr. Ali Aghazadeh Habashi
Major Advisor

Dr. Jared Barrott,
Committee Member

Dr. Srinath Pashikanti,
Committee Member

Dr. Prabha Awale,
Committee Member

Dr. René Rodriguez,
Graduate Faculty Representative

Animal Welfare Research Committee Approval

Idaho State
UNIVERSITY
Office for Research - Research Outreach & Compliance
921 S. 8th Avenue, Stop 8046 • Pocatello, Idaho 83209-8046

March 5, 2019

Ali Habashi, PhD
921 S. 8th Ave
Stop 8333
Pocatello, ID 83209

RE: Your application dated 3/5/2019 regarding study number 772: Pharmacokinetics and Pharmacodynamics Study of Small Molecule and Peptide Conjugate Anti-inflammatory Drugs in Adjuvant Arthritis Rat Model

Dear Dr. Habashi:

Thank you for your response to requests from a prior review of your application for the new study listed above. Your study is eligible for Designated Member Review under OLAW guidelines.

This is to confirm that your application is now fully approved. The protocol is approved through 3/5/22.

You are granted permission to conduct your study as most recently described effective immediately. The study is subject to annual review on or before 3/5/2020, unless closed before that date.

Please note that any changes to the study as approved must be promptly reported and approved. Some changes may be approved by expedited review; others require full board review. Contact Tom Bailey (208-282-2179; fax 208-282-4723; email: anmlcare@isu.edu) if you have any questions or require further information.

Sincerely,

Curt Anderson, PhD
IACUC Chair

Idaho State
UNIVERSITY
Office for Research - Research Outreach & Compliance
921 S. 8th Avenue, Stop 8046 • Pocatello, Idaho 83209-8046

June 15, 2020

Ali Habashi, PhD, PharmD
Biomedical & Pharmaceutical Sciences
921 S. 8th Ave. Stop 8333
Pocatello, ID 83209

RE: Designated Member Review regarding study number *790: Pharmacokinetics and Pharmacodynamics of PEGylated-Bone Targeting Peptide Conjugates and Small Molecules*

Dear Dr. Habashi:

Thank you for your responses to a full-board review of the study listed above. Your responses are eligible for Designated Member Review (DMR) per OLAW guidelines. This is to confirm that your protocol has been approved.

You are granted permission to conduct your study as submitted effective immediately. The date for annual review is 6/15/21, unless the study closes before that date.

Please note that any further changes to the study must be promptly reported and approved. Contact Tom Bailey (anmlcare@isu.edu; 208-282-2179) if you have any questions or require further information.

Sincerely,

Erin Rasmussen, PhD
IACUC Chair

Idaho State University

February 8, 2021

Ali Habashi, PhD
Pharmacy
921 S. 8th Ave., Stop 8333
Pocatello, ID 83209

RE: AMENDMENT regarding study number *772: Pharmacokinetics and Pharmacodynamics Study of Small Molecule and Peptide Conjugate Anti-inflammatory Drugs in Adjuvant Arthritis Rat Model*

Dear Dr. Habashi:

Your request for revision of the study listed above was reviewed at the 2/8/21 meeting of the Idaho State University IACUC.

The requested revision involves including both sexes in the animal study and investigate the gender effect on the its outcome. This is to confirm that your application for revision has been approved.

You are granted permission to conduct your study as revised effective immediately. The date for the next annual review remains unchanged at 3/5/21, unless the study closes before that date.

Please note that any further changes to the study must be promptly reported and approved. Contact Tom Bailey (anmlcare@isu.edu; 208-282-2179) if you have any questions or require further information.

Sincerely,

Erin Rasmussen, PhD
IACUC Chair

Idaho State University

February 26, 2021

Ali Habashi, PhD, PharmD
Biomedical & Pharmaceutical Sciences
921 S. 8th Ave., Stop 8333
Pocatello, ID 83209

RE: DMR regarding study number *798: Pharmacokinetics and Pharmacodynamics of PEGylated-Bone Targeting-Small Peptide Conjugates*

Dear Dr. Habashi:

Thank you for your responses to a full-board review of the study listed above. Your responses are eligible for Designated Member Review (DMR) per OLAW guidelines.

This is to confirm that your application for revision has been approved. The date for annual review is February 26, 2022, unless the study closes before that date.

Please note that any further changes to the study must be promptly reported and approved. Contact Tom Bailey (anmlcare@isu.edu; 208-282-2179) if you have any questions or require further information.

Sincerely,

Erin Rasmussen, PhD
IACUC Chair

Office for Reseach - Research Outreach & Compliance
921 South 8th Ave., Stop 8386 | Pocatello, ID 83209-8286 | (208) 282-1336 | isu.edu/research

Idaho State University

September 22, 2021

Ali A. Habashi, PhD, PharmD
Biomedical & Pharmaceutical Sciences
921 S. 8th Ave., Stop 8333
Pocatello, ID 83209

RE: AMENDMENT regarding study number *772: Pharmacokinetics and Pharmacodynamics Study of Small Molecule and Peptide Conjugate Anti-inflammatory Drugs in Adjuvant Arthritis Rat Model*

Dear Dr. Habashi:

Your request for revision of the study listed above is eligible for Veterinary Verification and Consultation (VVC) per OLAW guidelines.

The requested revision involves studying the effect of drinking hydrogenated water on alleviation of adjuvant arthritis sign and symptoms in SD rats. The whole procedure of arthritis induction and animal group assignments will be followed similarly to the original protocol with a simple modification on drug treatment. The animals will drink hydrogenated water instead of receiving drug treatment by injection. The H2 Theraputics device will produce hydrogenated water, and animal water bottles will be filled to let animals drink hydrogenated water daily for three weeks. The rest of the procedure will follow as described under "Procedure, subsection: PD study." This is to confirm that your application for revision has been approved. Please coordinate with Mia Benkenstein to make sure the appropriate supplies are available when needed.

You are granted permission to conduct your study as revised effective immediately. This study is set to expire on 3/5/22. If work needs to continue past that date, you will need to submit a new protocol at least a month in advance of the expiration date to avoid any gaps.

Please note that any further changes to the study must be promptly reported and approved. Contact Tom Bailey (anmlcare@isu.edu; 208-282-2179) if you have any questions or require further information.

Sincerely,

Erin Rasmussen, PhD
IACUC Chair

Idaho State University

April 14, 2021

Ali Habashi, PhD, PharmD
Pharmacy
921 S. 8th Ave., Stop 8333
Pocatello, ID 83209

RE: AMENDMENT regarding study number *798: Pharmacokinetics and Pharmacodynamics of PEGylated-Bone Targeting-Small Peptide Conjugates*

Dear Dr. Habashi:

Your request for revision of the study listed above is eligible for Administrative Review per OLAW guidelines.

The requested revision involves adding Caleb Wilson as personnel to the protocol. This is to confirm that your application for revision has been approved.

You are granted permission to conduct your study as revised effective immediately. The date for annual review remains unchanged at 2/26/22, unless the study closes before that date.

Please note that any further changes to the study must be promptly reported and approved. Contact Tom Bailey (anmlcare@isu.edu; 208-282-2179) if you have any questions or require further information.

Sincerely,

Erin Rasmussen, PhD
IACUC Chair

Office for Reseach - Research Outreach & Compliance
921 South 8th Ave., Stop 8386 | Pocatello, ID 83209-8286 | (208) 282-1336 | isu.edu/research

Idaho State University

June 14, 2021

Ali Habashi, PhD, PharmD
Biomedical & Pharmaceutical Sciences
921 S. 8th Ave., Stop 8333
Pocatello, ID 83209

RE: AMENDMENT regarding study number *798: Pharmacokinetics and Pharmacodynamics of PEGylated-Bone Targeting-Small Peptide Conjugates*

Dear Dr. Habashi:

Your request for revision of the study listed above is eligible for Veterinary Verification and Consultation (VVC) per OLAW guidelines.

The requested revision involves performing routine animal urine collection using standard metabolic cages and adding Logan Cano as personnel to the study. This is to confirm that your application for revision has been approved.

You are granted permission to conduct your study as revised effective immediately. The date for annual review remains unchanged at 2/26/22, unless the study closes before that date.

Please note that any further changes to the study must be promptly reported and approved. Contact Tom Bailey (anmlcare@isu.edu; 208-282-2179) if you have any questions or require further information.

Sincerely,

Erin Rasmussen, PhD
IACUC Chair

Idaho State University

March 15, 2022

Ali Habashi, PhD, PharmD
Biomedical & Pharmaceutical Sciences
921 S. 8th Ave., Stop 8333
Pocatello, ID 83209

RE: DMR regarding study number *805: Pharmacokinetics and Pharmacodynamics Study of Chemical and Peptide Conjugate Anti-inflammatory Drugs in Adjuvant Arthritis Rat Model*

Dear Dr. Habashi:

Thank you for your responses to a full-board review of the study listed above. Your responses are eligible for Designated Member Review (DMR) per OLAW guidelines.

This is to confirm that your protocol has been approved.

You are granted permission to conduct your study as revised effective immediately. The date for annual review is 3/15/23, unless the study closes before that date.

Please note that any further changes to the study must be promptly reported and approved. Contact Tom Bailey (anmlcare@isu.edu; 208-282-2179) if you have any questions or require further information.

Sincerely,

Erin Rasmussen, PhD
IACUC Chair

Dedication

I dedicate this dissertation to my mom, dad, and my sister. Without their unconditional support, patience, and encouragement to move forward and most of all love, the completion of this work would not have been possible.

Acknowledgments

I am deeply grateful to everyone who has contributed to the completion of this dissertation. First and foremost, I would like to express my sincerest appreciation to my major advisor, Dr. Ali Aghazadeh Habashi, for his unwavering support, invaluable guidance, and continuous motivation throughout my PhD journey. His expertise, insights, and constructive criticism have been instrumental in shaping this work.

I am also indebted to my committee members, Dr. Jared Barrott, Dr. Srinath Pashikanti, Dr. Prabha Awale, and Dr. René Rodriguez, for their invaluable feedback and suggestions that have helped me to improve and refine my work. I would also like to thank Dr. Kavita Sharma for being my go-to person for any technical help and writing.

Furthermore, I would like to acknowledge the support and camaraderie of my former and current lab partners, Sana Khajehpour, Biwash Ghimire, and Emma Summerill. Their contributions have been instrumental in my academic growth and personal development.

I would also like to extend my deepest gratitude to my family, my mom, dad, and sister, for their unwavering support, encouragement, and belief in me. I am forever grateful for their sacrifice and patience, without which I would not have been able to make it this far.

Lastly, I would like to thank everyone in the department of biomedical and pharmaceutical sciences at Idaho State University for being part of my journey here. This has been a life-changing and valuable learning experience that I will always cherish in my memories.

This dissertation research was supported by Idaho State University. Once again, thank you all from the bottom of my heart for your support and encouragement.

Table of Contents

List of Figures

List of Tables

List of Abbreviations

Abbreviations	Full name
BcL-2	β-cell lymphoma-2
DAB	3,3'-diaminobenzidine
cGMP	3,5 Cyclic guanosine monophosphate
HPETEs	4-hydroperoxyeicosatrienoic acid
AIAA	Abdominal aortic aneurysm
ACN	Acetonitrile
AP-1	Activator protein-1
ATP	Adenosine triphosphate
AIA	Adjuvant-induced arthritis
ATCC	American type culture collection
ANOVA	Analysis of variance
Ang	Angiotensin
Ang 1-7	Angiotensin 1-7
Ang 1-9	Angiotensin 1-9
ACE	Angiotensin converting enzyme
ACE2	Angiotensin converting enzyme 2
Ang II	Angiotensin II
AT1R	Angiotensin II type 1 receptor
AT2R	Angiotensin II type 2 receptor
AT4R	Angiotensin II type 4 receptor
Ang III	Angiotensin III
Ang IV	Angiotensin IV
ARBs	Angiotensin receptor blockers
ACCPA	Anti-cyclic citrullinated peptide antibody
$ApoE^{-/-}$	Apolipoprotein E knockout
CL	Apparent clearance
ArA	Arachidonic acid
AUC	Area under curve
AI	Arthritis index
ADMA	Asymmetric dimethylarginine
$AT2R^{-/-}$	AT2R knockout mice
a.m.u	Atomic mass unit
ANP	Atrial natriuretic peptide
BP	Bisphosphonate
BSL	Biosafety level
Bac	Bladder Cancer cell
BBB	Blood brain barrier

Boc/Bzl	tert-butyloxycarbonyl /Benzyl
BK	Bradykinin
B2R	Bradykinin 2 receptor
BHT	Butylated hydroxytoluene
CRP	C-reactive protein
CK	Cathepsin K
Cav-1	Caveolin-1
CNS	Central nervous system
CDS	Chromatography data system
CV%	Coefficient of variation percentage
CE	Collision energy
CXP	Collision cells exit potential
cDNA	Complementary Deoxyribose nucleic acid
C21	Compound 21
CT	Computed tomography
cAMP	Cyclic adenosine monophosphate
COX	Cyclooxygenase
CYP450	Cytochrome P450
D	Deuterium
DP	Declustering potential
DMARDS	Disease-modifying antirheumatic drugs
D.D	Double distilled
DMEM	Dulbecco’s Modified Eagle’s medium
DiHTs	Dihydroxyeicosatrienoic acid
Ke	Elimination rate constant
eNOS	Endothelial nitric oxide synthase
EETs	Epoxyeicosatrienoic acids
EP	Entrance potential
ESR	Erythrocyte sedimentation test
EDTA	Ethylenediaminetetraacetic acid
ECM	Extracellular matrix
ECL	Extracellular loop
ERK	Extracellular signal-regulated kinase
EIC	Extracted ion chromatogram
FPPS	Farnesyl pyrophosphate synthase
FBS	Fetal bovine serum
FLS	Fibroblast-like synoviocytes
GC	Gas chromatography
GPCR	G-protein-coupled receptor
GDP	Guanosine Diphosphate
GTP	Guanosine triphosphate

Fmoc	Fluorenyl methoxycarbonyl protecting group
HETEs	Hydroxyeicosatetraenoic acids
HPLC	High-pressure liquid chromatography
HDL	High-density lipoprotein
HQC	High-quality control
HRP	Horseradish peroxidase
hCAECs	Human coronary artery endothelial cells
hCAVSMCs	Human coronary artery vascular smooth muscle cells
HAT	Hypoxanthine-aminopterin-thymidine
H_2O_2	Hydrogen peroxide
HA	Hydroxyapatite
HEK-293	Human embryonic kidney-293
HF	Hydrofluoric acid
IPF	Idiopathic pulmonary fibrosis
I2	Imidazoline 2 receptor
IgG	Immunoglobulin G
IgM	Immunoglobulin M
iNOS	Inducible nitrogen oxygen species
IP3	Inositol 1,4,5-trisphosphate
INS-1	Insulinoma-1
IS	Internal standard
IL-1	Interleukin-1
IL-6	Interleukin-6
IL-8	Interleukin-8
IL-12	Interleukin-12
IL-18	Interleukin-18
IL-21	Interleukin-21
IL-32	Interleukin-32
IL-33	Interleukin-33
ILD	Interstitial lung disease
ICL	Intracellular loop
i.c.v.	Intracerebroventricular
i.p.	Intraperitoneal
I.V	Intravenous
JAK	Janus kinase inhibitors
LTs	Leukotrienes
LOD	Limit of detection
LOQ	Limits of quantification
LXs	Lipoxins
LOX	Lipoxygenase

LC	Liquid chromatography
LDS	Lithium dodecyl sulfate
LDL	Low-density lipoprotein
LLOQ	Lower limit of quantifications
LQC	Lower quality control
Q-TOF	Quadrupole-time of flight
MRI	Magnetic resonance imaging
MHC	Major histocompatibility issue
MAL-PEG NHS	Maleimidopropionyl-PEG N-hydroxysuccinamide
MasR	Mas receptor
MMPs	Metalloproteinases
MRI	Magnetic resonance imaging
mRNA	Messenger Ribose nucleic acid
MT	Metabolism
MQC	Middle-quality control
MAP	Mitogen-activated protein
MAPK	Mitogen-activated protein kinase
MKP-I	Mitogen-activated protein kinase phosphatase-I
MRM	Multiple reaction monitoring
MI	Myocardial infarction
L-NAME	N- nitro-L-arginine methyl ester
NGF	Nerve growth factor
NG108-15	Neuroblastoma/glial
NADPH	Nicotinamide adenine dinucleotide phosphate
NO3	Nitrate
NO2	Nitrite
NO	Nitric oxide
NOS	Nitric oxide synthase
NSAIDs	Non-steroidal anti-inflammatory drugs
Novo Conj	Novokinin Conjugate
p.o	Oral
OPG	Osteoprotegerin
PTH	Parathyroid hormone
PPAR γ	Peroxisome proliferator receptor γ
PEG	Polyethylene glycol
PET	Positron emission tomography
PK	Pharmacokinetics
PI3-K	Phosphoinositide 3-kinase
PLA2	Phospholipase A2
PLC	Phospholipase C

PLD	Phospholipase D
PBS	Phosphate buffer saline
PBT	Phosphate buffered saline with 0.1% tween
PRCP	Prolyl carboxypeptidase
PGs	Prostaglandin
EP4	Prostaglandin E receptor 4
IP	Prostaglandin I2
PKG	Protein kinase G
PP2A	Protein Phosphatase 2A
PT1B	Protein tyrosine Phosphatase 1B
P-O-P	Pyrophosphate
QC	Quality control
Rab 5	Ras-related protein 5A
Rac1	Ras-related C3 botulinum toxin substrate 1
ROS	Reactive oxygen species
RANKL	Receptor activator of nuclear factor kappa beta ligand
RIPA	Radioimmunoprecipitation assay
RAS	Renin-angiotensin system
Tregs	Regulatory T cells
RE	Relative error
RP	Reverse Phase
RT-PCR	Reverse transcriptase-polymerase chain reaction
Rpm	Revolution per minute
RA	Rheumatoid arthritis
RF	Rheumatoid factor
RNA	Ribonucleic acid
RPMI	Rosewell Park Memorial Institute
STAT	Signal transducers and activators of transcription
SIR	Single ion recording
SPE	Solid-phase extraction
SPPS	Solid-phase peptide synthesis
she	Soluble epoxy hydrolase
SHR	Spontaneously hypotensive rats
SpD	Sprague Dawley
SHP-1	Src-homology-2-domain-containing tyrosine phosphatase-1
SD	Standard deviation
SE	Standard error
SPPS	Statistical Package for Social Sciences
SLE	Systemic lupus erythematous

TRAP	Tartrate-resistant phosphatase
$t_{1/2}$	Terminal elimination half-life
TNFα	Tissue necrosis factor α
TIMPS	Tissue inhibitor of metalloproteinase
TLRs	Toll like receptors
T-EETs	Total-EETs
T-HETEs	Total-HETEs
T-DiHTs	Total-DiHTs
TGF-β	Transforming growth factor β 1
TFA	Trifluoroacetic acid
TXA2	Thromboxane A2
TXA2R	Thromboxane A2 receptor
TKDR	Tissue kallkrein-deficient receptor
TM	Transmembrane
TBST	Tween-containing tris base saline
Th1	Type 1 helper T cells
Th17	Type 17 helper T cells
VSMC	Vascular smooth muscle cell
VEGF	Vascular endothelial growth factor
WB	Western blot

List of Symbols

α	Greek small letter Alpha
ß	Greek small letter Beta
γ	Greek small letter Gamma
g	Gram
k	Kilo
Λ	Greek small letter Lambda
L	Liter
µ	Greek small letter Micro
M	Molar
m	Milli
n	Nano
p	Pico
mins	Minutes
hrs	Hours
secs	Seconds

List of Amino Acids and Abbreviations

Three letter symbols	Amino acid
Ala	Alanine
Arg	Arginine
Asn	Asparagine
Asp	Aspartic acid
Cys	Cysteine
Glu	Glutamic acid
Gln	Glutamine
Gly	Glycine
His	Histidine
Ile	Isoleucine
Leu	Leucine
Lys	Lysine
Met	Methionine
Phe	Phenylalanine
Pro	Proline
Ser	Serine
Thr	Threonine
Trp	Tryptophan
Tyr	Tyrosine
Val	Valine

Bone-Targeted Delivery of Novokinin, an Angiotensin II Type 2 Receptor Agonist, for Improved Pharmacokinetics and Therapeutic Effects

Idaho State University - (2023)

The renin-angiotensin system (RAS) is an intricate endocrine cascade that elicits diverse biological functions. Angiotensin II (Ang II), as a central component of the RAS, mediates inflammatory diseases by binding to the Angiotensin II type 1 receptor (AT1R). In contrast, its binding to Angiotensin II type 2 receptor (AT2R) provides functional antagonism to AT1R axes. Novokinin, a synthetic peptide, activates AT2R and can be considered a potential drug candidate for alternative therapy for RAS-related diseases if its plasma stability and pharmacokinetics could be improved. Hence, we have employed a novel bone-targeting approach where we conjugate bone to polyethylene glycol (PEG) spacer and bone-targeting moiety bisphosphonate (BP) that utilizes the bone as a reservoir and protects it from degradation. We have hypothesized that this delivery approach will improve stability to elicit superior pharmacodynamic characteristics.

To fulfill our hypothesis, we first synthesized Novokinin and Novokinin Conjugate (Novo Conj) by conjugation with PEG and BP. They were characterized by HPLC and LC-MS/MS. In addition to this our results indicated that Novo Conj has better stability and higher affinity to the bone.

Next, we outlined our second objective to determine and compare the biological activity of conjugated peptide *in vitro* and *in vivo*. Our result indicated that Novo Conj showed superior *in vitro* effects by increasing neurite outgrowth in NG108-15 and prolonging antiproliferative effects in breast cancer cell lines. Similarly, for the *in vivo* study we observed that Novo Conj

alleviated signs and symptoms of experimental arthritis by reducing the plasma nitric oxide level, restoring inflammation-induced weight loss, reducing joint swelling, and restoring the disrupted balance of the RAS.

Our final objective was to determine drug pharmacokinetic (PK) parameters in the healthy male Sprague Dawley (SpD) rats. For this study, we developed and validated the quantification of novokinin in the plasma, applied it to PK studies and established its complete drug profile.

Overall, we successfully established bone-targeted delivery of novokinin by testing several cell models and the RA model. We also showed a superior pharmacodynamic effect of conjugated peptide than its native due to its stability and likely improvement in its PK parameters.

Keywords*:* Renin-angiotensin system, Angiotensin II type 2 receptor, Novokinin, Pharmacodynamics, Pharmacokinetics

Chapter I: Introduction to Angiotensin II Type 2 Receptor (AT2R)

1.1 Renin Angiotensin System (RAS) and AT2R

RAS is an intricate, complex cascade of angiotensin (Ang) peptides that elicits diverse biological functions. Its unique feature is balancing the two opposite arms composed of enzymes/peptides/receptors within the system to maintain normal physiological conditions. Initially, it had been identified as a circulating endocrine system responsible for blood pressure, fluid, and electrolyte balance, and systemic vascular resistance (1). Detailed biochemical and molecular studies indicated that the concentration of Ang peptides in the blood is too high to be attributed to the systemic generation of these peptides alone as they present with a rapid clearance in the systemic circulation. These findings led to the consensus that a parallel tissue RAS and the circulating component exists. The widespread presence of Ang converting enzymes (ACE) and Ang peptides receptors in various tissues also supported the tissue RAS concept (2). As depicted schematically in Figure 1, angiotensinogen is a serum glycoprotein produced by the liver and serves as the precursor for all Ang peptides. The plasma renin cleaves angiotensinogen to form an inactive decapeptide, Ang I. Classically, membrane-bound metalloproteinase (ACE) cleaves Ang I into an octapeptide, Ang II, that binds to the angiotensin II subtype 1 receptor (AT1R). However, recent findings suggest that Ang I is also metabolized by other enzymes, such as ACE2, an ACE homolog enzyme, a carboxypeptidase, and neprilysin, to give other truncated peptides like Ang 1-9 and Ang 1-7 as well. Ang 1-7 binds to the mas receptor (MasR) and evokes the opposite action of AT1R (2, 3). The complexity of RAS does not end here as Ang II can itself bind to different subtypes of AT1R, i.e., angiotensin II subtype 2 receptor (AT2R) (4). Ang II can be further metabolized by aminopeptidase A to give Ang III or by ACE2 to give Ang 1-7. Furthermore, Ang III has also been found to be cleaved by aminopeptidase N to give rise to

Ang IV. It has been reported that Ang III and Ang IV can bind to AT1R and AT2R, but they have more selectivity to AT2R (1).

With several different peptides acting in the RAS, a delicate balance exists between the peptides working on opposite functional arms of the system. On one arm, the ACE/Ang II/AT1R forms a dominant axis where Ang II evokes vasoconstriction and aldosterone secretion, increases sympathetic tone, and promotes cellular growth and proliferation. Its overactivation has been implicated in cardiovascular, cancer, metabolic, inflammation, and neurological disorders (5, 6, 7). On the other less common arm, ACE/Ang II/AT2R acts as a protector by eliciting functional antagonism to that of AT1R. As the AT2R is scarcer in its expression than AT1R, the effects observed are subtle but cannot be neglected as their stimulation causes vasodilation, antiproliferation, natriuresis, and anti-fibrosis, thus serving as a protective arm (8). In addition, another axis, ACE2/Ang 1-7/MasR, also functions as a protective arm acting opposite to that of AT1R signaling. As the research focuses on the ACE/Ang II/AT2R axis, here we discuss more the structure, distribution, and mechanism of action of AT2R.

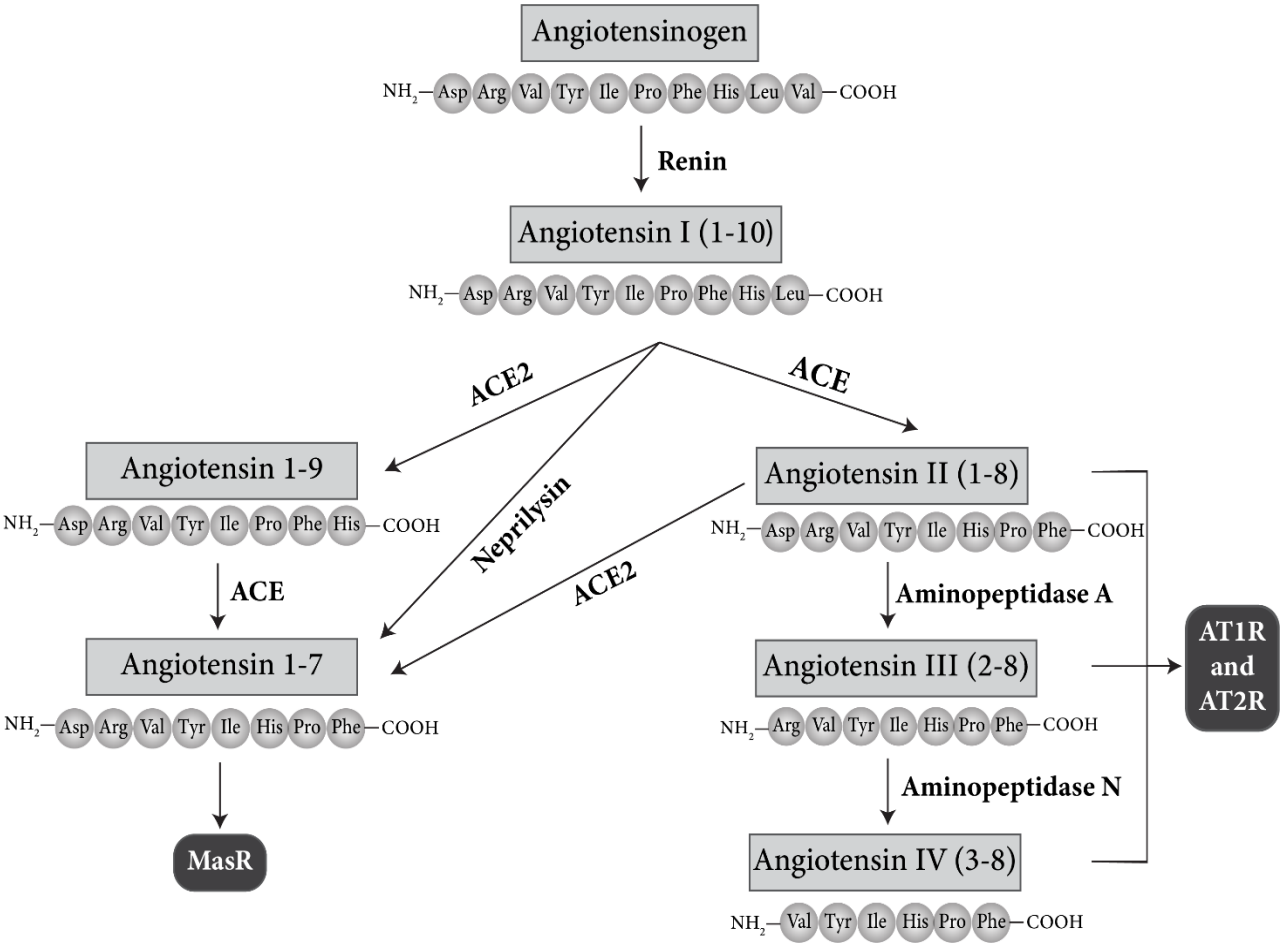

Figure 1. Schematic diagram of the renin-angiotensin system (RAS).

1.2 AT2R Protein Structure

The AT2R is a member of the superfamily G-protein-coupled receptor. It has seven transmembrane (TM) helical domains with an extracellular N-terminal and intracellular C-terminal on either side of the membrane (9). The receptor contains 5 N-glycosylation sites, 5 Ser/Thr phosphorylation sites, and 14 Cys residues. AT2R shows β hairpin conformations in the extracellular loop2 (ECL2), forming two disulfide bridges linking N-terminus with ECL3 (Cys^{35}-Cys^{290}) and helix III with ECL2 (Cys^{117}-Cys^{195}). The reading frame of cDNA encodes a 363 amino acid protein with an approximate molecular weight of 41 kDa, although the molecular weight varies according to cell types due to differences in glycosylation (10, 11).

The AT2R is encoded by the gene residing on the X-chromosome and has three exons with the entire coding region on the third exon (12). The promoter activity of the AT2R gene (Agtr2) is regulated by several cis-regulatory regions, and its expression is downregulated by cyclic adenosine monophosphate (cAMP) with the inhibition of both the gene transcription and messenger ribonucleic acid (mRNA) stability (13). The confinement of AT2R in the long arm of the X-chromosome may contribute to the variation of AT1R/AT2R level according to gender, with this ratio being higher in males than females (14).

1.3 The Divergent State of AT2R

Although AT1R and AT2R are same receptor type, they share just 34% of homology, which can explain their polar apart biological activity. The highest level of homology occurs in a TM domain, and only a few commonalities are observed in the N-terminal and the loops between both receptors (9). The third intracellular loop (ICL) and C-terminal have the lowest homology. The third ICL is regarded as the main site for G-protein coupling, accounting for its atypical signal transduction (15).

As Ang II receptors have a similar affinity to endogenous ligand Ang II (3-4 nM), it gave rise to the theory that receptors share homogeneity in the Ang II binding site. The earlier receptor mutational studies suggest some essential commonalities between the two receptors exist, but there were divergent mechanisms within each subtype to complement the shared basic binding processes (16).

Apart from divergent amino acid residues between Ang receptors, they also differ in the conformational structure in their basal state. Generally, agonists activate G-protein-coupled receptors (GPCRs), but atypical AT2R remains constitutively active state without agonist receptor activation. The crystallography studies done in the human AT2R bound to the high-affinity antagonist revealed that it displays active-like conformation. The unusual conformation of the helix VIII in AT2R regulates AT2R non-canonical activity by sterically blocking G-protein/β arrestin but can also switch to coupling with G-protein/β arrestin depending upon post-translational modifications and the environment it is in (17).

A series of AT1R/AT2R receptor chimeras were designed to characterize structural determinants responsible for cell signaling. This study revealed that unlike hydrophobic residue in GPCRs, the intracellular loop1 (ICL1) of AT2R has polar and charged residues, namely Gln^{72} and Lys^{73}. This polar residue destabilizes the interaction between helix VIII and ICL1 but promotes the interaction of this helix with TM6 leading to the atypical conformation of the AT2R helix VIII domain. Other than this, the divergent C-terminal also aided in the atypical AT2R active conformations (18). Additionally, the internal lock (Asn^{111}-Asn^{295}) of AT1R, which must be dismantled for active conformation, was also observed in AT2R (Asn^{127}-Ser^{311}), but there were no hydrogen bonds between internal locks. This difference in the internal lock hinted at the fact that AT2R remains in a different basal state compared to typical AT1R (19).

The ligand-independent apoptosis was observed in the AT2R transfected cultured fibroblasts, epithelial cells, and vascular smooth muscle cells (VSMC) (20). The GPCRs undergoing homo or hetero oligomerization is a common effect to induce cell signaling. The presence of Cys residue in the extracellular loops in the AT2R leaves an open site for both inter and intramolecular disulfide bonds. In another study, homooligomerization of AT2R in the serum-free pheochromocytoma cell line (PC12W) was proved by immunoblotting, and apoptotic cell signaling was observed without the input of any agonist for AT2R (21). The overexpression of AT2R by gene transfection in the lung adenocarcinoma (22), rat insulinoma (INS-1) (23), and human bladder cancer cell lines (Bac) (24) promoted apoptosis. Ang II or AT2R antagonists did not modulate this apoptotic effect, implicating that it was due to the constitutive activation of AT2R. Along with the apoptotic effect, the overexpression of AT2R also impaired insulin secretion in INS-1 and inhibited angiogenesis in the Bac.

Consistent with the constitutively active conformation theory, AT2R does not undergo desensitization and internalization, unlike its AT1R counterpart. The immunofluorescence microscopy studies in the human embryonic kidney cell line detailed that AT2R is not internalized into endosomes but localized in the plasma membrane upon agonist stimulation (25). In the rat mesenteric artery, the administration of Ang II or CGP42112A, an AT2R agonist, evoked concentration-dependent vasorelaxation in the presence of an AT1R blockade. There was attenuation of vasoconstriction effects evoked by the Ang II via AT1R, but AT2R-mediated relaxation was seen consistently in the same low dose of agonist, suggesting a lack of AT2R internalization during the short-term or long-term AT1R blockade (26).

1.4 Distribution and Expression of AT2R

1.4.1 Tissue Distribution

The early studies conducted on the tissue distribution of AT2R were based on autoradiography, ligand binding, and in situ hybridization. They revealed that AT2Rs are predominantly found in fetal tissues whose expression decreases rapidly after birth. In adults, their expressions were limited to the tissues of the brain, heart, adrenal glands, vascular endothelium, kidney, myometrium, and ovary (27, 28). This led to the opinion that AT2R is essential in the growth, development, and differentiation processes.

1.4.2 AT2R expression in pathological condition

Another unique feature of the AT2R is that its expression is upregulated in pathological conditions compared to standard physiological settings. The study done by Ortega et al. (29) showed that renal expression of AT2R increased when Ang II was systemically infused in the different experimental models of renal injury due to inflammation, apoptosis, and proteinuria . Similar results were obtained when AT2R expression was analyzed by real-time reverse transcriptase-polymerase chain reaction (RT-PCR), WB, and immunofluorescence labeling in cerebral ischemic models of rats. An increase in the density of AT2R was found centered around the peri-infarct zone when focal cerebral ischemia was induced, but the expression of AT1R remained unaltered (30). A single-cell RT-PCR performed in the adult rat cardiomyocytes one day before and after myocardial infarction (MI) also showed augmented AT2R expression after MI (31). Not only was this observed in various rat models of tissue and vascular injury, but sciatic and optic nerve transection models also showed a marked surge in the AT2R expression suggesting its role in the healing process and maintaining normalcy (32).

1.4.3 Factors Affecting AT2R Expression

The expression of AT2R is tightly regulated by intracellular and extracellular growth factors, including the growth stage of the cell and cell type. In the fibroblast cell line R3T3, known to express AT2R alone, the density of AT2R was low in the actively growing state but substantially increased in the confluent state. When serum and growth factors like bovine fibroblast factor, insulin-like growth factor-I, and transforming growth factor-β (TGF-β) were added to quiescent R3T3, and another exclusively AT2R expressing cell line, PC12W, the AT2R expression was found to be inhibited. The decreased AT2R expression was attributed to their negative influence on the gene transcription of AT2R. The time frame in the incubation of nerve growth factor (NGF) also affected the AT2R mRNA expression in primary neuronal cell culture. Extracellular factors like Ang II or AT2R agonist CGP42112A stimulated AT2R in a time and concentration-dependent manner in the R3T3 cell line. Apart from this, the cell type on which growth factors are acted upon also influenced AT2R expression. For example, treatment of insulin in cultured neurons downregulates the AT2R and in VSMC upregulates the AT2R expression (33). Likewise, growth factors (phorbol ester, lysophosphatidic acid, and basic fibroblast growth factor) markedly suppressed mouse AT2R mRNA expression in the R3T3 but not in the VSMC (9).

1.5 Signaling Pathway for the AT2R

After the establishment of AT2R as a GPCR, similarities and divergent characteristics between Ang receptors were drawn. It was found that AT1R acts as a typical GPCR and couples to a wide variety of G-proteins in the same cell type, whereas AT2R is atypical and limited to Gi (34) and some unknown G-proteins (35). This receptor is known to follow three different molecular events: 1) activation of protein phosphatases and protein dephosphorylation, 2) regulation of the

nitric oxide (NO), 3,5-cyclic guanosine monophosphate system (cGMP), and 3) stimulation of phospholipase A2 (PLA2) and release of arachidonic acid (ArA) (36).

1.5.1 Activation of Protein Phosphatases and Protein Dephosphorylation

The AT2R stimulation has been widely accepted to cause downregulation of growth factor-induced intracellular cascades, leading to kinase activation and protein dephosphorylation. Here the AT2R mediates the activation of 3 different Tyr, Ser, or Thr phosphatases, and they are Src homology -2 domain-containing tyrosine phosphatase-1 (SHP-1), protein phosphatase 2A (PP2A), and mitogen-activated protein (MAP) kinase phosphatase (MKP)-I. All three phosphatases are responsible for AT2R mediated inactivation of the extracellular signal-regulated kinase (ERK) cascade in different cell types. The inactivation of the ERK causes obstruction in the signaling transmission receptor on the surface of the cell to the DNA in the nucleus of the cell, thus inhibiting cell growth, proliferation and aiding in apoptosis (Figure 2). SHP-1 is a widely expressed inhibitory protein tyrosine phosphatase (PTP) in cells, acting as a checkpoint for unwanted cell growth. In the study done in the N1E-115 neuroblastoma cell line, AT2R mediated the activation of SHP-1 and interrupted the growth factor-induced ERK pathway. The activation of SHP-1 mediated by AT2R is pertussis toxin insensitive independent of Gi signal (37). Rather, SHP-1 coupling may actually involve an atypical G-protein scaffolding mechanism, Gβγ-independent constitutive association of the receptor with Gs and SHP-1 (38). Similarly, PP2A is another important and versatile enzyme acting as the regulator of the cell cycle. The activation of PP2A by AT2R in cultured neurons from newborn rats has been reported to show the inhibition of ERK MAP kinase (MAPK) activities important for apoptosis (39).

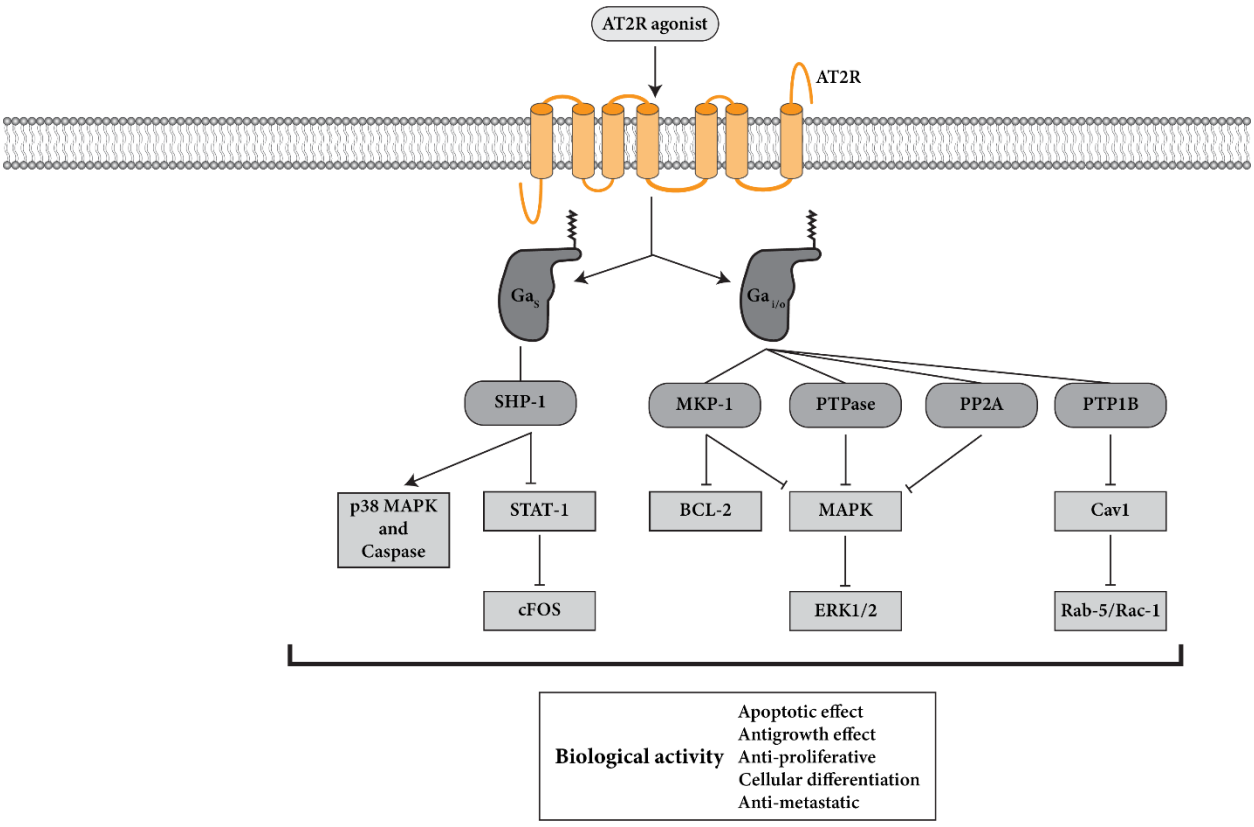

Figure 2. Schematic diagram for signaling mechanism protein phosphatases and protein dephosphorylation Src homology -2 domain-containing tyrosine phosphatase 1 (SHP-1), protein phosphatase 2A (PP2A), mitogen-activated protein (MAP) kinase phosphatase (MKP)-I, signal transducers and activators of transcription (STAT), β-cell lymphoma-2 (Bcl-2), caveolin-1 (CAV1) protein tyrosine phosphatase 1B (PTP1B) Ras-related protein 5A (Rab5), Ras-related C3 botulinum toxin substrate 1 (Rac1).

Another highly conserved phosphatase, MKP-1, is also involved in down-regulating ERK cascades. The AT2R stimulation in the cardiac myocytes resulted in the activation of vanadate sensitive dual-specificity (Tyr and Thr) phosphatase leading to the inactivation of the MAP kinase ERK. In the PC12W cells, the treatment of Ang II via AT2R caused stimulation of MKP-1 and impairment in the ERK MAPK activation. The interference in this intracellular level led to the inactivation of cell survival factor β-cell lymphoma-2 (Bcl-2) cell survival factor in those cells, thus resulting in apoptosis (40).

The AT2R-mediated SHP-1 activation is also known to cause dephosphorylation of signal transducer and activator of transcription (STAT) pathway responsible for mediating cell differentiation, migration, and cell growth. In the study done in AT2R complementary deoxyribonucleic acid (cDNA) transfected VSMCs, inactivation of STAT was observed via the inhibition of serine phosphorylation, thereby resulting in the decrease of proto-oncogene c-fos transcription (41). This is how AT2R recruits diverse intracellular pathways in various cell lines to show the same effect, i.e., protein dephosphorylation. Some of the pathways are reported in a similar cell line, hinting that more than one mechanism is involved and acts as an efficient cell lock system at different levels at various time points (36, 42). Furthermore, the level of AT2R protein expression also determines the apoptosis of cultured fibroblasts, epithelial cells, and VSMCs. Ligand-independent apoptosis was also observed that involved a signaling pathway that included activation of p38 MAPK and caspase 3 (43). The AT2R activation has been found to be a negative regulator of scaffold in G-protein caveolin-1 (CAV1), inducing melanoma and breast cancer migration and invasion. This ability of AT2R is linked to the activation of the protein tyrosine phosphatase 1B (PTP1B), dephosphorylation of (pY14) CAV1, and inhibition of the CAV1/ Ras-related protein 5A (Rab5)/Ras-related C3 botulinum toxin substrate 1 (Rac1) signaling axis. The AT2R stimulation was also shown to block CAV1-enhanced melanoma metastasis in a preclinical animal (44).

1.5.1 Regulation of the NO–cGMP Pathway

Being an endogenously produced autacoid, NO controls various biological processes, including vasodilation, neurotransmission, cell growth, apoptosis, and inflammation. Most of the biological effects of NO are thought to be mediated via stimulation of cGMP. The AT2R stimulation increases protein and gene expression of endothelial nitric oxide synthase (eNOS), facilitating

NO production (45). This increased NO generation and subsequent rise in cGMP was observed in various cell lines like cultured bovine endothelial cells, dog coronary arteries, and isolated perfused rat renal arteries (28). The activation of cGMP promotes vasodilation by inhibiting cytosolic free calcium levels by several mechanisms. These mechanisms include i) inhibition of inositol 1,4,5-trisphosphate (IP3)-mediated calcium release from intracellular stores, ii) removal and sequestration of intracellular calcium through calcium pump mechanisms, and iii) both direct and indirect inhibition of the extracellular calcium influx through voltage-gated calcium channels (46).

The enhanced AT2R-mediated NO/cGMP pathway promoted neuronal differentiation and outgrowth in NG108-15, neuroblastoma, and glial cell lines (47). Later AT2R-mediated NO/cGMP pathway and AT2R-mediated mitogen-activated protein kinases (p42/p44 MAPK) were also found going hand in hand for the neuron differentiation in the same cell line model, suggesting more than one way for AT2R-mediated action (48) and different cell lines like PC12W (49). On the other hand, AT2R encourages gastrointestinal sodium and water absorption by a pathway that induces stimulation of the sympathetic nervous system and NO/cGMP cascade. This way, AT2R acts as a functional antagonist for AT1R-mediated inhibition of sodium and water absorption (50).

The RAS and kinin pathway have long been considered partners for cardiovascular homeostasis. AT2R and kinins play essential role in cardio protection and vasodilation opposing the biological effects of AT1R. Siragy et al. (51) attributed the increase of renal bradykinin (BK) to non-AT1R and hinted at the possible role of AT2R. It was confirmed that the renal production of BK mediates the protective vasodilator response and NO through AT2R (51). Similarly, in the stroke-prone spontaneously hypertensive rats (SHR), continuous infusion of Ang II causes an

increase in cGMP level (Figure 3). This response was abolished by N- nitro-L-arginine methyl ester (L-NAME), an inhibitor of NO-synthase (NOS), AT2R blocking as well as using BK receptor antagonist, suggesting supporting the role of BK/NO/cGMP (52).

The mechanism by which AT2R influences direct BK release or mediates its cofactor has been tried to be explored in multiple pathways. One of the earliest pieces of evidence was given by Tsutsumi et al. (53), where they overexpressed the vascular smooth muscle-specific (VSM-specific) AT2R gene in mice. AT2R-mediated acidosis by inhibiting Na^+/H^+ exchanger activity, thus promoting kininogenase activity in aortic VSM cells and releasing BK. The increased level of BK-enhanced endothelial BK2 receptor (B2R) mediated vasodilation by activating the NO/cGMP system, resulting in an AT2R-mediated depressor effect.

Bergaya et al. (54) explored the vascular kallikrein-kinin system, which is responsible for producing vascular kinins, including BK. They recorded and compared the increase in the flow rate of perfused arteries in wild-type animals ($TK^{+/+}$) and in tissue kallikrein-deficient mice ($TK^{-/-}$). They discovered that the AT2R antagonist PD123319 significantly reduced flow-induced dilation in $TK^{+/+}$ mice but had no significant effect in $TK^{-/-}$ mice. Furthermore, the B2R antagonist, HOE-140, significantly reduced the response to flow in the wild-type animals ($AT2R^{+/+}$) but not in $AT2R^{-/-}$ mice, stating that functional AT2R and B2R are codependent on each other to elicit flow-dependent dilation. It has been confirmed that the cardioprotective effect of AT1R blockade is mediated via B2R and AT2R (55).

Dimerization between Ang II and BK receptors has added a new dimension to understanding the nature of RAS and kinins pathway interaction. AT1R and BK2R have been shown to undergo heterodimerization and demonstrate an inverse physiological relationship (56). Similarly, Abadir et al. (57) showed a direct molecular interaction between AT2R and B2R. The authors illustrated

that AT2R and B2R in the membrane of the PC12W cells are in close molecular proximity that gives rise to receptors dimerization resulting in enhanced NO and cGMP production. This emphasizes that AT2R and B2R work in concert to amplify the expected biological effect in a mutually dependent way. Although this concept seems very novel with little literature support, this information gap has given rise to questions about whether this phenomenon is particular to PC12W cells or can be observed in various cell lines. Therefore, more investigation is needed to validate this concept in detail.

Furthermore, Zhu et al. (58) attempted to shed light on the relationship between AT2R and kinins and their signaling mechanism using mouse coronary artery endothelial cells concerning kallikrein activation. It has been reported that AT2R-stimulation increases in prolyl carboxypeptidase (PRCP; a plasma prekallikrein activator) activation mediated by the tyrosine phosphatase SHP-1, which in turn stimulates the PRCP-dependent prekallikrein-kallikrein pathway. Subsequently, PRCP cleaves the high molecular weight kininogen complex and plasma prekallikrein to kallikrein generating BK. These events trigger the activation of serial cascades of NO/cGMP and subsequently cause vasodilation.

AT2R is also found to inhibit proximal tubular Na^+/K^+-ATPase, an active tubular sodium transporter, via NO/cGMP pathway in proximal tubules isolated from Sprague-Dawley (SpD) rat, thus unraveling the mechanism by which the AT2R mediates dilation and natriuresis (59).

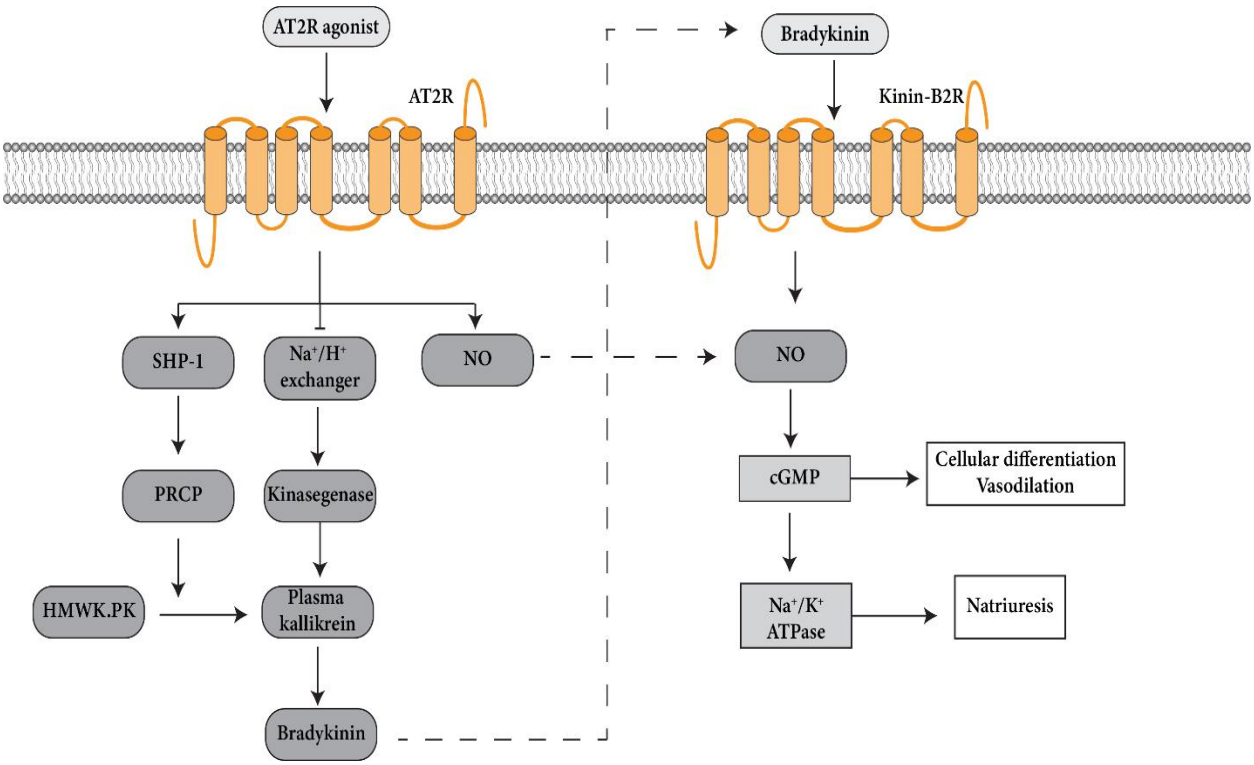

Figure 3. Schematic diagram AT2R mediated NO and cGMP pathway. Bradykinin (BK), nitric oxide (NO), cyclic guanosine monophosphate (cGMP), prolylcarboxypeptidase (PRPC), high molecular weight kininogen plasma kallikrein (HMWK.PK).

1.5.2 Stimulation of PLA2 and Release of Arachidonic Acid (ArA)

PLA2-ArA is a crucial mechanism that plays a diverse range of cellular functions. It involves the action of the enzyme PLA2, which hydrolyzes phospholipids into arachidonic acid (ArA). The released ArA then serves as a precursor to produce various biologically active compounds by cyclooxygenase, lipoxygenase, or cytochrome P450 monooxygenase. The elevated ArA level resulting from PLA2-ArA activation influences ion transport, which is crucial in regulating natriuresis and intracellular pH. In proximal renal tubule epithelial cells and cardiac myocytes, activation of PLA2-ArA by Ang II through its AT2R leads to sustained release of ArA. This process affects ion transport and regulates natriuresis and intracellular pH.

Similarly, in the brain, Ang II binding to neuronal AT2R results in the modulation of membrane ionic currents and firing rate through ArA release and its metabolism by 12-lipoxygenase via serine/threonine phosphatase PP2As. An association has been observed between the amplified generation of metabolites of epoxyeicosatrienoic acid (EETs) and the activation of PP2A. Thus, the stimulation of PP2A modulates membrane ionic current and neuronal activity.

The sustained release of the ArA by the AT2R pathway also gives rise to the various epoxy derivatives of ArA, dependent on cytochrome P450 (CYP450). These metabolites serve as an upstream mediator of MAPK in the renal cells (60). Another study reported it was reported that Ang II activates the Tyr kinase- Shc-Grb2-Sos complex pathway, which is a growth factor modulating the signaling pathway. This unique pathway activates the p21 ras protein, an important cell signalinG-protein, due to the exchange of guanosine diphosphate (GDP) to guanosine triphosphate (GTP) in the renal cell. These studies provided a basis for the linkage between AT2R and receptor tyrosine kinase through lipid secondary messenger (61).

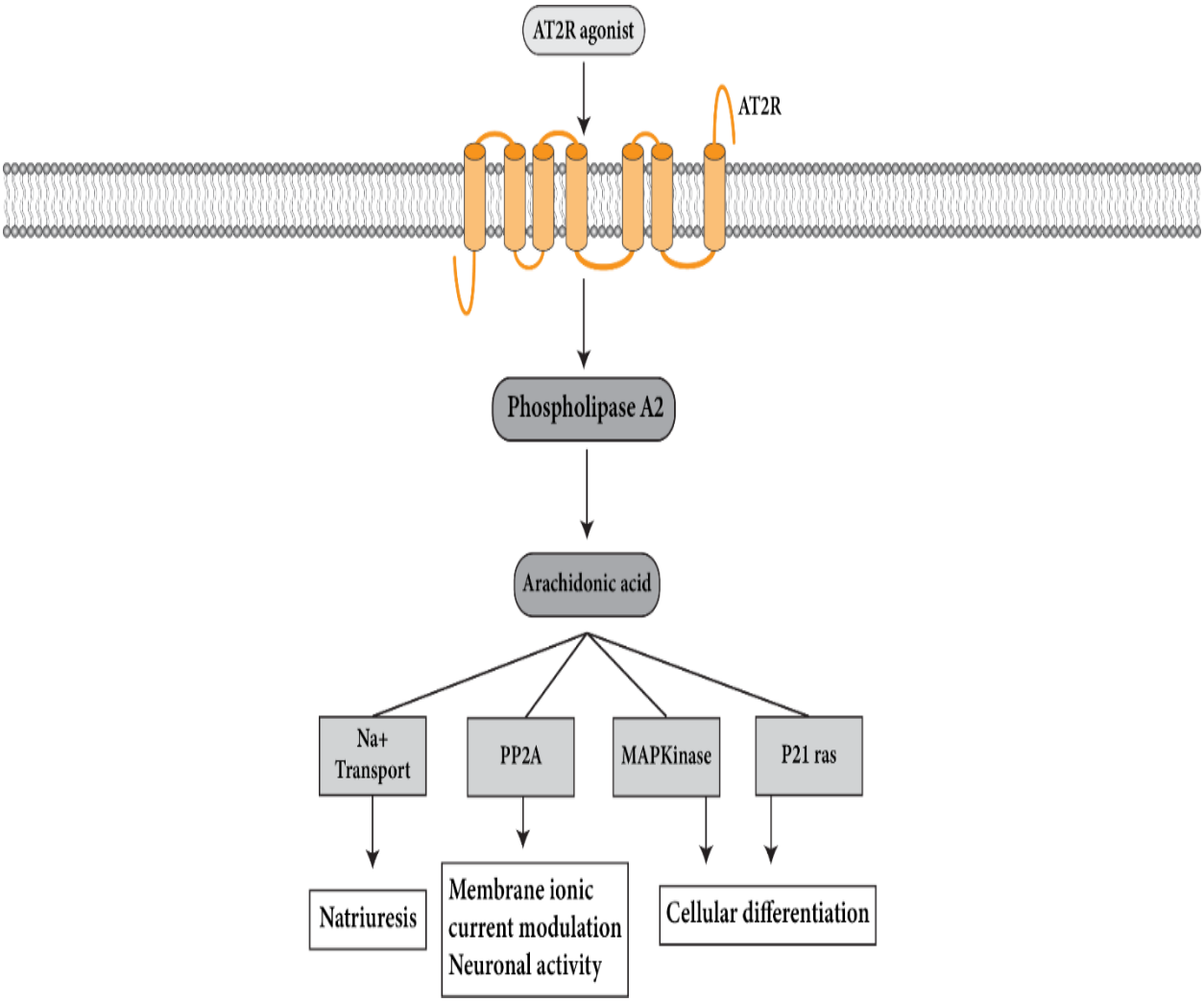

Figure 4. Schematic diagram for phospholipase A2/arachidonic acid (PLA2/ArA) pathway, protein phosphatase 2A (PP2A), mitogen-activated protein kinase (MAP Kinase), p21 ras protein.

1.6 AT2R Agonist

1.6.1 Ang II and its Peptide Derivatives

Ang II, a main effector peptide in the RAS, is considered the primary endogenous agonist for AT2R. These eight amino acid peptides (Asp^{1}-Arg^{2}-Val^{3}-Tyr^{4}-Ile^{5}-His^{6}-Pro^{7}-Phe^{8}) have a similar binding site for both receptors but with different pharmacophores for each receptor subtype (62). The modifications of all Ang II side chains affected binding to the AT2R to nearly

similar extents, whereas binding to the AT1R is significantly affected by modifications at side-chain positions of amino acids 2, 4, 6, and 7. They further revealed that the AT1R is in a constrained conformation and is activated only when bound to Ang II. In contrast, the AT2R is in a relaxed position, and no single interaction is critical for binding. When glycine scans were performed for each amino acid in Ang II, it divulged that Arg^2 and positive charge in the N-terminal side chain were important for Ang II binding to the AT2R (63). CGP42112A, a synthetic peptide, was also developed by retaining the carboxy-terminal of Ang II with the end aromatic chain replaced by aliphatic Ile, thus favoring even more affinity and selectivity. The retrospective analysis of the chemical evolution of AT2R peptide agonists by molecular binding modes and affinity estimations with the free energy perturbation method has shown that CG42112A presents a guanidine group on a branched-like structure mimicking the sidechain of Arg^2 in Ang II which explains its strong affinity to AT2R.

When Ang II binds to the Ang II receptors, the side chains of amino acids Val^3 and Ile^5 of Ang II are involved in productive hydrophobic interaction with one another in the receptor cavity. This produces turn conformations centered at Tyr^4 that generally serve as a recognition trigger in the peptide receptor interaction. Small variations of the turn geometry in the 3-5 region of Ang II result in drastic loss in the AT1R binding affinity, while having a minor impact on the AT2R binding affinity (64). Ang II was optimized to make several derivatives of Ang II by mimicking the γ-turn scaffold for AT2R selective activity.

Apart from the γ-turn mimetic scaffold, it is discovered that the position of the guanidine group of the Arg^2 residue in space, in relation to the Tyr^4 side chain and the N-terminal end, was also critical for AT2R binding affinity (63). The synthesized Ang II analog encompassing a benzodiazepine-based γ-turn-like scaffold having a suitable Arg^2 position in the

sequence displayed high AT2R selectivity and exhibited AT2R affinity in the low nanomolar range.

The Ang II binding to AT2R, other than being tolerant to the alteration in the amino acid structure, is also insensitive to the truncation of the Ang II sequence unlike the AT1R counterpart as reported previously (65). The acetylated pentapeptides Ac-Tyr-Val-His-Pro-Phe and Ac-Tyr-Val-His-Pro-Ile were reported to have high selectivity and Ki values in the nanomolar range but no information was divulged regarding agonistic and/or antagonistic properties. Taking these compounds as lead compounds, several different bicyclic aromatic scaffolds were introduced in the Tyr^4-Val^5 region, which gave rise to 13 other pseudo peptides. Among them, the compound having 1,3,5-trisubstituted aromatic scaffolds with Ile in C-terminal is found to have an equivalent affinity as Ang II to AT2R, whereas more than 10000-fold less as Ang II to AT1R. This compound also exerted agnostic effects at the AT2R based on its ability to induce neurite outgrowth. This study highlighted the lipophilic aliphatic C-terminal more favors AT2R interaction than the aromatic side chain (66).

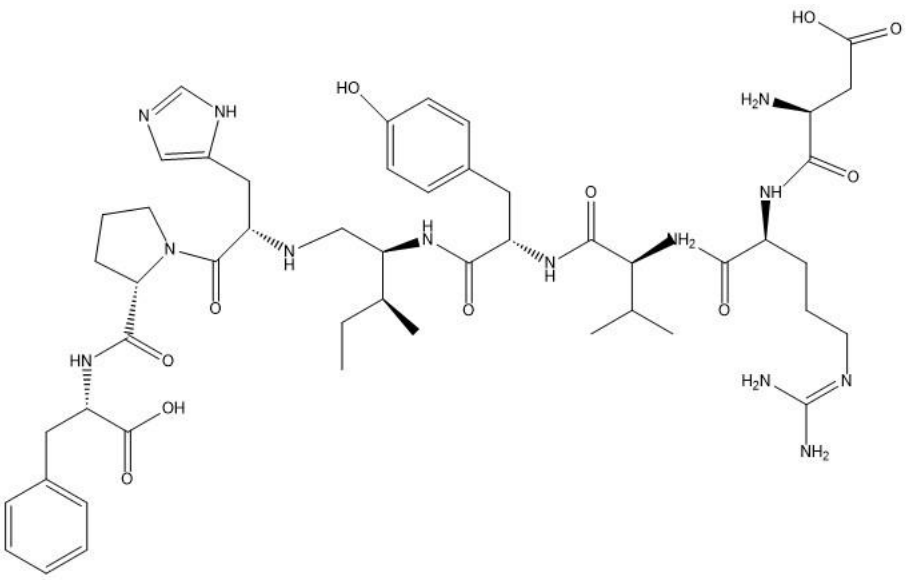

Figure 5. Structure of angiotensin II (Ang II).

1.6.2 Non-Peptide AT2R Agonist

A selective non-peptide agonist named C21 was developed based on mimicking of the three C-terminal amino acids His-Pro-Phe of Ang II essential for binding to Lys^{215} of AT2R (67). A compound containing a biaryl scaffold responsible for Ang receptor bindings which are connected to three functional groups, was designed having: i) a lipophilic side chain, ii) a sulfonyl carbamate group, and iii) a methylene group attached to a bicyclic nitrogen heterocycle (Figure 6).

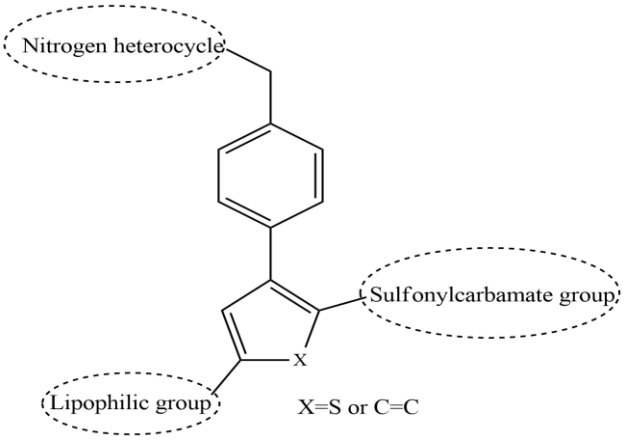

Figure 6. Scaffold for angiotensin II type 2 Receptor (AT2R) agonist. Adopted from (68) with permission.

Structural activity relationship studies show that methyl imidazole or triazole structure is essential for specific binding to AT2R with high affinity. Regarding the lipophilic side chain, it has previously been reported that small structural alterations of this group also seemed to reduce the affinity of the ligands to the AT2R, therefore the isobutyl group was considered as most suitable. Similarly, the alkoxy part of the sulfonyl carbamate group was crucial to improving AT2R selectivity. Vasile et al. (69) reported a detailed structural activity relationship of C21 by the binding modes and affinity estimations with the free energy perturbation method. It has been stated that C21 is anchored by electrostatic interactions of the central sulphonyl carbamate with charged sidechains of TM2 and TM5. The isobutyl group would be located in a deeper hydrophobic cavity within the TM region, facilitating the active receptor conformation. The ligand binding and pharmacokinetic studies of C21 showed that it has K_i = 0.4 nM to AT2R, $K_i \geq$ 10 µM to AT1R and bioavailability is 20-30% after (*p.o*) with a half-life of 4 hrs in the rat (70, 71).

1.7 Conclusion

AT2R plays a crucial role in maintaining the body's homeostasis through its protective arm within the RAS. This receptor has the potential to offer significant pharmacological benefits by opposing the AT1R-mediated action. Targeting AT2R offers promising clinical applications in various pathological conditions such as anti-proliferative, apoptotic, anti-inflammatory, cell differentiation, vasodilatory, and neuronal modulation activities. In the disease state, the upregulation of AT2R can be beneficial if correctly channeled, making it a potential therapeutic target. Ang II, the endogenous ligand for AT2R, has been a focus of research to develop AT2R agonists with enhanced metabolic stability and selectivity over AT1R. Several attempts have been made to modify the peptide structure of Ang II to enhance its pharmacological properties and make it a more effective therapeutic agent for targeting AT2R. Therefore, the AT2R presents an exciting avenue for future research and drug development, potentially providing significant clinical benefits.

Chapter II: Synthesis, Characterization, Test Stability and Bone-targeting Capacity of Novokinin and Novo Conj

2.1 Introduction to Novokinin

The advancements in molecular research of the RAS have led to the discovery of AT2R, which provides a promising approach to counterbalance the overactivated AT1R spectrum. This discovery has renewed hope that AT2R can be utilized to combat diseases caused by imbalances in the RAS. One area of focus in this field is the development of drugs that produce AT2R agonism, which is essential to channelizing therapeutic efficacy.

One promising drug candidate is novokinin, a synthetic peptide derived from chymotrypsin digest, ovokinin (2-7) (Arg-Ala-Asp-His-Pro-Phe), of egg albumin. The ovokinin (2-7) elicited vasorelaxation mediated by AT2R with a binding affinity of 210 μM. It evoked a hypotensive effect in SHR at the dose of 10 mg/kg after oral administration (*p.o*). Later this was modified to the (Pro^2, Phe^3)-ovokinin (2-7), which evoked anti-hypertensive effects at a dose of 0.3 mg/kg corresponding to more than 30-fold times less amount compared to ovokinin (2-7) after oral administration (72).

In the quest to design more potent bioactive peptides, the alanine scan was performed, which aided in determining suitable amino acid residues for each individual position. Like, Arg^1 residue at N-terminal is crucial for anti-hypertensive effects. Similarly, Pro at the 2nd and 5th positions conferred resistance to gastrointestinal degradation by protecting it from the action of enzymes like aminopeptidase and carboxypeptidase without affecting vasorelaxant activity. The aromatic Phe^3 is replaced with aliphatic Leu to escape degradation by chymotrypsin-type protease. They also established that aromatic amino acid residue with high hydrophobicity is required at the carboxyl-terminal, and Trp gives them the best results in terms of anti-hypertensive activity.

Replacing 4 amino acids from the original 6 [ovokinin (2-7)] gives them a more potent peptide called novokinin. This peptide (Arg-Pro-Leu-Lys-Pro-Trp) has superior binding affinity at 7×10^{-6} M, and its bioactivity is seen at a lesser dose than its parent peptide (73, 74).

Novokinin induced relaxation in the mesenteric artery pre-constricted by phenylephrine at the concentration of 10^{-5} M. They also showed encouraging anti-hypertensive effect in the SHR at a dose of 0.03 mg/kg (saline) intravenous (*i.v*) and 0.1 mg/kg (emulsified in 30% egg yolk) after (*p.o*) but no effect in normal hypotensive Wister Kyoto rat. This hypotensive effect was blocked by AT2R antagonist, COX inhibitor and prostaglandin I2 receptor antagonist but also insignificantly by NOS inhibitor. This proved the observed biological action was majorly mediated through the IP receptor downstream of the AT2R, but the contribution of NO cannot be ruled out completely. Similarly, it did not induce hypotension in normal and AT2R-deficient mice (74). The study by Mutlu et al. (75) tried to shed light on the role of the NO pathway for novokinin. In this study, novokinin was administered intraperitoneally (*i.p*) at a 0.1 mg/kg dose for two weeks to the salt-fed and L-NAME-induced hypertensive rats. Novokinin showed a decline in the enzymes responsible for end-organ damage like asymmetric dimethylarginine (ADMA), nicotinamide adenine dinucleotide phosphate (NADPH) oxidase and Rho kinase level induced in the hypertension; however, these changes did not reach statistical significance.

Beside the vasorelaxant and anti-hypertensive effects, novokinin was also found to affect the central nervous system. In the study done by Ohinata et al. (77) novokinin presented with anorexigenic effects at 100 mg/kg/mice (*p.o*) and 30 nmol/mouse intracerebroventricular (*i.c.v*) administration. This effect was mediated by the prostaglandin E receptor 4 (EP4) system via AT2R as it was reversed by AT2R antagonist, cyclooxygenase (COX) inhibitor and EP4 antagonist (76). Similarly, another central nervous effect of novokinin was reported by, which

exerted an anti-opioid effect. Here, centrally administrated novokinin (30 nmol/mouse) inhibits the antinociceptive effect of morphine (μ agonist) in mice, as evaluated by the tail-pinch test. The EP3 system mediated this effect via AT2R as this was reversed by AT2R antagonist, COX inhibitor and EP3 antagonist.

In addition, novokinin also exerted gastroprotective effects via AT2R-Prostaglandin (PG)s pathway (78). Here, it inhibited basal gastric acid secretion and protected gastric mucosa from alcohol-induced injury in a dose-related manner in rats after (*i.c.v.*) administration at the dose of 50 and 100 nmol/rat, respectively. AT2R antagonist and COX inhibitor occluded this effect.

Further exploration of the multitude of therapeutic effects of novokinin revealed that it also had a beneficial role in asthma (79). Novokinin was found to lower lung inflammation and airway reactivity at the dose of 0.3 mg/kg, (*i.p*) in allergen-sensitized mice mediated via AT2R.

While peptide drugs like novokinin offer potential therapeutic benefits, there are potential drawbacks to consider. Therefore, a detailed study of peptide drugs is very essential to make informed decisions about their development and use in clinical settings. The major advantages and disadvantages are explained below.

In conclusion, novokinin is a synthetic peptide modified to improve its bioactivity and potency. It has shown promising therapeutic effects, including vasorelaxant and anti-hypertensive effects, anorexigenic effects, inhibition of the antinociceptive effect of morphine, gastroprotective effects, and potential use in treating asthma. While further studies are needed to fully understand its mechanism of action and evaluate its safety and effectiveness in clinical settings, the potential applications of novokinin highlight the importance of continued research and development of AT2R agonist drugs.

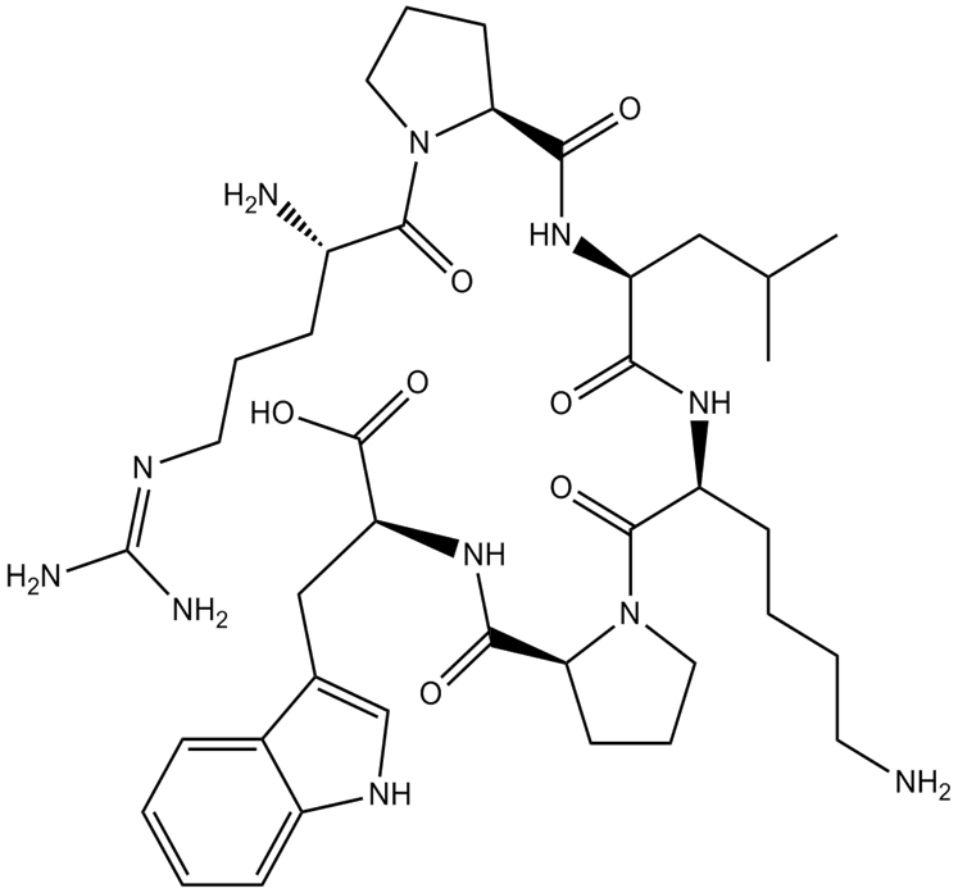

Figure 7. Structure of novokinin

2.2 Peptide Drugs

2.2.1 Advantages

Peptide drugs carry massive potential in filling the gap between two successful drugs by offering specificity and potency of large molecules compared to small molecules (<500 Da) but the smaller size and more accessibility and easiness to manufacture using chemical methods as compared to biologics (>5000 Da) (80). Peptides have a superior potency and selectivity due to their larger size than traditional small molecules, allowing them to capture more binding interactions with target receptors, resulting in high affinity and selectivity. Likewise, it has a probability to modulate undruggable sites due to its ability to regulate protein-protein interaction in the intracellular space. Moreover, many peptides are natural ligands for various cell surface

receptors, including GPCRs, ion channels, and growth factor responses, initiating signal transduction processes inside the cell, which makes them useful as agonist drugs or as starting points for lead discovery. As agonist drugs are more potent at binding to and activating their cognate receptor, they require lower concentrations to achieve a pharmacological response, which means that they can generally be administered at lower doses and may have more favorable dosing schedules than antagonist drugs (81, 82).

Peptide drugs possess several advantages over biologics, such as ease of synthesis, handling, and purification via chemical methods. This makes them more accessible and cost-effective, while still maintaining similar levels of potency and selectivity. Peptide drugs can also be modified at individual amino acids to achieve specific therapeutic outcomes, which results in a broad range of chemical and biological diversity that aids in their detailed investigation from a therapeutic perspective. Moreover, peptide drugs have optimal sizes that reduce activation of the immune system, making them less likely to induce autoimmune responses. Peptide drugs are considered the "holy grail" of personalized medicine as they can be modified at specific sites to tailor therapeutics to individual patients, accounting for different protein expressions and diverse patient responses to drugs (83).

However, peptide drugs have some limitations because of their susceptibility to proteolytic enzymes and rapid filtration from the body. However, their metabolites are usually amino acids that can be quickly taken up by the body to synthesize proteins, leading to less tissue accumulation. Peptide drugs are highly selective and tightly bind to receptors, thereby reducing the risk of off-target effects and adverse side effects. Additionally, they undergo minimal hepatic metabolism, making non-mechanistic toxicology and drug-drug interactions rare. These factors make it easier to predict peptide drug doses through allometric scaling and determine clinical

dose ranges with greater accuracy than small molecules. In some cases, the inability of peptides to penetrate barriers like the blood-brain barrier (BBB) can be beneficial, as it prevents unwanted harmful effects in the central nervous system (CNS). Likewise, peptide drugs with rapid clearance rates can also be advantageous for fast-acting treatments like diabetes, allowing for flexible dosing schedules (84).

2.2.2 Disadvantages

Despite their potential, peptide drugs have limited success in clinical development, primarily due to several challenges and limitations. One of the significant challenges associated with peptide drugs is their short circulation half-life. Peptides are hydrophilic and small, which makes them prone to rapid renal clearance. Additionally, they are susceptible to enzymatic degradation by enzymes that occur in blood, liver, and kidney, leading to ineffective treatment. As a result, peptide drugs cannot provide sufficient therapeutic concentrations over an extended period to reach target tissues (81, 84).

Another drawback of peptide drugs is their poor membrane permeability. Peptides cannot achieve para and transcellular passive diffusion due to their size and low lipophilicity. As a result, the distribution of peptide drugs is mainly limited to the vascular system and excludes most intracellular targets. Furthermore, the inability of peptide drugs to cross barriers, such as the BBB, makes them unsuitable for the developing of CNS drugs (85).

In terms of drug development in oral drugs, peptide lag far behind traditional small molecules. This is because peptides are rapidly degraded by gastric enzymes and are rarely absorbed by the intestinal mucosa owing to their impermeability to the gastric physical barrier. This leads to a low oral bioavailability of peptide drugs. Moreover, the high manufacturing and purification costs make large-scale peptide synthesis around ten times more expensive than small molecule

synthesis. Some lipophilic peptide drugs are also prone to aggregation and have low solubility, which hinders the overall development of peptide drugs (86).

Finally, the storage of most peptide drugs requires cool conditions, increasing the cost of production and making them less marketable than traditional drugs. These challenges and limitations of peptide drugs pose significant barriers to their development and use as therapeutic agents.

2.2 Strategies to Overcome the Shortcoming of Peptide Therapeutics

Various approaches have been employed to counteract the issue of peptide instability in drug development. One method involves resolving the metabolic instability of peptides by recognizing the cleavage specificity of specific proteolytic enzymes and modifying the peptide structure accordingly. For instance, terminal modifications like N-acetylation, methylation, and C-amidation are made into peptides that are particularly susceptible to exopeptidases such as aminopeptidase and carboxypeptidase. These optimizations not only make the peptide resistant to enzymes but also enhance its permeability by reducing the H-bond donating potential (85, 87). Moreover, the susceptibility of the peptide to proteolytic degradation can be minimized by replacement of natural L-amino acids with non-canonical amino acids or introduction of D-amino acids. Similarly, other modifications such as including isomeric amino acid surrogates, using reduced amide instead of amide bond, or incorporating azapeptides and peptoids into the peptide sequence can also be made in extending the peptide's circulation half-life (88).

In addition to this, cyclization of the peptide has also proven to be a successful strategy as it makes the peptide less accessible to enzymes and restricts its flexibility, thereby increasing its passive permeation. However, modifying the peptide structure can sometimes result in a loss of biological activity due to its effect on binding affinity and selectivity (89).

Due to limitations linked with structural modification of peptides, alternative conjugation has emerged as a more feasible option for extending the half-life and enhancing the membrane permeability of peptide therapeutics. The principle of covalent conjugation chemistry has been used to attach peptides to highly abundant plasma proteins such as albumin or transthyretin, polymers like PEG, or fatty acids (90, 91, 92). However, conjugation of a peptide to a large fatty acid or albumin can lead to steric hindrance, which may be particularly detrimental for short peptides if their binding epitope is in close proximity to macromolecules (93).

Therefore, PEGylation of peptides are considered as an excellent choice for improving peptide therapeutics due to easy chain length optimization, its non-toxic and hydrophilic properties. PEGylation increases their systemic circulation time and reduces macrophage intake of peptide drugs as it contribute in increment of molecular weight, resulting in longer half-life and reduced immunogenicity (91).

Furthermore, favorable therapeutic outcomes can be achieved by active targeting of PEGylated peptide drugs restrict their non-specific distribution, thereby reducing systemic toxicity (94). This approach augments the concentration of drugs and improves their bioavailability at the target site, which is particularly beneficial in the treatment of skeletal diseases such as RA. In our study, we have focused on bone-targeted drug delivery to facilitate the optimal delivery of the peptide for improved therapeutic outcomes in treating RA.

2.3 Bone Drug Delivery

The bone-targeted drug delivery approach is a method that facilitates drugs to achieve optimal therapeutic effectiveness by targeting the bone as the primary organ for drug delivery. Compounds like BPs, tetracycline, and oligopeptides are employed as bone-seeking agents as they all have affinity to hydroxyapatite [$Ca_{10}(PO_4)_6(OH)_2$] (HA), a primary mineral component

in the bone (95). However, tetracycline has less affinity to pathological skeletal sites compared to healthy ones, while oligopeptides have low affinity to the target site, which may cause the possibility of off-target effects (96). So, BPs are the favorable choice for bone-targeted drug delivery, as they offer high specificity and efficacy in delivering drugs to the bone (97).

BPs are a synthetic class of compounds having structural similarity to the endogenous calcium regulator pyrophosphate (P-O-P) as they contain two terminal phosphate groups bound to a central carbon atom. BPs exhibit their affinity to HA due to their ability to function as bidentate chelator as they chelate calcium ions on the surface of bone apatite crystals via the two phosphonate groups in close vicinity. The covalent side chains R1 and R2 attached to the central carbon atom of BPs can be modulated for their affinity and pharmacological effects. Due to the formation of a tridentate bond BPs containing a hydroxyl group as R1 (etidronate) show enhanced affinity to HA than non-hydroxyl-containing BPs (clodronate). Similarly, BPs containing nitrogen in the R2 group show a higher affinity for HA (alendronate). They also inhibit bone resorption by reducing osteoclast activity than non-nitrogen-containing BPs (etidronate), which cause osteoclast apoptosis.

BPs are categorized into three generations based on their chemical structures, with different antiresorptive potencies. Non-nitrogen-containing BPs compounds like etidronate, clodronate, and tiludronate belong to the first generation. Similarly, nitrogen-containing BPs compounds with an alkyl chain, like pamidronate, alendronate, and ibandronate, are classified into the second generation. The nitrogen atom in the BP has a special role in the potency as they enhance it by 10-10000 times to the non-nitrogen atom. This is because the nitrogen atom allows the binding of BP to the mineral surface of the bone which subsequently increases affinity to the negatively charged phosphonate group resulting from electrostatic interaction and aid in the

hydrogen bond formation between the BP group and HA surface. BPs with nitrogen-containing ring structures like risedronate and zoledronate belong to the third generation also boast of more potency, enhanced distribution and long duration of action owing to added aromatic structures (98, 99).

BPs are bone-targeting moiety, so they have major impacts on the bone cells like osteoblast and osteoclast. Depending on the structure, BPs exert different biochemical mechanisms on osteoclasts. For example, nitrogen-free BPs are metabolically incorporated into adenosine triphosphate (ATP) analogs, leading to a deficiency of functional ATPs within osteoclasts and subsequent apoptosis. While nitrogen-containing BPs interfere with the mevalonate biosynthetic pathway and inhibit farnesyl pyrophosphate synthase (FPPS), which is involved in the production of cholesterol and isoprenoid lipids necessary for the posttranslational prenylation of small G-proteins. Thus by inhibiting G-protein function, nitrogen-containing BPs can affect various processes essential for the function of osteoclasts, including their maturation and survival (100).

In addition to their effects on osteoclasts, BPs can prevent the formation of new bone minerals by binding them to HA crystals and inhibiting their growth. This effect can also be attributed to their ability to chelate calcium ions and form stable complexes with HA. Furthermore, BPs stimulate the differentiation and activity of osteoblasts, leading to increased bone formation. This effect is likely mediated by their ability to inhibit osteoprotegerin (OPG), which normally inhibits osteoblast activity. BPs have complex and dynamic impact on bone metabolism, with both anti-resorptive and anabolic actions (101).

Regarding physicochemical properties, BPs are water-soluble and acidic, making them highly concentrated in bone tissue. Only a small amount (1-3%) of the dose is absorbed, with 50% of

that being rapidly excreted by the kidneys, and a small fraction being excreted in the bile when administered orally. Much of the dose accumulation happens in the bones. Due to a P-C-P moiety, nitrogen-containing BPs are not metabolized in the human body and have very long skeletal elimination half-lives, thus making them less susceptible to hydrolysis. Although the benefits of using BPs generally outweigh the risks, caution must be taken in patients with special medical conditions such as renal failure, as BPs can accumulate and cause adverse effects. While their potential risks could be a matter of concern in some cases, BPs still remain an important treatment option for conditions characterized by excessive bone resorption, such as osteoporosis, osteoarthritis, Paget's disease of bone, osteomyelitis and bone cancer (metastasis) (95, 102, 103).

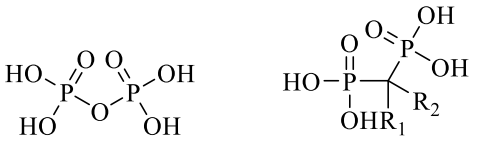

Pyrophosphate **Bisphosphonate**

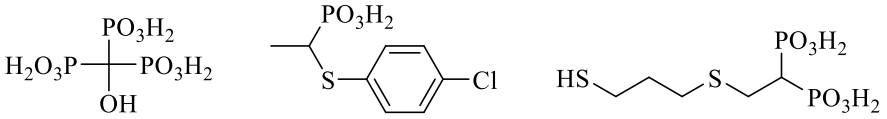

Etidronate **Tiludronate** **Thiol BP**

First generation : non-nitrogen containing structures

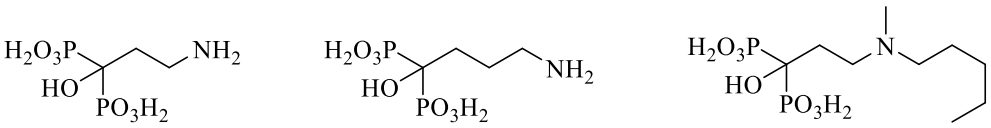

Pamidronate **Alendronate** **Ibandronate**

Second generation : nitrogen containing alkyl structures

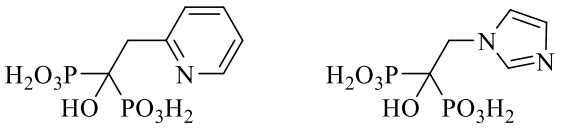

Risedronate **Zoledronate**

Third generation : nitrogen containing ring structures

Figure 8. Structure of bisphosphonates (BP) belonging to different generations

Beyond the use as a standalone drug, the application of BPs can be expanded through conjugation strategies, mainly by covalently linking BPs with other active drugs to form a new chemical entity. The conjugation can be achieved via a direct bond or a cleavable linker, but direct attachment can sometimes alter the intrinsic pharmacological activity of the drug, so a biodegradable linker is preferred. This conjugation of BP with other active drugs acts as a dynamic targeting system, limiting off-target systemic toxicity with reduced intrinsic metabolism to the liver. Thus, the optimal design of BP conjugates is warranted as it combines the bone-seeking properties of BPs, a biodegradable linker and an active drug that result in synergistic or additive drug efficacy for a longer duration of action (104, 105).

Successful skeletal drug delivery has improved pharmacodynamic and PK parameters in numerous instances. For example, the conjugation of a BP with estradiol and its administration to ovariectomized rats resulted in a prodrug that exhibited significantly greater antiresorptive activity compared to rats treated with estradiol alone (106). In a similar research setting, bone drug delivery of parathyroid hormone (PTH) conjugated with PEG and BP had demonstrated superior anabolic treatment efficacy over unmodified PTH in rats with osteoporosis (107). Additionally, a study involving salmon calcitonin, an antiresorptive drug, showed improved therapeutic efficacy and PK parameters when conjugated with PEG and BP in normal and osteoporotic rats (108). In our own laboratory, we demonstrated that the conjugation of Ang 1-7 with PEG and BP resulted in superior anti-inflammatory effects and improved PK parameters (109). These findings highlight the potential of bone drug delivery as a leading approach in improving therapeutic efficacy, which could help enhance small peptide drugs like novokinin to overcome the instability issue. The schematic design for the conjugation of novokinin (Novokinin Conjugate) has been given in Figure 9.

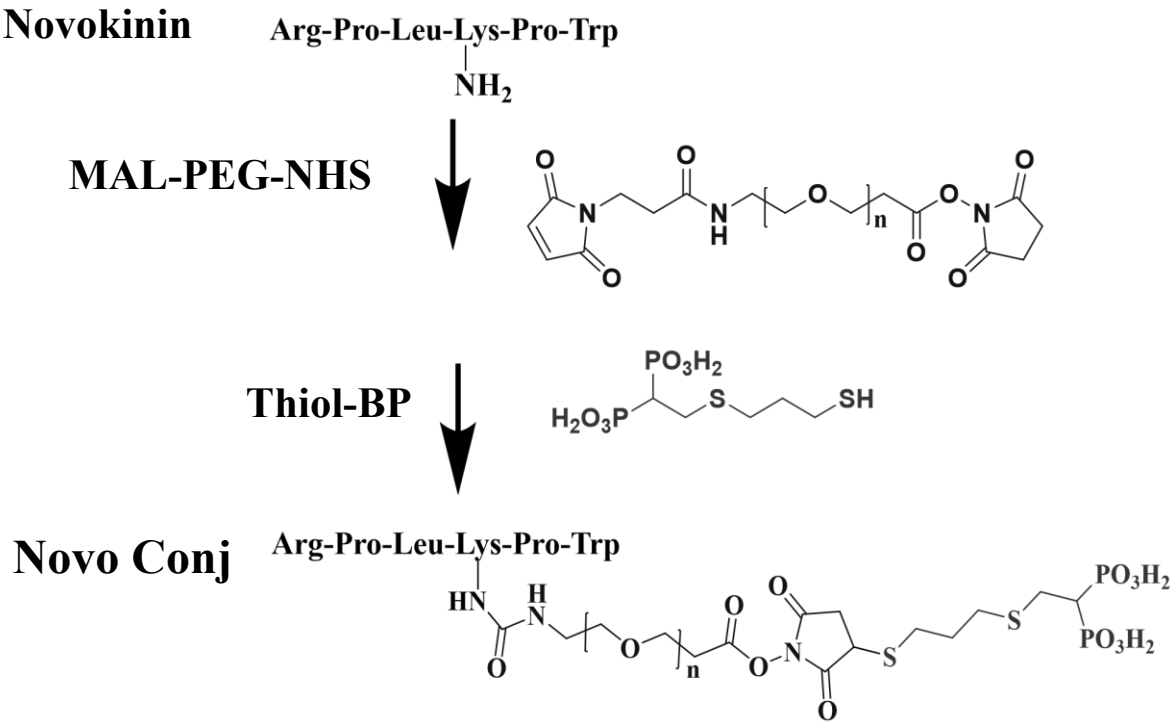

Figure 9. Schematic diagram of Novokinin Conjugate (Novo Conj) synthesis using Fmoc-mediated solid phase peptide synthesis. Maleimidopropionyl polyethylene glycol N-hydroxysuccinamide ester, (MAL-PEG-NHS) and thiol-bisphosphonate (Thiol-BP).

2.4 Hypothesis and Objectives

We have hypothesized that chemical conjugation of novokinin with the PEG as linker and BP as bone targeting moiety will prolong stability that will aid in the potentiation of its therapeutic effects. This approach aimed to synthesize and characterize the Novo Conj through analytical instruments, test its stability in different media and temperatures and confirm its bone-targeting capacity.

2.5 Experimental Materials and Method

2.5.1 Peptide Synthesis, Conjugation, and Characterization of Novo Conj

Novokinin was synthesized using a standard Fmoc-mediated solid-phase peptide synthesis (SPPS) using the AApptec Focus Xi peptide synthesizer (Louisville, KY, USA). All Wang resin, Fmoc-protected amino acids, solvents, and reagents needed for peptide synthesis were purchased from AApptec (Louisville, KY, USA). The chain elongation was performed by removing the Fmoc group from the resin-attached amino acid. Next, Fmoc-protected amino acid (based on the sequence) was added until the entire peptide was synthesized. After the synthesis, the final Fmoc group was removed and cleaved from the resin. After purification of the novokinin, it was coupled with Maleimidopropionyl-PEG NHS Ester (Polypure, Oslo, Norway) in an equimolar concentration for an hour to form an intermediate compound. A 10X solution of thiol-BP (Surfactis Technologies, Angers, France) was reacted with the intermediate compound for another hour. After completion of coupling, the conjugate was dialyzed to separate it from unreacted reagents.

The resultant peptide and conjugate were characterized by Agilent 6545 LC/Q-TOF. A US patent application for this innovative Novo Conj synthesis and pharmacological effect has been filed. For the animal study, a batch of Novo Conj was synthesized by AnaSpec (CA, USA) and used after structural and purity confirmation.

2.5.2 *In vitro* Hydroxyapatite Study

The bone-targeting ability of binding of Novo Conj was evaluated by *in vitro* (HA) binding affinity test according to our previously published protocol (27). Briefly, 20 µg of novokinin or an equivalent amount of Novo Conj was mixed with 5 mg of HA powder in 750 µL of various buffers like double distilled (D.D) water, 10 mM PBS (pH = 7.4), and acetate buffer (pH = 5.5).

An equivalent amount of novokinin and Novo Conj were mixed in corresponding buffers without HA and were used as a control. All the mixtures were shaken gently at room temperature for 1 hr and then centrifuged at 10,000 × g for 5 mins. The supernatant was collected and assayed for unbound drug using a fluorescence spectrometer at λ Ex 215 nm, λ Em 305 nm (Varioskan Lux, Thermo Scientific, MA, USA). The percentage of HA binding study was calculated as (Intensity of Control-intensity of supernatants/intensity of control × 100%). All the experiments were run in triplicate.

2.5.3 Stability Test

2.5.3.1 Instrumentation

The chromatographic assays were conducted using the Agilent 1220 Infinity II HPLC system (Santa Clara, CA, USA). This system comprised a degasser, a dual pump, an autosampler, a column oven, and a photodiode array. The Open Lab CDS software version 2.2.0 (Agilent Technologies, Santa Carla, CA, USA) was employed to monitor and integrate the signal detection.

2.5.3.2 Chromatographic Condition

For the chromatographic separation of novokinin and Novo Conj, an Eclipse XDB-C18 analytical column (4.6 × 150 mm i.d. 5 μm) (Agilent Technologies, Santa Carla, CA, USA) and a Security Guard Cartridge Polar RP (KJ0-4282, 4.0 mm × 3.0 mm i.d.) were employed. As Internal Standard (IS), [asn^{1}, Val^{5}]-Angiotensin II) (P/N A6402-1MG) from Sigma Aldrich (St Louis, MO, USA) was used. The mobile phase consisted of 0.1% trifluoro acetic acid (TFA) in water (A) and ACN (B). The gradient time program was initiated from 10% ACN to 25% ACN over 4 mins, with the composition being kept constant for 4 to 8 mins, followed by an increase to 50% ACN at 12 mins and a decrease to 10% ACN until 15 mins. The sample run time was 15

mins, and the column oven was set at 25 °C. The flow rate was 1 mL/min, and the injection volume was 50 µL. Although the analytes were detectable at different wavelengths, 210 nm was selected as the optimal wavelength for detection due to better sensitivity.

The HPLC method was subjected to validation for specificity, linearity, accuracy, and intra-day and inter-day variations. Working calibration curves were produced in three different media by serially diluting novokinin and Novo Conj in DD H_2O and PBS (pH 7.4). The stock solution (1000 µg/mL) was used to obtain standard sample concentrations of 0, 50, 75, and 100 µg/mL. The standard curves were generated by plotting the analyte/IS peak area ratio against each compound's given concentration. Three calibration curves were developed on the same day or three different days to assess intra- and inter-day variabilities. The accuracy percentage was computed from the observed concentration × 100/added concentration. The coefficient of variation (CV%) was employed to determine the assay's precision.

2.5.4 Statistical Analysis

A standard computer program analyzed data, GraphPad Prism Software PC software, and are expressed as mean ± standard deviation (Mean ± SD) of at least three independent experiments. Data were analyzed for normal distribution and homogeneity of variance before proceeding with the parametric statistical tests. The student’s t-test analyzed *in vitro* binding affinity and stability between two groups. *P*-values of less than 0.05 were considered statistically significant. The data labeled with different letters (a, b, c, or d) in tables or figures indicate a statistical difference between groups where $p < 0.05$.

2.6 Results

2.6.1 Synthesis and Characterization of Novokinin and Novo Conj

Novokinin and Novo Conj were successfully synthesized by FMOC SPPS and in-solution methods, respectively. The characterization of synthesized novokinin and Novo Conj was performed on LC/Q-TOF. Extracted Ion Chromatogram (EIC) depicted in Figure 10A shows precursor ions (Q1) of charge states with value *m/z* values of novokinin at 796 and 398 ions, which correspond to ($[M+1H]^{1+}$) and ($[M+2]^{2+}$), respectively, for the novokinin with a molecular weight of 796 amu. Similarly, in Figure 10B, the EIC shows that 1274, 850, and 637.82 ions correspond to ($[M+2H]^{2+}$), ($[M+3H]^{3+}$), and ($[M+4H]^{4+}$) for Novo Conj with a molecular weight of 2546 amu.

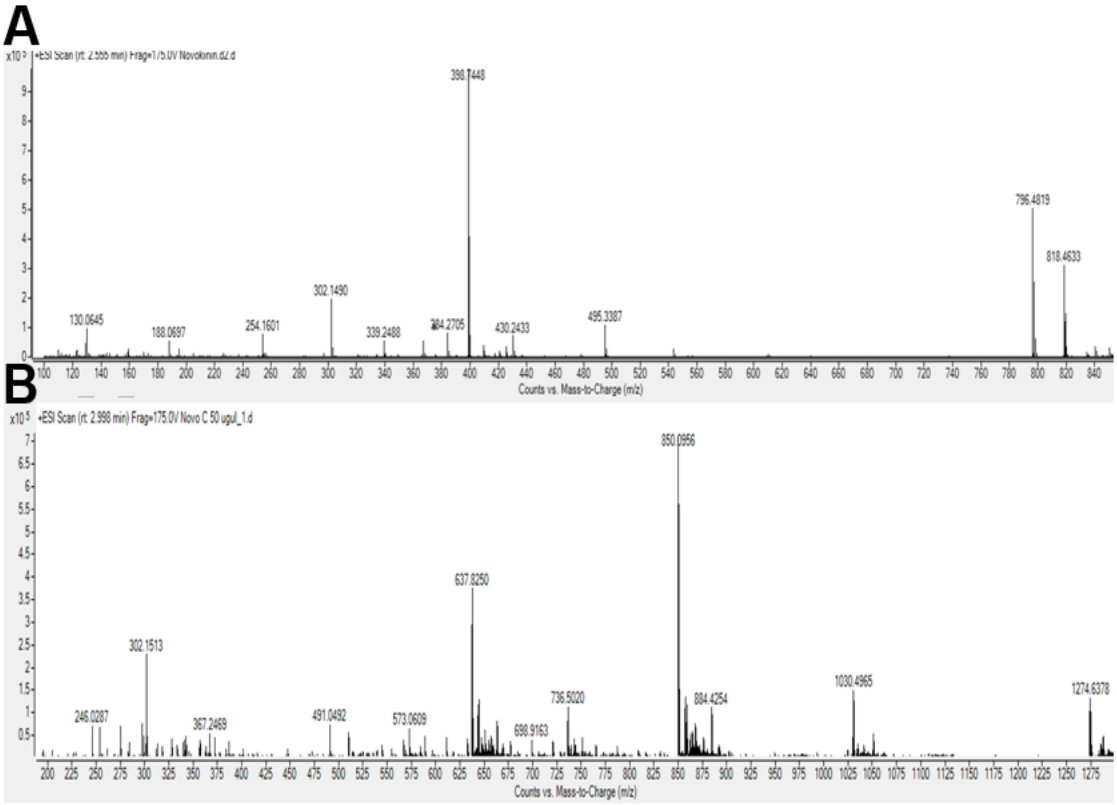

Figure 10. Extracted ion chromatogram (EIC) of (A) Novokinin and (B) Novokinin Conjugate (Novo Conj) through LC/Q-TOF.

2.6.2 *In vitro* Hydroxyapatite Binding Study

The bone mineral affinity of Novo Conj was compared with novokinin using *in vitro* HA binding affinity test. As shown in Figure 11, Novo Conj had 16.74 ± 1.0%, 6.89 ± 1.8%, and 7.65 ± 1.13% binding capacity, whereas in the case of novokinin it was 0.89 ± 0.29%, 1.52 ± 1.48%, and 2.14 ± 1.1% in D.D H_2O, acetate buffer, and PBS 10 mM respectively. This result shows that the bone mineral affinity of Novo Conj was significantly higher in each medium compared to novokinin.

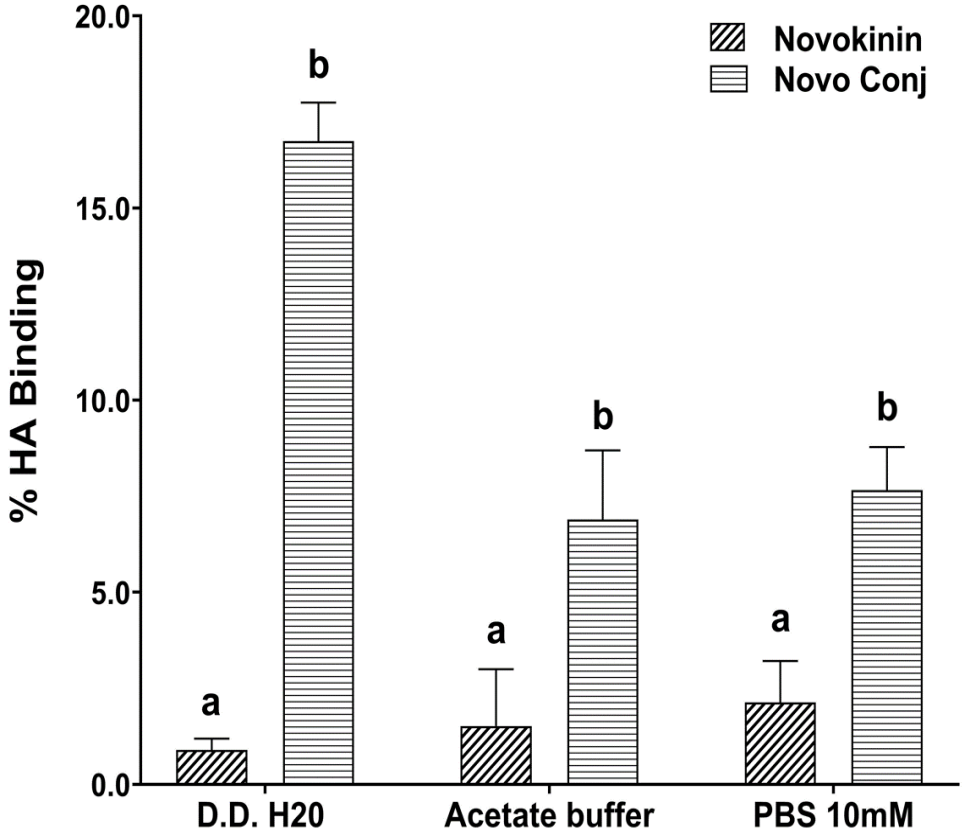

Figure 11. Novokinin Conjugate (Novo Conj) shows a higher percentage of hydroxyapatite (HA) binding affinity than novokinin. Mean ± Standard deviation (SD). Samples were run in triplicate. Data labeled with different letters (a or b) indicate a statistical difference between groups where p <0.05.

2.6.3 Stability Study

The HPLC-DAD method was validated for specificity, linearity, precision, intra-day, and inter-day variations. The working calibration curves were established in two different media (DD water and PBS, pH 7.4) by serial dilution of novokinin and Novo Conj stock solutions (1000 μg/mL), resulting in standard samples with concentrations of 0, 50, 75, and 100 μg/mL of each compound. The standard curves were plotted by graphing the ratio of the analyte peak area to the internal standard peak area against the concentration of each compound. To evaluate intra- and inter-day variances, three calibration curves were generated on the same day or on three different

days. Accuracy% was calculated by observed concentration×100/added concentration. The coefficient of variation (CV%) was utilized to assess assay precision Table 1. Representative chromatograms showed the peaks of the IS, Novo Conj, and novokinin in Figure 12. The stability of novokinin and Novo Conj was examined in DD water and PBS (pH 7.4). This experiment was conducted at three temperature storage conditions: (i) room temperature (25 °C), (ii) refrigerator (4 °C), and (iii) freezer (-20 °C) for four weeks to ensure the stability, storage, and shelf-life of the compound. Results showed that Novo Conj was more stable than novokinin in both PBS and water for four weeks under all three storage conditions. There was significant percentage degradation of novokinin at room temperature compared to Novo Conj in PBS (54.70 ± 3.34% vs. 83.79 ± 4.70%) and water (63.31 ± 1.74% vs. 88.89 ± 5.27%) as shown in Figure 13.

Table 1. Intra-day and inter-day precision (coefficient of variation, CV) and accuracy for HPLC of novokinin and Novo Conj in different media.

Compound	Medium	Conc. µg/mL	Inter-day		Intra-day	
			Precision (CV%)	Accuracy (%)	Precision (CV%)	Accuracy (%)
Novokinin	DD water	50	0.80	105.93	7.93	105.63
		75	3.79	102.51	3.26	101.08
		100	2.03	96.89	2.81	96.69
Novo Conj	DD water	50	0.73	94.52	1.06	96.14
		75	0.40	100.89	0.95	100.27
		100	1.19	100.93	2.43	103.58
Novokinin	PBS	50	3.85	105.61	7.90	105.33
		75	2.24	100.89	3.30	101.04
		100	2.83	98.58	2.93	96.80
Novo Conj	PBS	50	3.92	93.73	2.36	97.86
		75	0.82	97.89	4.24	101.61
		100	0.72	99.69	2.82	102.13

Conc.; concentration

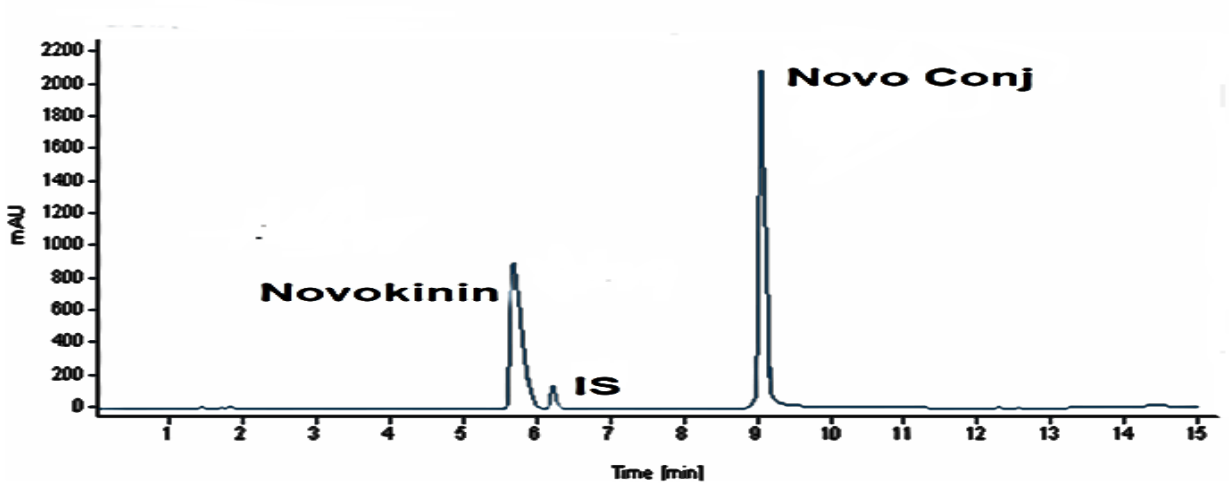

Figure 12. Representative chromatograph of novokinin, Novokinin Conjugate (Novo Conj) and internal standard (IS).

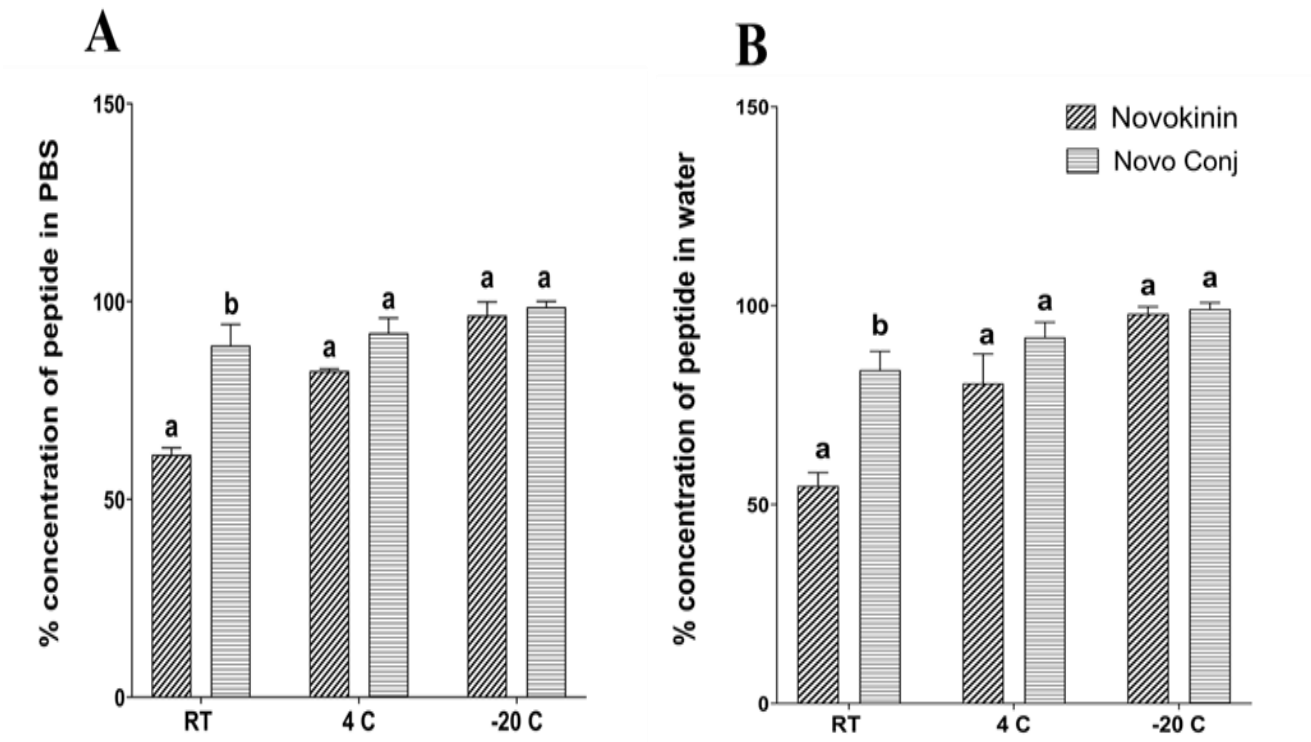

Figure 13. Novokinin shows a lower percentage peptide concentration than Novo Conj in (A) PBS and (B) water. Mean ± Standard deviation (SD) (n = 3). Triplicates samples were run. Data labeled with different letters (a or b) indicate a statistical difference between groups where p <0.05.

2.7 Discussion

Peptide drugs such as novokinin possess a range of benefits due to their hydrophilicity, and non-toxic metabolites. They also boast high selectivity and minimal off-target effects, which ultimately reduce tissue accumulation and lower immunogenicity (88).

Despite its multitude of therapeutic potentials known for more than a decade in the scientific realm, the AT2R agonistic activity of novokinin has not been studied in receptor confirmation studies. Consequently, we have tried to understand the selectivity and affinity of novokinin toward AT2R by comparing it with other AT2R agonists.

A glycine scan study performed on endogenous Ang II revealed the importance of Arg at the N-terminal for strong affinity to AT2R. The guanidine group of Arg interacts with Asp^{279} in TM6 and Asp^{297} in TM7 of AT2R, forming a salt bridge interaction that stabilizes the ligand-binding pocket of the receptor (63). Similarly, the glycine scan on novokinin showed that Arg at the N-terminal was essential for its anti-hypertensive activity. As already mentioned, there are no receptor conformational studies done on novokinin; the positive charge at the N-terminal, however, can be assumed to confer it with the necessary AT2R affinity (73, 74).

In addition, a study involving the first agonist, CG42112A, revealed that Ile with a hydrophobic side chain is crucial for its selectivity and affinity towards AT2R over AT1R (110). This is due to the C-terminal forming a hydrophobic core with Leu^{124} (TM3), Met^{128} (TM3), Trp^{269} (TM6), Phe^{272} (TM6), and Phe^{308} (TM7) of the AT2R for a ligand-binding pocket. This explains why novokinin, having Trp at the C-terminal, is highly selective for AT2R over AT1R but still has less affinity than CGP42112A because the aliphatic side chain of Ile can form a superior hydrophobic core (19).

Regarding synthesis of novokinin, we employed the SPPS method, which uses definite solid support provided by the resin to grow the chain of amino acids via the Fmoc strategy. This orthogonal protecting group strategy is based upon the base-labile N-Fmoc group, which protects the α amino function, acid-labile sidechain protecting groups, and acid-labile linkers that constitute the C-terminal amino acid protecting group. This approach mitigated the harmful acidic conditions that could affect the structural integrity and reduce toxicity compared to the traditional Boc/Bzl strategy, which employs hydrofluoric acid (HF) (111).

Similarly, we used wang resin loaded with the first amino acid Fmoc Trp, which allowed us to skip the critical step of attaching the first amino acid, thereby confirming for easy synthesis that could yield a pure compound. Five times excess reagents were used at a high concentration of 1 M to ensure the completion of the coupling reaction. The repeated washing cycle was included in the process, which led to removing excess reagents and probable side chains. Moreover, this method gave us the added advantage of using the same vessels without any material transfer, resulting in the low material loss (111, 112). Thus, we can synthesize our peptide successfully with purity (> 95%) as shown in Figure 10.

Despite peptide drugs having multiple benefits, it is a known fact they face biological instability issues. Several approaches, like modification of amino acids and cyclization, have been traditionally utilized as they offer resistance against enzymatic degradation. However, these approaches often alter the efficacy of peptides and require more complex remodeling to restore biological activity. PEGylation of peptides provides appropriate alternatives for these approaches. It not only enzymes and original structure of the peptide but also increases the hydrophilicity, decreases renal clearance, reduces accessibility for proteolytic enzymes, and diminishes immunogenicity and antigenicity (40). On the other hand, the bone targeting

approach that attaches BP to the peptide-PEG complex helps to increase stability by utilizing bone as a drug reservoir. This conjugation improved PK and bone tissue accumulation of parathyroid and Ang 1-7 peptides (113, 114).

For the synthesis of Novo Conj, MAL-PEG-NHS was used as a linker, which is a water-soluble heterobifunctional cross agent. This linker contains an NHS ester and a MAL group that allow the covalent conjugation of amine and sulfhydryl-containing molecules. First, the NHS group of the PEG linker reacted with the primary amine of novokinin to form an amide bond through a nucleophilic substitution reaction. Next, this intermediate compound was further reacted with thiol BP through a nucleophilic thiol-ene addition reaction to form Novo Conj (113) .

In our current study, we successfully synthesized novokinin and performed subsequent PEGylation and conjugation with BP, as confirmed by mass spectrometric detection in figure 6. Although solution synthesis was more feasible for the experimental synthesis of Novo Conj without a proper purification system, we could not isolate pure mono PEGylated product. This prompted us to outsource its production to ensure the required purity for *in vitro* and *in vivo* studies following confirmation of the archetype compound. The presence of an amine group at Lys and a guanidine group at Arg in novokinin may result in the formation of mono and diPEGylated products, which made the isolation a challenging task.

PEGylation is a widely-used technique for improving the stability and immunological recognition of peptides; however, there are concerns regarding its prolonged half-life and reduced bioactivity of PEGylated peptides (115). This can lead to tissue accumulation and toxicity if the drugs are not cleared from the body. However, studies have shown that the increased circulation time of PEGylated medications is directly proportional to the molecular weight of PEG, and our PEG molecule is 2 kDa, which should allow for renal filtration at a

slower pace (116, 117). Although PEG is generally considered non-degradable, there is evidence of alternative chemical and biological chain cleavage. Specifically, a study has shown that PEG molecules can be oxidized by CYP450-dependent enzymes and by aldehyde and alcohol dehydrogenases. Our PEGylated peptides are conjugated with an optimum chain length that undergoes slow kidney elimination and excretion through bile, and this chain length has not shown any serious defects (117). We are confident that our PEGylated peptides will not have any toxic side effects, but a detailed scientific study is necessary to validate our results. The reduced bioactivity resulting from conjugation can be addressed by conjugating the peptide to non-essential amino acids, such as Lys in novokinin, for binding. This approach can help circumvent the loss of bioactivity while benefiting from the improved stability and immunological recognition provided by PEGylation (91).

The BP moiety used in the conjugate resembles therapeutic BP, but it does not have a significant pharmacological effect when compared to second and third-generation BPs. Additionally, this moiety has less affinity compared to nitrogen-containing BPs and can be excreted through the kidney (118). Numerous studies, including those conducted in our laboratory, have shown that the thiol-BP used in the conjugate is safe for use and has no significant pharmacological effects (107, 113).

The HA binding studies presented in Figure 11 demonstrate that Novo Conj has a considerably higher bone mineral affinity than native BP. The decrease in the percentage of binding observed in phosphate buffer as opposed to water can be explained by the fact that both PBS and BP contain functional HA-binding phosphate groups, resulting in competition for binding to the HA component (114). Furthermore, the reduction in the percentage binding in acetate buffer can be linked to pH levels, as lower pH values decrease the ionization state of the phosphate group of

BP. In addition, the stability assay depicted in Figure 13 reveals that Novo Conj is more stable than novokinin, particularly at room temperature. This information sheds light on their suitability for storage and shelf-life.

2.8 Conclusion

In summary, we successfully synthesized novokinin and Novo Conj and accurately characterized them using analytical instruments. Using an optimal chain length of PEG and BP for the synthesis of Novo Conj assures its safety as a pharmacological drug. The simple chemical conjugation of PEG and BP has significantly improved the bone binding capacity and stability of Novo Conj compared to its native peptide.

Chapter III: Test and Compare Biological activity of Novokinin and Novo Conj in vitro

3.1 AT2R-Mediated *in vitro* Pharmacodynamics

Besides its role in regulating cardiovascular function, recent research has shown that AT2R plays a vital role in promoting neurite outgrowth-a critical process in the development of the nervous system (119). Studies have highlighted that AT2R activation can stimulate neurite outgrowth in various cell types, including both neuronal and non-neuronal cells. To determine AT2R agonistic activity, the neurite outgrowth observed in cell lines such as NG108-15 (48, 67, 120), PC12W (49, 121, 122) and R3T3 (123) are used as preliminary quantitative tests. Amongst them, NG108-15 is considered as the gold standard for assessing AT2R-mediated activity, as it predominantly expresses AT2R in its non-differentiated state (70). With the presence of both subtypes of ang receptors, it has become essential to identify cell lines that can exclusively establish AT2R-mediated biological effects.

In addition to its role in neurite outgrowth, the AT2R exhibits other biological activities that can be quantified through *in vitro* assays. One such activity is its ability to inhibit cell proliferation upon stimulation. This anti-proliferative effect has garnered significant attention due to its potential application in treating fibrotic disorders and cancer (124). Numerous scientific studies have demonstrated the ability of AT2R stimulation to inhibit cell proliferation in various cell types, including coronary endothelial cells, vascular endothelial cells, pheochromocytoma, and fibroblasts (6, 124). Breast cancer cell lines are often used as a model for anti-proliferative effects that can be mediated through the RAS pathway (125). Therefore, investigating the anti-proliferative activity of AT2R stimulation in breast cancer cell lines such as MCF-7 and 4T1.2 may shed light on the link between overactivation of the classical RAS pathway and cancer.

The evidence from these studies suggests that the functional antagonism provided by AT2R has significant potential in counteracting various RAS-mediated disorders. However, it is worth noting that the beneficial AT2R-mediated activity relies on agonist drug use. One such drug is novokinin, a peptide designed based on ovalbumin, which has been shown to exhibit receptor-mediated agonistic activity, making it an attractive target for extending AT2R-mediated effects (74).

The confirmation of biological activity through *in vitro* assays is a crucial step in drug development, as it provides a reductionist approach that allows for insight into the mechanism of action of compounds without confounding factors. Therefore, any novel compound needs to have their biological activity confirmed through cell lines first. Our drug of interest, novokinin, has elucidated *in vivo* therapeutic effects since the 2000s, but there has been a lack of *in vitro* work reflecting its cell-based activity. This knowledge gap made our research objectives challenging, exciting, and novel. Moreover, to ensure that the conjugation model does not compromise the biological efficacy of our peptide, it was imperative to conduct *in vitro* assays.

3.2 Hypothesis and Objective

We have hypothesized that increased stability due to the chemical conjugation of novokinin with PEG linker and BP will help to improve the biological effects of peptide. Our current work aimed to determine that our conjugation model does not interfere with the AT2R-mediated biological efficacy but instead establishes its supremacy over native peptide. Moreover, we aimed to diversify the effectiveness of novokinin and Novo Conj by confirming AT2R-mediated activity in neuroblastoma cell lines and extending its antiproliferative effects in breast cancer cell lines.

3.3 Experimental Materials and Methods

3.3.1 Cell lines and Culture Media

3.3.1.1 Chemicals

The chemicals used in the present study were obtained from the following sources: 6 wells culture plates (P/N 703001, NEST Scientific, Woodbridge, NJ, USA), 96-well microplates, Polystyrene, (P/N 655085, Greiner Bio-One, Monroe, NC, USA), Nonc® EasYflask™ Tissue culture 75 cm^2 cell vented (P/N 156499, Thermo Fisher Scientific, Waltham, MA, USA), HAT supplement (50X) (P/N-21060017, Thermo Scientific, Waltham, MA, USA), 15 mL Centrifuge Tube- Sterile, Polypropylene, 12000 g (P/N-229411, Cell Treat, Pepperell , MA, USA), Reagent reservoir, 25 mL, Sterile, (P/N S255100, GMP Sales, Leominster, MA, USA), Fetal bovine serum (FBS) (P/N FBS001, Neuromics, Edita, MN, USA), Trypsin-EDTA solution (P/N T4049-500ML), (Sigma Aldrich, St Louis, MO, USA), Dulbecco's Modified Eagle's medium-high glucose, with 4500mg/L glucose, L-glutamine, and sodium (P/N D5796-6X500ML) (Sigma Aldrich, St Louis, MO, USA), Real Time -GLO MT Cell viability assay (P/N G9713, Promega, Madison, WI, USA), Cytosolic Tracer and Related Reagents , Biotium, Calcein AM (P/N 80011-3 Biotium , Fremont, CA, USA), Molecular Probes NucBlue Ready Probes reagent (P/N R37605, Thermo Fisher Scientific, Waltham, MA, USA), Gentamicin Solution (P/N G137-10ML, Sigma Aldrich, St Louis, MO, USA), PD123319 (P/N B2206, ApexBio, Houston, TX, USA), Val^5 Angiotensin II peptide (P/N-350452, Abbiotec, Chicago, IL,USA), PBS 1X (P/N 25-507, Genesee Scientific, San Diego, CA,USA), Invitrogen countess Cell counting chamber slides (P/N C10228, Fisher Scientific, Waltham, MA, USA), Rosewell Park Memorial Institute (RPMI) 1640 medium (P/N 11-835-030, Fisher Scientific, Waltham, MA, USA), Penicillin-Streptomycin (P/N B21110, R& D system, La Jolla, CA,USA), Quick-RNA™ Miniprep Plus kit (Zymo

Research, Irvine, CA, USA) ,qScript cDNA super mix (P/N 84034, Quanta Bio, USA) and qScript cDNA super mix (P/N 84034, Quanta Bio, USA). The cell lines used were American Type Culture Collection ATCC (Manassas, VA, USA), NG108-15 Neuroblastoma/glial (P/N HB12317, 4T1.2 (P/N CRL-3406) and MCF-7 (P/N HTB-22).

3.3.1.2 Cell Culture

NG108-15 were cultured passages (5-15) in DMEM culture medium with 10% FBS, HAT supplement and 50 mg/L of Gentamycin at 37 °C in 75 cm^2 Nunclon Delta flasks in a humidified atmosphere. Subcultures were performed at sub confluency. 4T1.2 cells were cultured (10-20) in DMEM medium with 10% FBS and 1% 50 units of Penicillin/Streptomycin. MCF-7 were cultured in (10-20) RPMI medium with 10% FBS and 1% 50 units of Penicillin/Streptomycin. Cells were cultured in their corresponding culture medium and kept in an incubator equipped with 5% carbon dioxide at 37 ˚C. They were passaged or collected for further assays at about 70% confluency. For this purpose, cells were removed from the incubator and washed once with 5 mL PBS, and 2 mL trypsin-EDTA (used to detach the adherent cells from the surface) was added to the tissue culture flask containing the cells. Then, after cells were transferred to the incubator for 3 mins, they were checked under the microscope for detachment and transferred to a sterile plastic tube. They were centrifuged at 2000 × revolution per minute (rpm) for 4 mins to remove the trypsin-EDTA. Then, cells were reconstituted in the corresponding medium to achieve the desired concentration and prepared for further analysis. All procedures were done under a BSL-2 biosafety hood to avoid contamination of the cells' environments.

3.3.2 Quantitative Polymerase Chain Reaction (qPCR) for the Analysis of RAS Components

The Quick-RNA™ Miniprep Plus kit was utilized to extract total RNA from cell samples in accordance with the manufacturer's protocol. Briefly, cultured cells were passaged, and centrifugation was performed (≤ 500 × g for 1 min). The supernatant was removed and resuspended in 300 µL RNA lysis buffer according to (for ≤ 5 x 10^6 cells, add ≥ 300 µL of RNA lysis buffer, and for 5 x 10^6 - 10^7 cells, add ≥ 600 µL of RNA Lysis Buffer). The particulate debris was removed by centrifugation (≤ 500 × g for 1 min) and the supernatant was transferred into a nuclease-free tube.

Initially, the samples were transferred into a Spin-Away™ filter in a collection tube and centrifuged to eliminate the majority of genomic DNA. The flow-through was then collected, and 1 volume of 95-100% ethanol was added and mixed thoroughly. This mixture was transferred into a Zymo-Spin™ III CG column in a collection tube, centrifuged, and the flow-through was discarded. Next, the samples were treated with DNAase I, where 400 µL of RNA wash buffer was added, centrifuged, and the flow-through was discarded. In a nuclease-free tube, 5 µL of DNase I and 75 µL of Digestion buffer were mixed, added to the column matrix, and then incubated at room temperature for 15 mins. Following DNase treatment, the column matrix was washed with 400 µL, 700 µL, and 400 µL of RNA wash buffer, and centrifuged for 30 secs, except for the last 400 µL of the wash, where it was centrifuged for 1 min and the flow-through was discarded. The remaining solution was transferred to nuclease-free tubes. Finally, 100 µL of DNase/RNase was added directly to the column matrix and centrifuged to elute the RNA.

RNA purified samples were then subjected to the reverse transcriptase process, where 500 ng of RNA was transcribed into cDNA using 4 µL of qScript cDNA super mix, and the volume was made to 20 µL by RNase/DNase free water. The mixtures were gently vortexed and centrifuged

at 3000 × g for 30 secs. The samples were then incubated for 5 mins at 25 °C, 30 mins at 42 °C, 5 mins at 85 °C, and finally held at 4 °C in a Master cycler Epgradient S (Eppendorf, USA). After completing the cDNA synthesis, 20 ng of cDNA samples in triplicate were used as templates, 7 µL of PerfectaSYBR Green fast master mix and the desired primer mix of 10 µM were added before incubating again in a Master cycler Epgradient S (Eppendorf, USA). The expression of target genes was normalized by GAPDH in the same cDNA sample (Table 2). GAPDH normalized the expression of target genes in the same cDNA sample (Table 2). The relative expression of target genes was determined using the $2^{-\Delta\Delta Ct}$ method, where ΔCT (control) = CT (Target gene) - CT(GAPDH), ΔCT (test) = CT (Target gene) - CT(GAPDH). The mRNA expressions were normalized to the house GAPDH and presented. All the primers were designed based on the published papers from rat species for NG108-15 and 4T1.2 and humans for MCF-7, and a list of reverse and forward primers is shown below in Table 2.

Table 2. Primer sequences of genes with the accession number and amplicon size

Gene	Sequence	AN	AS	Ref
AT2R-Rat	5'-GGTCTGCTGGGATTGCCTTAATG-3' 5'-ACTTGGTCACGGGTAATTCTGTTC-3'	NM_00138562 4.1	142	(126)
AT1R-Rat	5'-GGAAACAGCTTGGTGGTGAT-3' 5'-ACTAGGTGATTGCCGAAGG-3'	NM_00877159 4.3	171	(127)
GAPDH - Rat	5'-CCTGCACCACCAACTGCTTA-3' 5'-TGTCCAAAACTACCCCACATAT-3'	NM-017008.4	95	(33)
AT2R-Human	5'- CCACCCTTGCCACTACTAGCA -3' 5'- CATTGTTGCCAGAGATGTTCACA -3'	NM_00138562 4.1	75	(128)
AT1R-Human	5'- CAGCGTCAGTTTCAACCTGTACG -3' 5'- GCAGGTGACTTTGGCTACAAGC -3'	NM_004835.5	130	(128)
GAPDH -Human	5'- GAAGGTGAAGGTCGGAGTCAAC -3' 5'- CAGAGTTAAAAGCAGCCCTGGT -3'	NM_00135794 3.2	71	(129)

AT2R; Angiotensin II type 2 receptor, AT1Ra; Angiotensin II type 1 receptor a, ACE2; Angiotensin type converting enzyme 2, ACE; Angiotensin type converting enzyme, GAPDH; Glyceraldehyde-3-phosphate dehydrogenase, AN; Accession number, AS; Amplicon Size

3.3.3 Neurite Outgrowth Assay

NG108-15 cells were plated at a density of 6×10^4 cells in 6 well plates. After 24 hrs of plating, cells were stimulated in culture medium for three days (treated daily once) with Ang II (100 nM), Ang II (100 nM) + PD123319 (10 μM), novokinin (1 μM), novokinin (1 μM) + PD123319 (10 μM), Novo Conj (1 μM), Novo Conj + PD123319 (10 μM) or no treatment. Media was removed at the end of the third day and cells were incubated with 1 μM Calcein CM and 2 drops of NucBlue Ready Probes in Hank's balanced salt solution for 30 mins. After the incubation, the staining solution was replaced with PBS with 0.1% FBS for image capture.

Images were captured using the ImageXpress Pico Automated Cell Imaging system (Molecular Devices, LLC, Sunnyvale, CA, USA) using 10 × Plan Fluor objective. The light source was a solid-state white light engine with emissions from 380 nm to 680 nm. A FITC filter cube (Ex 482/35, Em 536/40) was used for calcein AM, and a DAPI filter cube (Ex 377/50 and Em 447/60) was used for NucBlue Ready Probes. Analysis was run on-the-fly CellReporterXpress software which contains analysis modules for neurite tracing. Cells having neurite longer than cell body was considered as positive.

3.3.4 RealTimeGlo™ MT Cell Viability Assay

The RealTimeGlo™ MT Cell Viability Assay kit was used to measure the real-time cell viability of breast cancer cell lines. This assay method utilizes a nonlytic, homogenous bioluminescent approach to determine viability based on cell metabolism. The kit contains NanoLuc® luciferase and a cell-permeant pro-substrate that are stable in a complete cell culture medium for up to 48 hrs at 37 °C. The substrate diffuses from viable cells into the surrounding culture medium, where the NanoLuc® Enzyme rapidly uses it to produce a luminescent signal. The assay was conducted in a continuous-read measurement format, allowing all RealTime-Glo™ reagents (MT Cell

Viability Substrate and NanoLuc® Enzyme) to be added to the wells at the same time as the cells or test compound or any point during the assay. We prepared fresh reagents for each experiment and equilibrated the cell suspension, test compound diluent, and cell culture medium to 37 °C before adding them to the cell culture.

For this assay, substrate and enzyme were added to the cell culture medium to prepare a 1X dilution. Before conducting the test, we determined the assay linearity by measuring a range of cell densities to assess the varying capacities of cells to reduce the MT Cell Viability Substrate. We performed this test 4T1.2 and MCF-7 cell lines and determined each cell's best density. To prepare the RealTime-Glo™ reagents, we added 2 μL of MT Cell Viability Substrate, 1000X, and 2 μL of NanoLuc® Enzyme, 1000X, to 996 μL of cell culture medium to make a 1 mL of 2X concentration. An equal volume of the 2X RealTime-Glo™ reagent was added to the cells simultaneously to obtain the desired cell concentration determined based on the linearity assay. The cells were incubated in a cell culture incubator at 37 °C and 5% CO_2 for 1 hr. Then, the test compounds (novokinin and Novo Conj) prepared in PBS at their final concentrations of 1 μM for each compound of 10 μL were added such that the final volume of each well was 100 μL. The luminescence was measured at different time points using a plate-reading luminometer for 48 hrs. All samples were done in triplicates.

3.3.5 Statistical Analysis

Data were analyzed by a standard computer program, GraphPad Prism Software PC software, version 9.3.1, expressed as mean ± standard deviation (Mean ± SD) of at least three independent experiments. Data were analyzed for normal distribution and homogeneity of variance before proceeding with the parametric statistical tests. The student’s t-test was used in RT-PCR experiments to determine the difference between two groups. One-way ANOVA analyzed

differences between mean values of multiple groups with Tukey's test for post-hoc comparisons were utilized for neurite outgrowth and cell viability assay. *P*-values of less than 0.05 were considered statistically significant. The data labeled with different letters (a, b, c, or d) in tables or figures indicate a statistical difference between groups where $p < 0.05$.

3.4 Results

3.4.1 Quantitation of mRNA Expression of RAS Receptors in NG108-15

The mRNA expression of AT1R and AT2R are analyzed in the NG108-15 cell lines. AT2R (0.04 ± 0.002) was significantly expressed compared to AT1R (0.01 ± 0.001) in the cell lines. This dominant expression of AT2R confirms the suitability of NG108-15 cell lines for the AT2R-mediated agonistic activity.

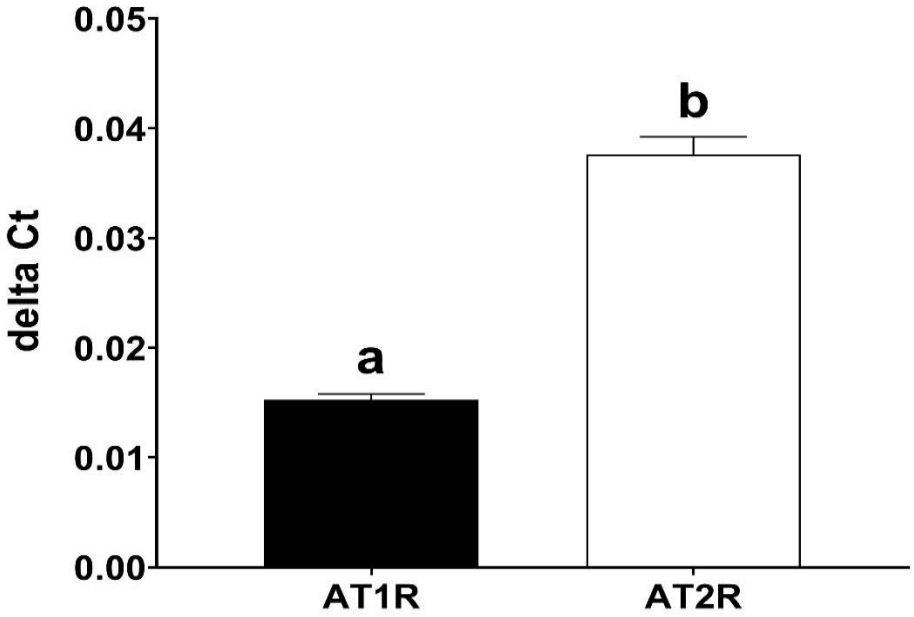

Figure 14. The mRNA expression of angiotensin II type 2 receptor (AT2R) and angiotensin II type 1 receptor (AT1R) in NG108-15. Mean ± Standard deviation (SD) (n = 3). Triplicates samples were run. Data labeled with different letters (a or b) indicate a statistical difference between groups where $p < 0.05$.

3.4.2 Quantitation of Neurite Outgrowth in NG108-15

The NG108-15 cells were incubated with drugs for three days, and the resulting neurite outgrowth was imaged and quantified. When agonists such as Ang II, novokinin, and Novo Conj were introduced, there was a noticeable increase in neurite branching and extension. Conversely, the presence of an agonist drug and an antagonist prevented neurons' outgrowth. Figure 15 illustrates the representative images of NG108-15 in the presence of both agonist and antagonist under drug treatment.

The neurite outgrowth per field was quantified, and data from four fields were taken. As shown in Figure 16, the treatment with Ang II increased neurite extending from the cell body to 36.17 ± 1.84 μm, novokinin increased it to 26.17 ± 1.01 μm, and Novo Conj increased it to 33.15 ± 1.84 μm. However, treatment with the antagonist PD123319 inhibited the extension of neurite outgrowth. Specifically, Ang II + PD123319 showed 13.91 ± 1.01 μm, novokinin + PD123319 showed 12.66 ± 1.46 μm, and Novo Conj + PD123319 showed 10.49 ± 0.72 μm.

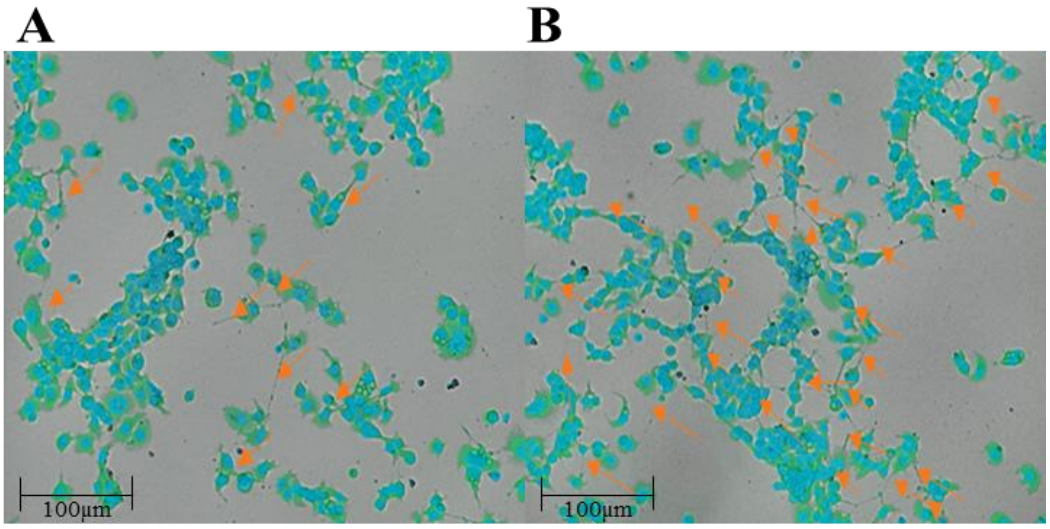

Figure 15. Neurite outgrowth in presence of (A) Antagonist (B) Agonist in NG108-15 cells.

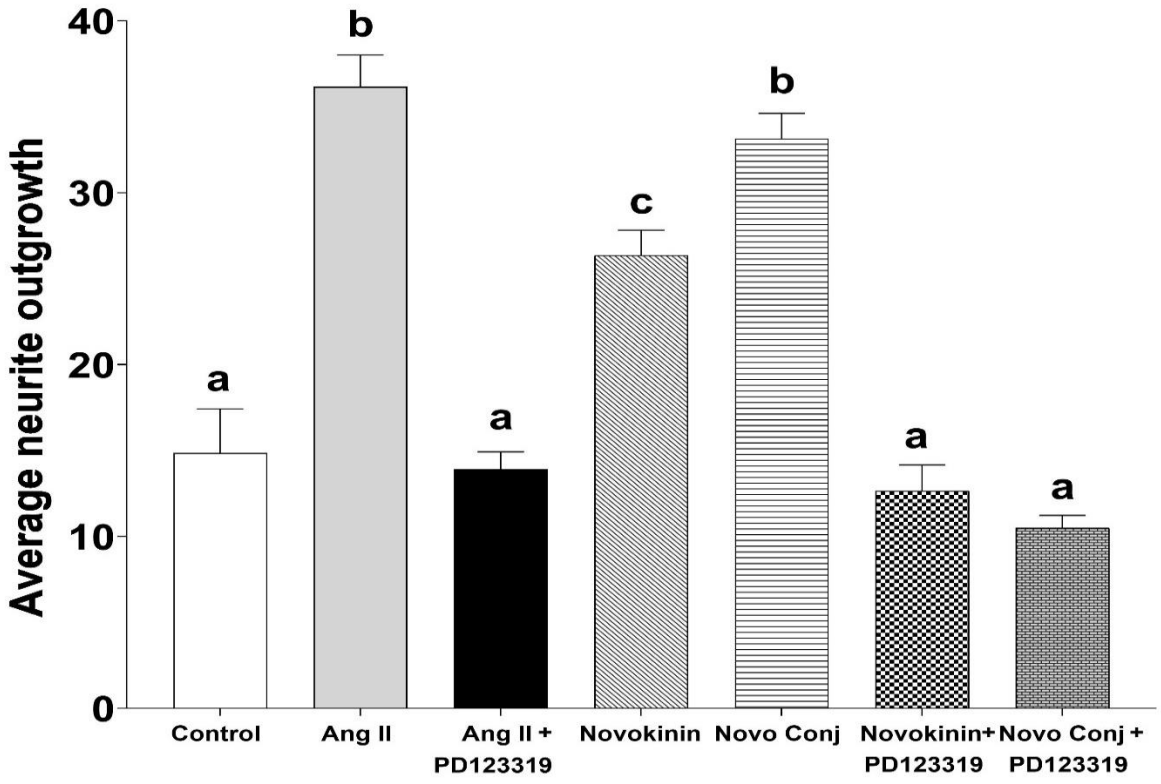

Figure 16. Average neurite outgrowth was observed with the treatment of drugs or media alone in NG108-15 cells. Mean ± SD (n = 4). Data labeled with different letters (a, b, or c) indicate a statistical difference between groups where p <0.05.

3.4.3 Quantitation of mRNA Expression of RAS Receptors in Breast Cancer Cell Lines

The mRNA expression levels of AT2R and AT1R were evaluated in two breast cancer cell lines, and the resulting ratio was determined by computing the delta CT expression of AT2R relative to AT1R. In the 4T1.2 cell line, the AT2R/AT1R ratio was observed to be 0.25 ± 0.01, markedly greater than that of MCF-7, where the ratio was also 0.25 ± 0.01.

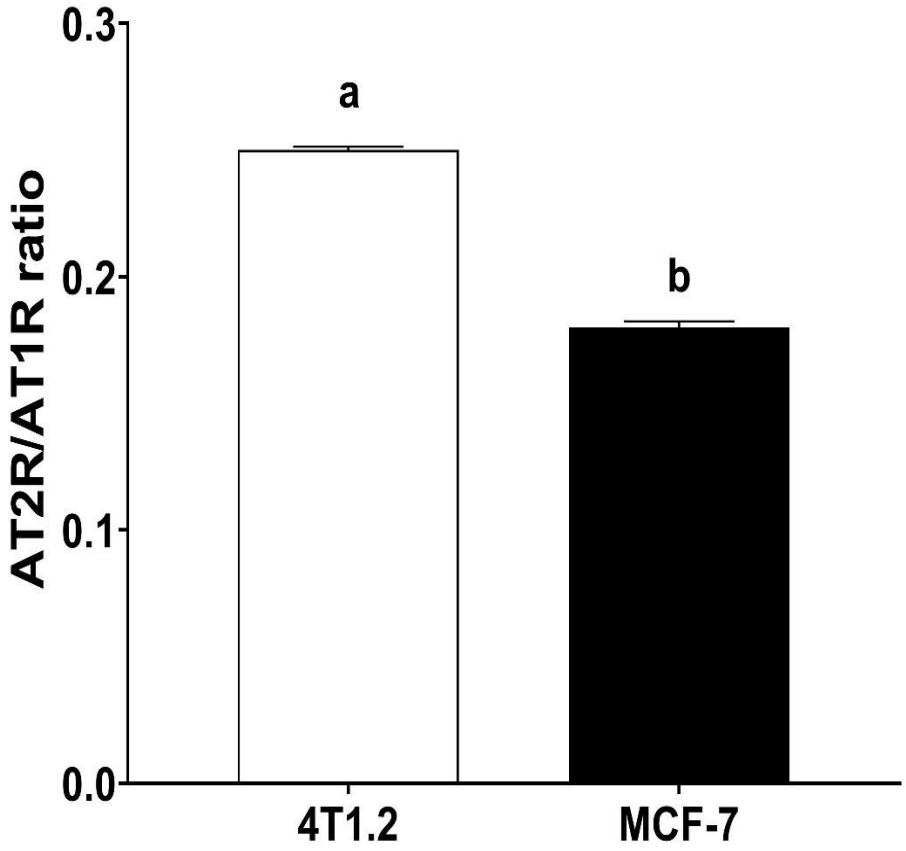

Figure 17. The ratio of mRNA expression of angiotensin II type 2 receptor (AT2R) and angiotensin II type 1 receptor (AT1R) in 4T1.2 and MCF-7 cells. Mean ± SD (n = 3). Triplicates samples were run. Data labeled with different letters (a or b) indicate a statistical difference between groups where p <0.05.

3.4.4 RealTime MT Assay on Breast Cancer Cell Lines

The RealTime cell viability effect by vehicle, novokinin and Novo Conj was studied and compared using two breast cancer cell lines (4T1.2 and MCF7), as shown in Figure 18. Absorbances were measured at different time points (0, 6, 24, 48), and the results were normalized to the control and highest absorbance. In the 4T1.2 cell line, novokinin (14.21 ± 1.3%) and Novo Conj (12.10 ± 0.8%) significantly decreased proliferation at 6 hrs compared to media alone (23.22 ± 0.6%). However, at 24 and 48 hrs, Novo Conj was able to significant decrease proliferative activity compared to novokinin, with Novo Conj showing significant effects at 24 hrs (23.40 ± 1.3%) and 48 hrs (23.40 ± 1.3%), while novokinin showed results at 24 hrs (30.8 ± 0.7%) and 48 hrs (55.6 ± 4.7%). In the MCF-7 cells, novokinin (15.1 ± 0.27%) and Novo Conj (13.14 ± 0.8%) significantly decreased proliferation at 6 hrs compared to media alone (21 ± 0.56%). However, with increasing time, only Novo Conj showed significant antiproliferative activity at 24 hrs (49.11 ± 1.98%) and 48 hrs (58.28 ± 0.6%), compared to media at 24 hrs (54.37 ± 0.13%) and 48 hrs (66.21 ± 1.64%).

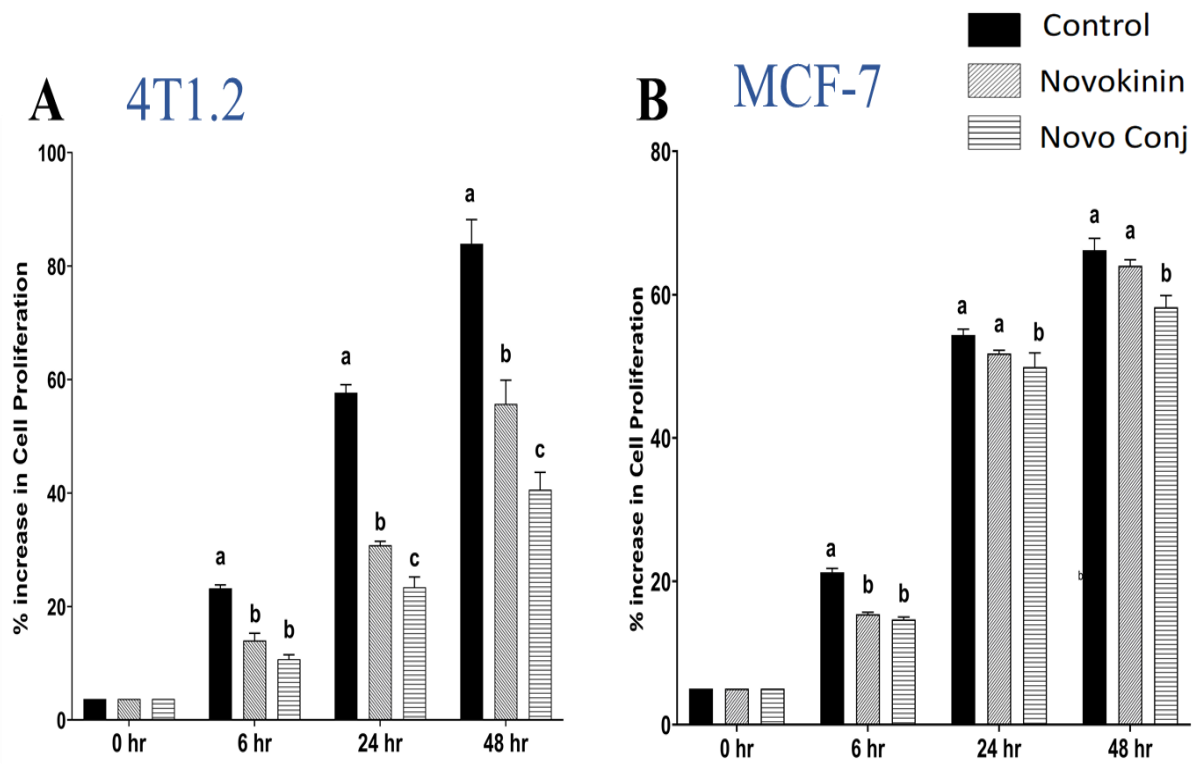

Figure 18. Cell proliferation in (A) 4T1.2 and (B) MCF7 breast cancer cell lines after 48 hours of a single treatment of vehicle, novokinin and Novokinin Conjugate (Novo Conj). Mean ± SD (n = 3). Triplicates samples were run. Data labeled with different letters (a, b, or c) indicate a statistical difference between groups where p <0.05.

3.5 Discussion

For assessing AT2R agonistic activity, neurite outgrowth has been considered as s a reliable and reproducible method, and the current study demonstrated that both novokinin and Novo Conj could induce neurite outgrowth in NG108-15 cells. Moreover, our RT-PCR results showed that AT2R was primarily present in NG108-15 cells. Using a selective AT2R antagonist and the blockade of neurite outgrowth further confirmed that the observed biological activity was due to AT2R stimulation. Figure 16 provided interesting results, showing that Ang II had the highest neurite outgrowth, which can be attributed to its higher binding affinity to AT2R than novokinin. Additionally, Novo Conj displayed higher neurite outgrowth due to its increased stability in treated cells. This study chose a 1 μM dose of novokinin and an equivalent dose of Novo Conj based on previous studies that synthesized and tested the agonistic effects of AT2R synthetic agonists using neuroblastoma cell lines.

AT2R-mediated neurite outgrowth has been shown to occur through two primary signal transduction mechanisms. The first mechanism involves the activation of AT2R, which modulates the tyrosine phosphorylation of various cytoplasmic proteins, leading to the inhibition of p21ras but sustained activation of p42 MAPK and p44 MAPK. The subsequent activation of MAPK promotes neurite elongation in NG108-15 cells (130). The second mechanism involves the stimulation of AT2R, which activates a complementary pathway that rapidly increases NOS activity through the dephosphorylation of neuronal NOS. This increase in NOS activity increases intracellular cGMP levels, eventually resulting in neuronal differentiation through the elongation and branching of neurites (48). These signal transduction mechanisms highlight the crucial role played by AT2R in cellular signaling, particularly in the development of the nervous system.

Apart from its role in neuronal signaling, RAS components have been found to play a role in breast cancer pathogenesis (131). Compared to normal breast cells, the classical ACE/Ang II/AT1R pathway is expressed more in cancerous breast cells (57). A study conducted on estrogen receptor-positive breast cancer cells revealed that Ang II activates phosphoinositide-3-kinase–protein kinase B/Akt (PI3K/Akt) pathway through AT1R and downregulated Caspase 9, thus attenuating apoptosis (57). Other classical RAS components create a favorable tumor microenvironment by upregulating inflammatory cytokines, chemokines, and transcription factors. In addition to this, they are found to promote epidermal growth factor receptor transactivation, which mediates cancer cell proliferation. This predominant AT1R stimulation has been associated with increased angiogenesis, cellular proliferation, and adipose inflammation in breast cancers (125, 132).

On the other hand, the AT2R, which has a functional antagonistic activity to AT1R, is reported to mitigate tumor progression and proliferation by activating the tumor suppression gene SHP-1 (125). The AT2R activation inhibits cell migration by targeting Akt and endothelial NOS phosphorylation in HEC, exerting a protective action against cancer progression (133). Moreover, AT2R activation has been linked to apoptosis in cancerous cells and has been found to play a crucial role in maintaining cell proliferation, apoptosis, and cell migration (6).

Our present study attempted to establish the link between breast cancer and possible AT2R activation. We confirmed the presence of AT2R in breast cancer cell lines using RT-PCR. The ratio of AT2R/AT1R in 4T1.2 was significantly higher compared to MCF-7. Although we do not have solid evidence for why AT2R is expressed more in 4T1.2 than MCF-7, it can be assumed that AT1R activation positively correlates with estrogen receptors. MCF-7, estrogen-positive

receptors, and 4T1.2, estrogen-negative receptors, might impact the genesis of AT2R and AT1R (134, 135).

We employed a RT cell viability assay against traditional destructive cell viability assays like MTT, owing to several advantages like non-lytic and continuous study. This assay allowed us to perform a non-lytic bioluminescent assay that can be measured over time, allowing us to investigate drug delivery efficiency. We observed from Figure 18 that treatment with novokinin and Novo Conj reduced cell proliferation, with more significant results in the latter time points. However, in Figure 18B, we did not see a statistically significant antiproliferative effect for Novo Conj until 48 hrs, which can only be attributed to the stability of the conjugate drug compared to the native one. We observed better antiproliferative effects of our AT2R-mediated drugs on 4T1.2 compared to MCF-7, which can be attributed to higher AT2R expression in 4T1.2.

Although the cell lines we used did not have a bone component, we were able to show that the conjugate model showed a superior pharmacodynamic effect compared to novokinin. This can be attributed to the fact that conjugation helps to increase the stability and sustained release of novokinin. However, proper release studies can explain the stability claim of our Novo Conj.

3.6 Conclusion

In summary, we were able to show the *in vitro* activity of AT2R-mediated agonistic novokinin and Novo Conj for the first time. With the help of neurite outgrowth and antiproliferative assays, we could also establish a superior therapeutic effect of our conjugated compound. There are some limitations to our study, such as dose-response and release studies, that would have facilitated a better understanding of our research.

Chapter IV: Test and Compare Biological activity of Novokinin and Novo Conj *In-Vivo*

4.1 Inflammation

Inflammation is integral to complex biological reactions to any bodily injury caused by harmful stimuli such as pathogens, damaged cells, toxicants and irritants (136). The cardinal signs of inflammation are marked by increased blood flow, elevated cellular metabolism, vasodilation, the release of soluble mediators, extravasation of fluids and cellular influx (137). It is the body's primary defense mechanism interplayed by immune cells, blood vessels, and molecular mediators, where they tend to remove harmful stimuli and initiate the healing process. Its primary motive is to stop the spread of infection, followed by resolution-restoring affected tissues to their standard and functional state (138).

Inflammation can generically be classified as acute and chronic. Acute inflammation is often considered an initial local response of the body toward harmful stimuli through the web of inflammatory mediators residing in tissue cells and inflammatory cells recruited from the blood into the injured tissues (139). It flares up quickly and becomes intense for some time then the body will resolve the inflammation. However, if inflammation does not subside or it is not self-limiting, it leads to a shift in the type of immune cells resulting in tissue destruction, fibrosis, and necrosis. This continuous non-resolving phenomenon is called chronic inflammation (140).

4.1.1 Mechanism of Inflammation

Within minutes of attack to host innate immune system, immune cells like macrophages, dendritic cells, mast cells, neutrophils, and lymphocytes, initiate a long chain of reactions and cellular activities of inflammation. These immune cells propagate the cell signals which mediate the stimulation of endotoxins, oxygen free radicals, cytokines (a family of small molecular signalinG-proteins, e.g., TNF-α, IL-1, IL-8), polypeptides (such as bradykinin, complement

fragments), coagulation and fibrinolytic factors, thrombin, leukotrienes, histamine, and oxidized low-density lipoprotein (LDL) in local cells. In response to these trigger mechanism, blood cells degranulate, forms pseudopod and initiate phagocytosis (140, 141).

Several microvascular consequences, like enhancement of endothelial permeability and blood flow, infiltration and aggregation of immune cells and escapement of plasma into tissue, are accompanied or followed by cellular responses. Along with immune mediators, immune cells work in tandem to create a positive feedback mechanism. These inflammatory chains of cascades lead to necrosis and apoptosis and are eventually cleared by phagocytic cells. These events promote new humoral mediators for cell growth and regeneration of new functional and connective tissues. Often characterized by scar formation, the latter stage of inflammation is known as inflammation resolution. However, suppose the stream of inflammation fails to subside to resolution. In that case, it leads to non-resolved chronic inflammation, where organ dysfunction might lead to death if timely intervention is not reached (140, 141, 142).

The etiology of non-resolved inflammation can be associated with various internal factors. These factors include failure of cellular checkpoints such as unsuccessful neutralization and elimination of inflammatory and biochemical inducers, futile cessation of inciting stimulus that signals pro-inflammatory mediators, unable to clear inflammatory cells from the site of action and regain tissue homeostasis (143). Similarly, the downregulation of anti-inflammatory factors like adenosine, adrenal glucocorticoids, and selected cytokines (e.g., IL-10) that ensure harmful feedback mechanisms also contribute hugely to chronic inflammation. In addition to this, the immune system sometimes defectively recognize normal component of the body as a foreign antigen, and attacks healthy tissues which contribute to inflammation called disorders (141, 142).

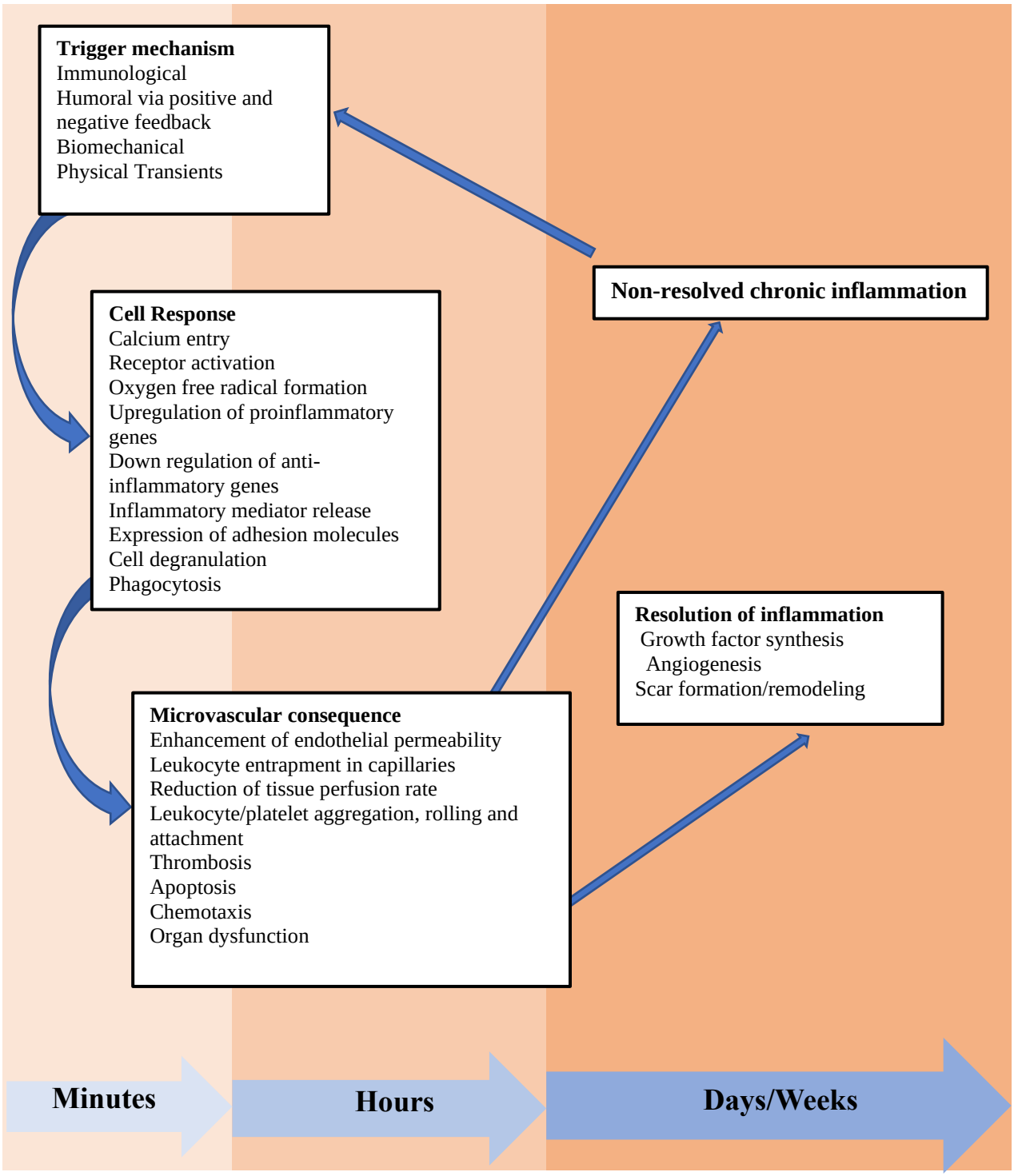

Figure 19. A schematic timeline outlining selected steps in the inflammatory cascade that lead to the resolution or chronic inflammation. Adopted from reference (141) with permission.

Often inflammation is considered as common soil of the multifactorial response of various disorders like cardiovascular disorders, metabolic disorders, neurodegenerative disorders, and cancer other than infectious disease. Several cardiovascular diseases like atherosclerosis, hypertension, myocardial infarction, and stroke are ignited by the activation of the innate and adaptive immune response. This interplay mainly initiates endothelial expression of cytokines, leukocytes and adhesion molecules that would pave the road for the manifestation of vascular disease (138). Similarly, chronic low-grade inflammation has historically been associated with metabolic disorders like diabetes and hypercholesterolemia because it brings dysmetabolism, causing homeostasis imbalance, resulting in loss of lipid control, oxidative stress, inflammation and insulin resistance (144). In addition, inflammation also mediates neurodegenerative disorders like Alzheimer's and Parkinson's disease due to endogenous or exogenous immune cell dysfunction (145).

Furthermore, inflammation induces cancer due to damage to DNA which increases the risk of mutation (146). Lastly, autoimmune disorders like RA, systemic lupus erythematosus (SLE), and myasthenia gravis are characterized by the failure to regulate inflammation which provokes to attack the immune system (147). As RA is our disease of concern, we have discussed it in detail below.

4.2 Rheumatoid Arthritis (RA)

RA is a chronic autoimmune disorder characterized by inflammation in the lining of joints causing warm, tender and swollen, painful joints but bringing stiffness, thus limiting mobility (148). It is a chronic inflammatory disease characterized by synovitis, an incursion of inflammatory cells, and progressive joint destruction. It primarily affects wrists, hands, feet and cervical spine, but larger joints like the shoulder and knee can also be involved (149).

4.2.1 Epidemiology and Risk Factors

RA is estimated to affect about 0.24 to 1% of the total world population. However, its prevalence in the United States, northern European and south Asian countries is higher, usually between 0.5 to 1%. The annual incidence of RA in highly prevalent areas is approximately 40 per 100,000 persons. RA is twice as common in women compared to men, so the lifetime risk of developing RA is 3.6% in women and 1.7% in men (150). Although RA can occur at any age, its risk of developing increases with age, except for juvenile idiopathic arthritis, which mainly affects children and younger teenagers (151). Similarly, people with a family history of RA, predisposed genes and translating factors, and a history of smoking, gum disease, obesity, or lung disease are more inclined to develop RA than those without such risk factors (152, 153).

4.2.2 Symptoms

The symptoms of RA vary among people. The most common symptoms are joint pain at rest and motion, tenderness, redness, swelling and warmth of the joints. Patients also complain of stiffness, particularly early morning after waking up, leading to prolonged activity. As the disease progresses, the inflammation may worsen, causing erosion and destruction of the joint surface, ultimately leading to deformity in the affected areas. Similarly, around 30% of people affected by RA have reported rheumatoid nodules in non-joint areas. This joint swelling and pain often interfere with mundane daily activities, such as buttoning clothes, bending knees, or combing hair. Other than these joint symptoms, RA patients also experience fatigue, low-grade fever and loss of appetite (154).

4.2.3 Diagnosis

In the early stages of RA, diagnosing RA is difficult as its symptoms are very mild and cannot be confirmed by X-rays or in blood tests. However, at the later stages, doctors can pinpoint by

physical examination of joints characterized by swelling, redness and rigidity while moving. Furthermore, blood tests such as Rheumatoid factor (RF) test, anti-cyclic citrullinated peptide antibody (ACCPA) test, completed blood count test, C-reactive protein (CRP) test and erythrocyte sedimentation rate (ESR) test can be used as confirmatory test. But to check the extent of joint damage, patients are suggested to undergo several imaging tests like X-rays, Magnetic resonance imaging (MRI), ultrasound, computed tomography (CT), bone scan and positron emission tomography (PET) (155, 156).

4.2.4 Treatment

Although there is no specific cure for RA, treatments are only available to alleviate the symptoms and slow the progression of the disease. Like in most cases, drugs work only with change in healthy lifestyle and inclusion of physical therapy. Anti-inflammatory drugs such as non-steroidal anti-inflammatory drugs (NSAIDs), corticosteroids and disease modifying antirheumatic drugs (DMARDs) are considered as the first line of treatment for the RA. In some cases, failure to these initial therapies, patients are moved to biological response modifiers DMARDs and Janus kinase (JAK) inhibitors. In addition to this, physical therapy focusing on the joints along with daily exercise and healthy food habits contribute to the management of symptoms. In some extreme cases, doctors might also opt for surgery like synovectomy to prevent pain or tendon rupture due to failure of drugs (155, 156).

4.2.5 Pathophysiology of RA

The onset of RA is marked by sustained cellular activation that can lead to autoimmunity and the formation of immune complexes. This manifests in the production of autoantibodies such as RF and ACCPA, synovial inflammation and hyperplasia, and cartilage and bone destruction (148). The disease progresses through initiation, amplification, and chronic inflammation (157).

The initiation stage is characterized by non-specific inflammation resulting from a complex interplay of genetic and environmental factors. For example, individuals with the CCR6DNP and HLA DRB1 genotypes have a significantly higher association with RA. Those with polymorphisms in the RANKL promoter are predisposed to the onset of RA at a younger age. Smoking, alcohol consumption, and infectious diseases are environmental risk factors that can trigger the initiation of RA. Smoking and alcohol consumption upregulate the production of pro-inflammatory cytokines, while infectious agents such as Epstein-Barr virus, Proteus species, and *Escherichia coli* can aid in the formation of immune complexes that induce RF and ACCPA production (158). Periodontitis and gastrointestinal imbalances can also stimulate autoimmunity through the citrullination of proteins. Genetic factors can sometimes interact with environmental risk factors, resulting in a high predisposition to the disease. Overall, understanding the complex interactions between genetic and environmental factors in the initiation and progression of RA is crucial for developing effective prevention and treatment strategies (156, 159, 160).

During amplification, B lymphocytes derived from plasma cells produce more RF and AACPA of IgG and IgM classes in large quantities. Toll-like receptors (TLRs) and lipoprotein molecules increase, leading to macrophages, mast cells, and natural killer cells infiltration through Fc receptor and complement binding, intensifying synovitis. Macrophage activation results in high levels of vasoactive amines, cytokines, chemokines, and proteases produced by cytokines, reactive oxygen species (ROS), inducible nitrogen oxygen species (iNOS), and prostaglandins. Macrophages and dendritic cells present antigens by expressing MHC class II molecules, allowing entry of activated T cells, mainly CD4 in microscopically nodular aggregates and CD8 in microscopically diffuse infiltrates. Neutrophils contribute to synovitis by synthesizing

prostaglandins, proteases, and reactive oxygen intermediates. Mast cells also produce high levels of vasoactive amines, cytokines, chemokines, and proteases (160, 161, 162).

Normal homeostasis in the synovium between type 1 helper T cells (Th1) and type 17 helper T cells (Th17) is dysregulated in RA due to the defective function of regulatory T cells (Tregs). Tregs are responsible for recruiting less protein kinase with less downstream NF-κB activation and regulated local inflammatory cytokine production. However, dysfunctional Tregs cause an increase in TNF α, IL-1, and IL-6, which activate leukocytes, endothelial cells, and synovial fibroblasts, inducing the production of cytokines, chemokines, adhesion molecules, and matrix enzymes. They suppress regulatory T-cell function, activate osteoclasts, and cause cartilage resorption. Additionally, there is an increase in IL-12, 18, 21, 32, 33, which promotes the activation of Th1, neutrophils, and natural killer cells and mediates metabolic and cognitive dysfunction. This marks the initiation and progression of synovial inflammation and hyperplasia (163, 164).

The third stage of RA is characterized by chronic inflammation, marked by the formation of granulation tissue and pannus at the synovial lining. Fibroblast-like synoviocytes (FLS) in affected joints exhibit an altered phenotype compared to normal cells, resulting in reduced apoptosis, impaired contact inhibition, increased migratory invasive potential, and the expression of high levels of cytokines, chemokines, adhesion molecules, matrix metalloproteinases (MMPs), and tissue inhibitors of metalloproteinases (TIMPs). This altered FLS phenotype leads to extensive angiogenesis and tissue damage caused by enzymes, as well as promotes cartilage destruction by sustaining T-cell and B-cell survival and adaptive immune organization (165). Additionally, the cytokines involved in RA initiate and amplify osteoclast differentiation and

inhibit OPG through the RANKL receptor. This can lead to bone erosion and deformity, inhibiting OPG promoting osteoclast activity and reducing osteoblast activity (166).

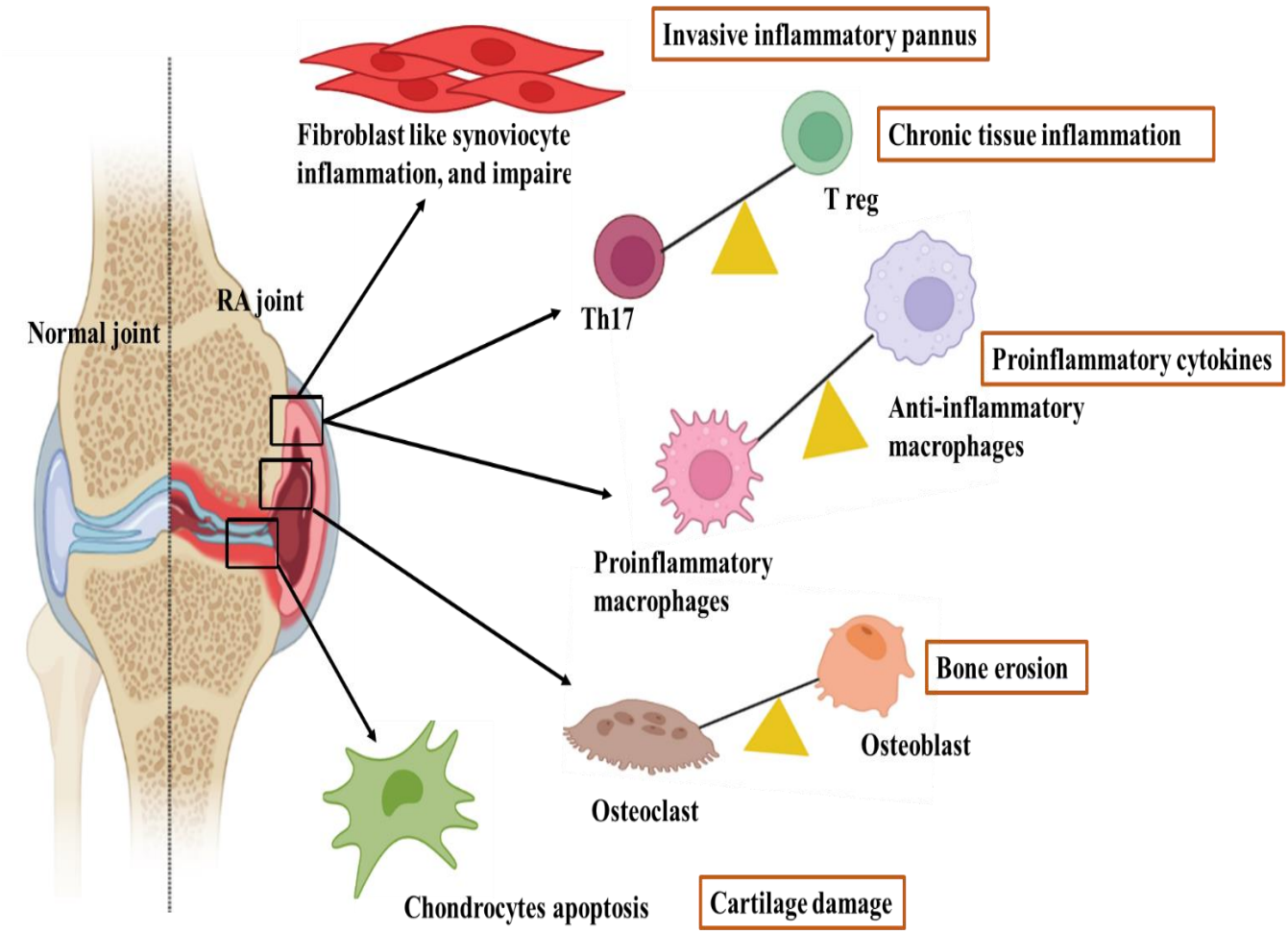

Figure 20. Pathophysiology of rheumatoid arthritis (RA) through different stages. Adopted and modified from (https://discoveries.vanderbilthealth.com/2022/04/for-rnas-non-coding-does-not-mean-non-essential/).

4.2.6 Complications Associated with RA

4.2.6.1 Cardiovascular and Metabolic Complications

Cardiovascular disease contributes a significant percentage of excess mortality in RA patients, almost 39.6% of deaths in the review of 50 studies that included 91618 patients and 33250 deaths (167). This is because RA patients have higher cardiac risk factors, inactive lifestyles and altered lipid profiles than the general population. Higher cardiac risk factors account for the elevation of inflammatory markers like TNF-α, IL-18, IL-33, ESR, CRP, ACPA, coronary artery calcification, oxidative stress, and endothelial dysfunction. Similarly, patients with RA have limited physical activity, which may result in lower muscle mass and higher fat mass. This visceral adiposity exacerbates metabolic syndrome, insulin resistance and hypertension, thus worsening cardiovascular disease. The lipid profile in RA patients is severely imbalanced in such a way that it alters the function of lipoprotein. High-density lipoprotein (HDL), an antioxidant lipoprotein, is impaired functionally as it loses most of its anti-oxidative properties. Similarly, LDL of RA patients has higher levels of glycated end products, enhanced phagocytosis by macrophages, higher fatty acid accumulation and three-fold greater oxidation than control (168). However, treatments available for RA, like high doses of corticosteroids, also pose a significant threat to cardiovascular disease. This can be credited to the effects of corticosteroids on weight gain, insulin resistance, dyslipidemia, and elevated blood pressure. Overall, inflammation forms the deep interconnection between cardiovascular disease and RA as they share a common mechanism for their pathogenesis (167, 168).

4.2.6.2 Pulmonary Complications

Pulmonary involvement is a substantial systemic effect of inflammation, resulting in another significant source of morbidity amongst RA patients (169). RA manifests several pulmonary

diseases like interstitial lung disease (ILD), pleural disease, rheumatoid nodules, and airway disease, and they become more prominent with the progression of RA. This happens due to defects in immunity and chronic inflammation caused by age, various environmental exposure like inhaled antigens, smoking and genetic predisposition. The chronic elevation of CCP and RF with local production of inflammatory cytokines coupled with epigenetic factors in RA patients has been the reason for the occurrence of ILD. These factors give rise to the differentiation and proliferation of fibroblasts, increased synthesis and deposition of extracellular matrix (ECM), and increased metalloproteinase activity resulting in ILD (170). Similarly, in the case of rheumatoid nodules and pleural disease, RA triggers impaired fluid resorption in inflamed pleura, necrosis of rheumatoid nodules and initiates a cascade of inflammatory mediators like cytokines and immune complexes leading to endothelial injury and capillary permeability. Additionally, rheumatoid nodules and vasculitis, seen in RA patients, can also influence upper and lower airway disease, which sometimes becomes fatal if a severe obstruction occurs (170, 171).

4.2.6.3 Renal Complications

RA, a systemic inflammatory disorder, has a significant occurrence of renal complications. These renal disorders can be classified into two types based on their causative mechanisms: (1) chronic inflammation caused by renal atherosclerosis and amyloidosis and (2) drug-induced kidney disease (172). The renal complications arising from chronic inflammation in RA are characterized by the infiltration of inflammatory cells like macrophages and mediators such as CRP, IL-6, and TNF α. These actions promote kidney injury by inducing inflammation in the glomerulus and tubulointerstitium (173). On the other hand, certain drugs used to treat RA, such as penicillamine, cyclosporine, and bucillamine, can have nephrotoxic effects. This is due to

these drugs' poor control of systemic inflammation, which can lead to mesangial proliferative glomerulonephritis or secondary amyloidosis. However, using methotrexate and targeted biologic agents in conjunction with treat-to-target therapeutic approaches has significantly reduced the incidence of drug-induced nephrotoxicity in RA patients in recent years (174).

4.2.6.4 Psychological and Socio-Economic Burden

RA is a degenerative disorder that is characterized by its progressive nature, and its impact goes beyond physical trauma. The loss of the ability to perform daily activities due to RA can cause patients to experience anxiety, depression, and low self-esteem, which can lead to high rates of mortality and suicide. These psychological effects not only affect patients but also their partners, families, and caregivers (175). Since RA cannot be cured completely by available medications and is only manageable through symptom management, it leads to chronic psychological distress for those suffering from the condition. Moreover, the economic burden of purchasing numerous medications to manage the various health complications arising from RA adds to the patients' worries (175, 176).

4.3 RA and RAS

RA is a complex disease with various mechanisms involved in its pathogenesis, and one mechanism that has gained attention is RAS. Identifying local functional RAS in multiple organs and tissues has highlighted the crucial role of RAS components in the development of RA (177). In particular, the classical ACE-Ang II-AT1R axis is a major contributor to the initiation and progression of inflammation in RA (178). The aggravation of angiogenesis is a significant mechanism that drives RA by facilitating the infiltration of inflammatory cells and subsequent damage to articular tissue. Ang II, a key functional peptide in RAS, plays a critical role in this process by acting as a cytokine and growth factor that actively promotes inflammatory responses

by binding to AT1R. Ang II stimulates the production of pro-angiogenic molecules and induces the migration of inflammatory cells and the production of cytokines, which increase inflammation-mediated tissue damage. In addition to exacerbating inflammation and tissue damage, Ang II also contributes to the development of periarticular osteopenia, leading to progressive destruction, deformation, and dysfunction of affected joints. ACE and Renin, active enzymes of RAS responsible for producing Ang II, have been found to have a positive correlation with VEGF, MMPs, and RFs (179, 180, 181).

Various studies have indicated that the administration of ARBs significantly reduces inflammation and arthritis-related parameters in arthritic rats. In particular, ARBs like Olmesartan, Candesartan, and Telmisartan have been shown to reduce neutrophil recruitment, hyper nociception, and the production of inflammatory markers (182, 183). Along with ARBs, ACE inhibitors like Ramipril and renin inhibitors such as Aliskiren have also been shown to decrease inflammation and oxidative stress biomarkers, making them useful as immunomodulatory agents (184).

Scientific research suggests that activation of the ACE2-Ang 1-7-MasR axis can help counter inflammation in RA beyond traditional enzyme inhibitors and blockers. This beneficial axis involves the production of Ang 1-7 by the ACE2 enzyme, which binds to MasR and reduces the production of proinflammatory genes. Ang 1-7 has also been found to play a critical role in bone metabolism, stimulating osteogenesis and inhibiting osteoclastic resorption. The effects of this axis are reversed when MasR antagonist A-779 is administered, but Mas agonists can reduce local cytokine production and decrease leukocyte adhesion at inflamed joints. Several studies have shown that the ACE2-Ang 1-7-MasR axis negatively correlates with inflammatory markers,

and the ratio of ACE/ACE2 in arthritis rats is significantly higher in arthritic rats than in control rats (184, 185).

Our study focuses on AT2R, a subtype of angiotensin receptors, which also belongs to the protective axis of RAS and plays a role in the pathogenesis of RA. In the synovium sample taken from RA patients, the expression of AT2R is upregulated in the chronically inflamed microenvironment compared to the control. When stimulated by its specific agonist CGP42112A, AT2R reduces the gene expression of cytokines such as IL-1, IL-6, and TNF-α while increasing the expression of anti-inflammatory cytokines such as IL-10 (186, 187, 188). Additionally, AT2R agonism inhibits cell proliferation, remodeling, vasodilation, migration of FLS, leukocyte adhesion, and endothelial inflammation (189).

Interestingly, the use of ARBs in arthritic rats has also been correlated with increased expression and activation of AT2R, making it a potential candidate for treating RA and other inflammatory conditions (190). These findings suggest that AT2R is a promising avenue for treating RA and other inflammatory conditions. Overall, this beneficial axis modulates intracellular signaling and downregulates inflammatory genes, presenting a potential route for treating RA and other inflammatory conditions.

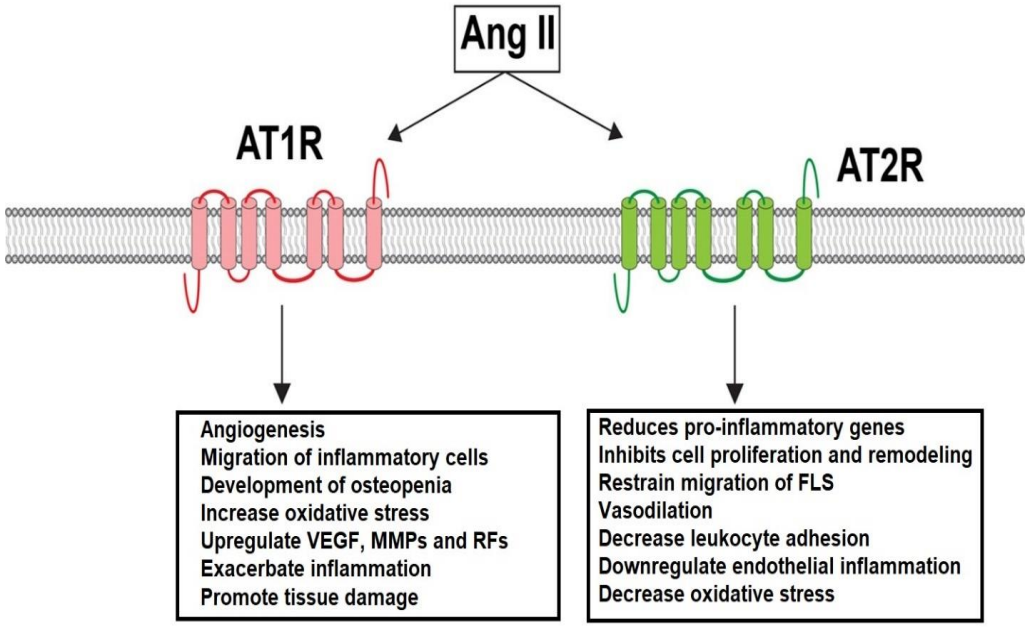

Figure 21. Role of renin-angiotensin system (RAS) in the pathogenesis of rheumatoid arthritis (RA). Angiotensin II (Ang II), angiotensin Type I receptor (AT1R), angiotensin type II receptor (AT2R), vascular endothelial growth factor (VEGF), matrix metalloproteinase (MMPs), rheumatoid factors (RFs) and fibroblast like synoviocytes (FLS).

4.4 Arachidonic acid (ArA)

ArA is a 20-carbon polyunsaturated omega-6 fatty acid with four double bonds in the cis position. These double bonds impart ArA with mobility, flexibility, fluidity, and selective permeability to cell membranes. Additionally, they facilitate interaction with molecular oxygen, which produces bioactive oxygenated molecules such as eicosanoids and isoprostanes. ArA is primarily found in the hairpin structure and incorporated into the phospholipid membrane of cells. It is abundant in phospholipids in the brain, muscles, liver, spleen, and retina (191). Phospholipases, specifically PLA2, phospholipase C (PLC), and phospholipase D (PLD), act on

phospholipids to release esterified ArA, with PLA2 being the primary contributor. Although the concentration of free ArA in the circulation is low, its release is regulated by various cellular activation signals from receptors such as TLRs, pyrogenic receptors, inflammation stimulation, calcium ionophores, P75, and P55 receptors, which activate PLA2. After the release, there are three possible outcomes for the three functional ArA 1) diffusion to other cells, 2) incorporation into the phospholipids and 3) metabolism via enzymatic reactions (192).

ArA is metabolized by three enzymes: COX, Lipoxygenase (LOX), and Cytochrome P450 (CYP450). These enzymes generate biologically active fatty acid mediators involved in various biological activities. COX enzymes, specifically COX1 and COX2, produce prostaglandins (PGs) and thromboxane (Tx), collectively known as prostanoids, which are vital in regulating blood clotting, blood flow, inflammation, and other essential bodily processes (193). LOX enzymes metabolize ArA into 4-hydroperoxyeicosatetraenoic acids (HPETEs), which are then converted into leukotrienes (LTs), lipoxins (LXs), and hepoxilins. These metabolites are critical in regulating cell proliferation, differentiation, apoptosis, and inflammatory mediators (194). CYP450 enzymes, specifically CYP450 epoxygenase and CYP450 ω-hydroxylase, are also involved in ArA metabolism. These enzymes produce metabolites involved in various biological activities such as cellular proliferation, inflammation, hemostasis, and intracellular signaling pathways. The CYP pathway is the primary focus of this study, and understanding its intricate details is crucial for understanding the diverse biological roles of ArA metabolites (195).

The CYP450 epoxygenase enzymes act on ArA to produce four EETs derivatives, which function as autocrine and paracrine mediators. EETs have been found to play a crucial role in regulating cellular proliferation, inflammation, and angiogenesis and modulate various cellular processes, including the growth and differentiation of smooth muscle cells. They are also

involved in vasodilation and are critical in regulating blood flow and pressure, making them cardioprotective and anti-inflammatory. EETs are further metabolized to less active dihydroxyeicosatrienoic acids (DiHTs) through soluble epoxide hydrolase (sEH) (196, 197).

The CYP450 ω-hydroxylase, on the other hand, enzyme catalyzes a hydroxylation reaction that produces biologically active compounds called hydroxyeicosatetraenoic acids (HETEs), specifically HETEs 16,17-,18,19-, and 20-. HETEs are involved in physiological processes and modulate inflammation by participating in leukocyte activation, adhesion, and chemotaxis. However, they also induce vasoconstriction, increasing blood pressure and participating in platelet aggregation. Due to these functions of HETEs, they are linked to proinflammatory and vasoconstrictive effects. Overall, the CYP pathway is critical in generating ArA metabolites involved in various biological activities, including cellular proliferation, inflammation, angiogenesis, blood flow regulation, and blood pressure control. This balance between the metabolites generated through the CYP pathway is essential for maintaining normal homeostasis. However, an imbalance in the CYP-mediated eicosanoids can contribute to the development and progression of various inflammatory diseases, including RA, cancer, and diabetes, as well as cardiovascular diseases such as hypertension, atherosclerosis, and stroke and neurological disorders like Alzheimer's disease (191, 198).

4.5 Effect of CYP-derived ArA in Inflammation/RA

CYP-derived eicosanoids play a significant role in inflammation and are associated with RA and ArA metabolism. EETs exhibit anti-inflammatory activity by binding to nuclear peroxisome-proliferator activated receptors (PPARγ and PPARα), which leads to reduced iNOS and ROS generation and inhibition of the transcription of proinflammatory genes such as cytokines, metalloproteinases, and acute phase proteins (199). This also inhibits NF-κB activation, LOX-5

and COX-2-mediated inflammatory responses and attenuates cytokine-induced leukocyte adhesion to the vascular wall. The negative correlation between EETs and proinflammatory cytokines promotes bone resorption and osteoclastogenesis (195). EETs also inhibit osteoclastogenesis by modulating multiple pathways upstream and downstream of RANKL signaling. This is associated with decreased receptor activation of NF-κB, OPG ratio, and serum levels of proinflammatory cytokines. At the molecular level, EETs downregulate RANKL-induced activation of NF-κB, activator protein-1 (AP-1), and MAPKs, including ERK and JNK, during osteoclast formation. Additionally, EETs prevent the production of ROS following RANKL stimulation, suppressing osteoclast-specific gene expression. EETs inhibit Tartrate-resistant acid phosphatase (TRAP), cathepsin K (CK), matrix metalloproteinase (MMP)-9, and receptor activator of NF-κB (RANK), providing an anti-inflammatory role (197).

However, DiHTs, metabolites of EETs, also exhibit anti-inflammatory activity but are less potent than their precursor. Thus, inhibiting the enzyme sEH, which metabolizes EETs to DiHTs, may be an alternative option for treating inflammatory diseases. Some studies have found that administering sEH inhibitors can improve arthritis in a mouse model. DiHTs are less active than EETs because the carbon chain's epoxy ring binds with more affinity to receptors than vicinal diol, which only shows partial binding (200).

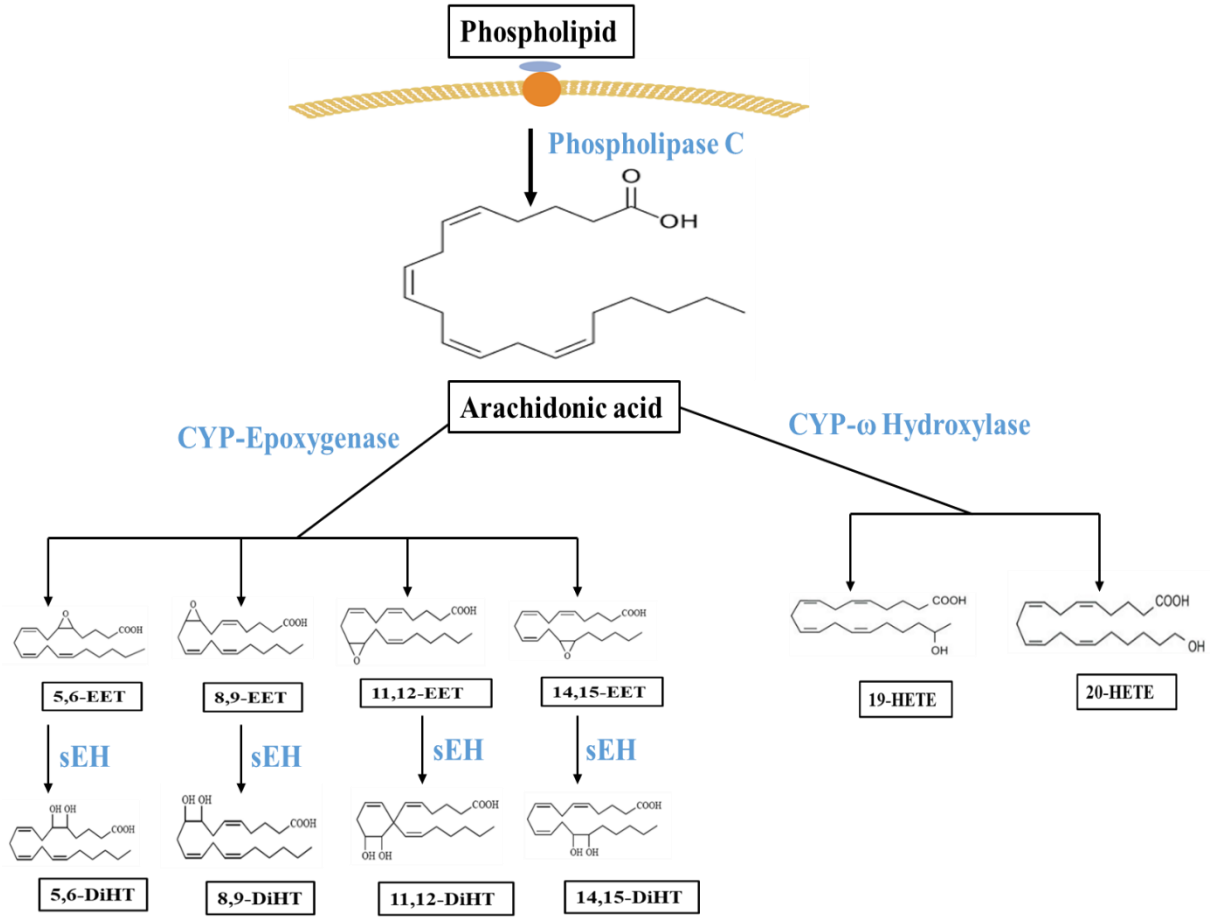

Figure 22. CYP450 (CYP) derived arachidonic acid (ArA) metabolism. 5,6-epoxyeicosatrienoic acid (5,6-EET), 8,9-epoxyeicosatrienoic acid (8,9-EET), 11,12-epoxyeicosatrienoic acid (11,12-EET), 14,15-epoxyeicosatrienoic acid (14.15-EET), 19-hydroxyeicosatetraenoic acid (19-HETE), 20-hydroxyeicosatetraenoic acid (20-HETE), 5,6-dihydroxyeicosatrienoic acids (5,6-DiHT), 8,9-dihydroxyeicosatrienoic acids (8,9-DiHT), 11,12-dihydroxyeicosatrienoic acids (11,12-DiHT), 14,15-dihydroxyeicosatrienoic acids (14,15-DiHT) and soluble epoxyhydroxylase (sEH).

4.6 Crosstalk between ArA and RAS

The evidence gathered so far has shed light on the significant role played by the crosstalk between ArA and RAS in both inflammatory and cardiovascular diseases. One of the key findings is that 20 HETE, a potent vasoconstrictor and pro-inflammatory agent, can stimulate the translocation of NF-κB and bind to the ACE promoter region, promoting the generation of ACE. ACE production is directly proportional to Ang II, a main effector peptide in the RAS. This leads to an increase in Ang II production, which induces AT1R expression. By binding through AT1R, Ang II facilitates vasoconstriction, inflammation, oxidation, and fibrosis. Moreover, 20 HETE antagonists abolished the ACE, Ang II generation increase and subsequent biological activity. The pro-inflammatory effect mediated by the AT1R involves CYP-dependent hydroxylation of arachidonic acid to 20-HETE and activation of NF-κB (203, 204).

Additionally, when sEH inhibitors were administered to Ang II-induced hypertensive mice, it resulted in a vasodilatory effect and increased sodium and potassium excretion. This biological effect is attributed to the inhibition of sEH, which increases EETs levels, known for their antioxidative and anti-inflammatory properties (205). Furthermore, direct stimulation of AT2R using agonist C21 has been shown to activate protein phosphatases, CYP-dependent epoxidation of arachidonic acid to EETs, and inhibition of NF-κB activation. Hence, activation of AT2R leads to the inhibition of cytokine-induced inflammation (206). These findings highlight the interplay between CYP-derived ArA metabolites and RAS in the disease manifestation (207).

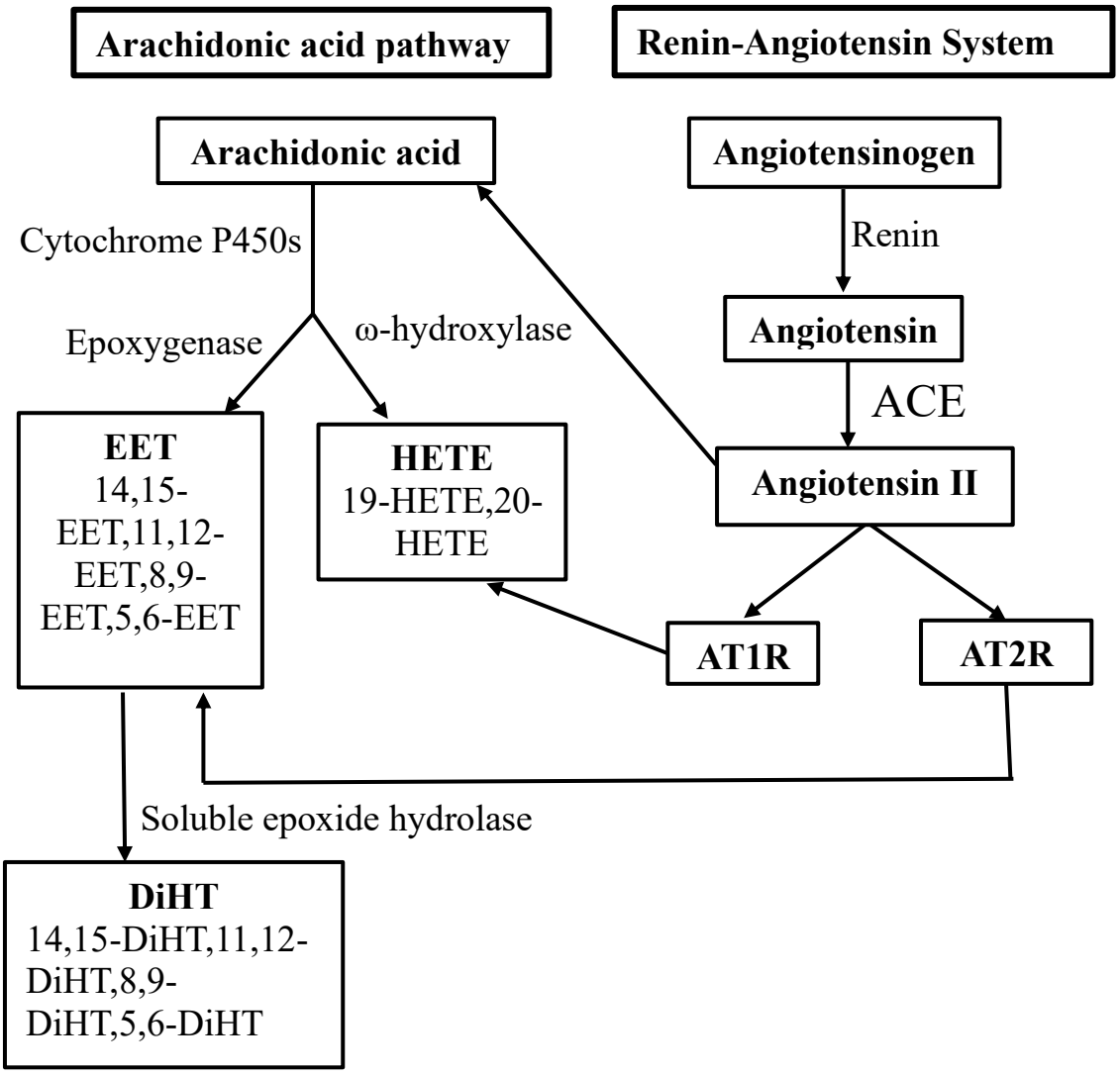

Figure 23. Correlation between CYP450 (CYP) derived arachidonic acid (ArA) metabolism and renin-angiotensin System (RAS). 5,6-epoxyeicosatrienoic acid (5,6-EET), 8,9-epoxyeicosatrienoic acid (8,9-EET), 11,12-epoxyeicosatrienoic acid (11,12-EET), 14,15-epoxyeicosatrienoic acid (14.15-EET), 19-hydrooxyeicosatetraenoic acid (19-HETE), 20-hydrooxyeicosatetraenoic acid (20-HETE), 5,6-dihydroxyeicosatrienoic acids (5,6-DiHT), 8,9-dihydroxyeicosatrienoic acids (8,9-DiHT), 11,12-dihydroxyeicosatrienoic acids (11,12-DiHT), 14,15-dihydroxyeicosatrienoic acids (14,15-DiHT) and soluble epoxyhydroxylase (sEH), angiotensin II (Ang II), angiotensin II type 1 receptor (AT1R), angiotensin II type 2 receptor (AT2R), angiotensin converting enzyme (ACE).

4.7 Bone Drug Delivery

Beyond the use as a standalone drug, the application of BPs can be expanded through conjugation strategies, mainly by covalently linking BPs with other active drugs to form a new chemical entity. The conjugation can be achieved via a direct bond or a cleavable linker, but direct attachment can sometimes alter the intrinsic pharmacological activity of the drug, so a biodegradable linker is preferred. This conjugation of BP with other active drugs acts as a dynamic targeting system, limiting off-target systemic toxicity with reduced intrinsic metabolism to the liver. Thus, the optimal design of BP conjugates is warranted as it combines the bone-seeking properties of BPs, a biodegradable linker and an active drug that result in synergistic or additive drug efficacy for a longer duration of action (104, 105).

Successful skeletal drug delivery has improved pharmacodynamic and pharmacokinetic (PK) parameters in numerous instances. For example, the conjugation of a BP with estradiol and its administration to ovariectomized rats resulted in a prodrug that exhibited significantly greater antiresorptive activity compared to rats treated with estradiol alone (106). In a similar research setting, bone drug delivery of parathyroid hormone (PTH) conjugated with PEG and BP had demonstrated superior anabolic treatment efficacy over unmodified PTH in rats with osteoporosis (107). Additionally, a study involving salmon calcitonin, an antiresorptive drug, showed improved therapeutic efficacy and PK parameters when conjugated with PEG and BP in normal and osteoporotic rats (108). In our own laboratory, we demonstrated that the conjugation of Ang 1-7 with PEG and BP resulted in superior anti-inflammatory effects and improved PK parameters (109). These findings highlight the potential of bone drug delivery as a leading approach in improving therapeutic efficacy, which could help enhance small peptide drugs like

novokinin to overcome the instability issue. The schematic design for the conjugation of Novo Conj has been given in Figure 9.

4.8 Hypothesis and Objective

We hypothesize that Novo Conj can effectively restore dysfunctional RAS by activating the AT2R protective axis, providing superior effects at both cellular and molecular levels compared to its parent peptide, novokinin. Additionally, we propose that stimulating AT2R with Novo Conj will positively impact ArA metabolism, which will combine to alleviate the signs and symptoms of RA.

Beyond simply assessing the physical manifestations of RA, the primary objective of our study was to investigate the impact of inflammation and its relationship with RAS. We aimed to determine how our drug conjugate shows their effects at the gene and protein level in various tissues. Additionally, we evaluated the systemic effects of Novo Conj through quantification of NO, RAS peptides, and ArA metabolites. We also compared the efficacy of our conjugate to its native form in terms of therapeutic activity.

4.9 Experimental Methods and Materials

4.9.1 Animals

The research procedure adhered to the approved protocols of the Institutional Animal Care and Use Committee at Idaho State University (protocol #772, 09/22/2021). Healthy adult male SpD rats weighing between 230-250 g were sourced from the Health Sciences Laboratory Animal Services. These rats were housed under standard conditions with controlled temperature, ventilation, and hygiene, and a 12-hr light-dark cycle, with unrestricted access to food and water. A period of 72 hrs was allowed for the rats to acclimatize to their environment before the experiment began.

4.9.2 Dose Calculation

For a period of two weeks, a subcutaneous injection of novokinin at a dosage of 0.4 mg/kg, or an equivalent dosage of Novo Conj, was administered every other day (three times per week).

4.9.3 Adjuvant Arthritis Induction and Assessment of Adjuvant Arthritis

To conduct our study, we utilized SpD rats due to their widespread availability, genetic similarity to humans, and affordability compared to other animals. We induced experimental adjuvant-induced arthritis (AIA) in healthy male SpD rats by administering a 0.2 mL solution of *Mycobacterium butyricum* (Difco Laboratories, Detroit, Michigan, USA) of 50 mg/mL in squalene via tail base injection on day 0. This induction method produces an immuno-inflammatory reaction that closely mimics human RA.

The arthritic rats were divided into three groups and given either saline (Arthritic, n = 6), novokinin (Arthritic + Novokinin, n = 5), or Novo Conj (Arthritic + Novo Conj, n = 5). In contrast, a group of healthy rats received saline (Control, n = 6). The treatment groups received an equivalent dose of 400 µg/kg of novokinin solution in saline via subcutaneous injection thrice a week for two weeks after arthritis emergence. We monitored the rats' body weight change using a regular balance and measured joint and paw diameter changes periodically with a caliper having 25 µm sensitivity (Mitutoyo Canada Inc., Toronto, Ontario, Canada).

The progression of AIA was observed daily, and we calculated the arthritis index (AI) using a macroscopic scoring system as described previously. The AI was determined based on the involvement of hind paws on a 0–4 scale and forepaws on a 0–3 scale. Scores from each paw were added to calculate AI, with a score of ≥5 indicating significant disease emergence and 14 being the highest possible index in AIA rats. Only rats with at least one paw or joint swelling were included in the study. The inclusion criteria for the rats to receive treatment was having at

least one paw or joint swelling. Any rats that developed AI ≥ 5 were excluded and euthanized as a humane masseur of animal use and handling. All animals were euthanized at the end of the experiment, and serum, plasma, and tissues were harvested. Serum samples were analyzed for total nitrate and nitrite (nitric oxide, NO). RAS enzymes and protein through qPCR, WB, IHC and the Ang 1-7, Ang II, and ArA metabolites were analyzed by LC-MS/MS methods.

4.9.4 Sample Collection

After completing the 14-day treatment regimen, and waiting for 24 hours since the last dose, the rats were given isoflurane/oxygen anesthesia and then euthanized. Blood samples were obtained by puncturing the heart and divided into three tubes. Various tissues, such as the heart, kidneys, liver, lungs, and joints, were surgically removed and prepared for subsequent experiments according to the methods described in the following experiments.

4.9.5 Processing of Blood Samples

1. To measure nitrate (NO_3) and nitrite (NO_2) levels, a sample of the collected blood was placed in a clean glass tube and kept at room temperature for 20 mins. The serum was then separated using a micropipette and transferred into Eppendorf tubes, which were snap frozen in liquid nitrogen and subsequently stored at -80 °C until analysis.
2. To analyze the components of RAS, a blood sample was collected in a glass tube containing 50 µL of Complete Mini Protease Inhibitor cocktail (Roche Diagnostics GmbH, Manheim, Germany), which was calculated for each 1 mL of blood. This protease inhibitor cocktail was prepared by dissolving one Complete mini protease tablet in 10 mL of normal isotonic saline. The protease inhibitor cocktail contained EDTA, inhibiting a broad range of proteases and protected proteins. Heparin was not added as it interfered with the analysis. After gently mixing the blood sample with the cocktail, it

was centrifuged at 15,000 rpm at 4 °C for 15 mins. The supernatant layer of plasma was collected in 1.7 mL Eppendorf tubes using micropipettes, snap-frozen using liquid nitrogen, and then stored at -80 °C for further analysis.

3. To measure ArA metabolites, another sample of blood was collected in glass tubes containing 50 USP units of sodium heparin (BD Diagnostics, NJ, USA). To every 1 mL of blood, 200 µL of 0.9% normal saline containing 0.113 mM butylated hydroxytoluene (BHT) and 10 µM of Indomethacin were added. After gently mixing, the tubes were centrifuged at 15,000 rpm at 4 °C for 15 mins. The supernatant layer of plasma was collected in 1.7 mL Eppendorf tubes using micropipettes, snap frozen using liquid nitrogen, and then stored at -80 °C for further analysis.

4.9.6 Processing of Tissue samples

All other tissues, such as the heart, kidneys, liver, and lungs, were washed with normal saline and collected in 2.0 mL labeled propylene tubes. They were then snap frozen using liquid nitrogen and stored at -80 °C until further analysis.

4.9.7 Colorimetric Assay of Nitrite (NO_3) and Nitrate (NO_2) Measurement

The biochemical assessment of RA involved using a nitrite/nitrate assay kit from Sigma-Aldrich to quantify NO metabolites in serum. This was done by measuring the stable metabolites of NO, NO_3 and NO_2 using the Griess reaction and colorimetric detection. The experiment was carried out in non-tissue culture 96 well-treated plates, with fresh standard solutions of 0, 20, 40, and 80 nmol/well prepared each time and run in duplicates. To prepare the serum samples, they were centrifuged using an Amicon® Ultra-4 centrifugal unit with Ultracel®-10 membrane to filter out hemoglobin and proteins. 70 µL of the filtered sample was added to each well in triplicates, along with 10 µL of nitrate reductase and 10 µL of enzyme co-factor solution. The plate was

mixed well on a horizontal shaker for 2 hrs, then 50 µL of Griess reagent A was added to each well and incubated for 5 mins, followed by adding Griess reagent B and shaking for 10 mins. The absorbance intensity was measured at 570 nm using a Varioskan Lux from Thermo Scientific, and the background absorbance was calculated and subtracted from the total values. A standard curve was drawn to determine the equation, and each absorbance correlated with the NO_3 and NO_2 concentration. According to the kit's manufacturer pamphlet, the lower limit of quantification (LLOQ) was approximately 82.5 ng/µL, much lower than the levels detected in the serum samples.

4.9.8 Quantitative Polymerase Chain Reaction (qPCR) for the analysis of RAS components

The Quick-RNA™ Miniprep Plus kit (Zymo Research, Irvine, CA, USA) was utilized to extract total RNA from rat tissue samples in accordance with the manufacturer's protocol. Briefly, the frozen samples were thawed at room temperature and 50 mg of the samples were weighed and submerged in 600 µL of DNA/RNA shield. For every 300 µL of samples, 15 µL of Proteinase K and 30 µL of PK digestion buffer were added, mixed, and incubated at room temperature for 5 hrs. The samples were centrifuged at 15000 rpm for 5 mins, and the supernatant was transferred to a nuclease-free tube to eliminate particulate debris. An equal volume of RNA lysis buffer was added to all RNA samples, mixed well, and then centrifuged at 15000 × g for 30 secs, unless specified.

Initially, the samples were transferred into a Spin-Away™ filter in a collection tube and centrifuged to eliminate the majority of genomic DNA. The flow-through was then collected, and 1 volume of 95-100% ethanol was added and mixed thoroughly. This mixture was transferred into a Zymo-Spin™ III CG column in a collection tube, centrifuged, and the flow-through was discarded. Next, the samples were treated with DNAase I, where 400 µL of RNA

wash buffer was added, centrifuged, and the flow-through was discarded. In a nuclease-free tube, 5 µL of DNAase I and 75 µL of Digestion buffer were mixed and added to the column matrix, which was then incubated at room temperature for 15 mins. Following DNase treatment, the column matrix was washed with 400 µL, 700 µL, and 400 µL of RNA wash buffer, centrifuged for 30 secs, except for the last 400 µL of the wash, where it was centrifuged for 1 min and the flow-through was discarded. The remaining solution was transferred to nuclease-free tubes. Finally, 100 µL of DNase/RNase was added directly to the column matrix and centrifuged to elute the RNA.

RNA purified samples were then subjected to the reverse transcriptase process, where 500 ng of RNA was transcribed into cDNA using 4 µL of qScript cDNA super mix (P/N 84034, Quanta Bio, USA), and the volume was made to 20 µL by RNase/DNase free water. The mixtures were gently vortexed and centrifuged at 3000 × g for 30 secs. The samples were then incubated for 5 mins at 25 °C, 30 mins at 42 °C, 5 mins at 85 °C, and finally held at 4 °C in a Master cycler Epgradient S (Eppendorf, USA). After completing the cDNA synthesis, 20 ng of cDNA samples in triplicate were used as templates, 7 µL of PerfectaSYBR Green fast master mix (P/N 84069, Quanta Bio, USA), and the desired primer mix of 10 µM was added before incubating again in a Master cycler Epgradient S (Eppendorf, USA). GAPDH normalized the expression of target genes in the same cDNA sample (Table 1). The relative expression of target genes was determined using the $2^{-\Delta\Delta Ct}$ method, where ΔCT (control) = CT (Target gene) - CT(GAPDH), ΔCT (test) = CT (Target gene) - CT(GAPDH). The mRNA expressions were normalized to the house GAPDH and presented in published papers from rat species, and a list of reverse and forward primers is shown in Table 3.

Table 3. Primer sequences of genes with the accession number and amplicon size

Gene	Sequence	AN	AS	Ref
AT2R	**5'**-GGTCTGCTGGGATTGCCTTAATG-**3'**	NM_0013856	142	(126)
	5'-ACTTGGTCACGGGTAATTCTGTTC-**3'**	24.1		
AT1R	**5'**-GGAAACAGCTTGGTGGTGAT-**3'**	NM_0087715	171	(127)
	5'-ACTAGGTGATTGCCGAAGG-**3'**	94.3		
ACE2	**5'**-ACCCTTCTTACATCAGCCCTACTG-**3'**	NM_0010120	74	(208)
	5'-TGTCCAAAACTACCCCACATAT-**3'**	06.2		
ACE	**5'**-TTTGCTACACAAATGGCACTTGT-**3'**	NM_012544.	67	(209)
	5'-CGGGACGTGGCCATTATATT-**3'**	1		
GAPDH	**5'**-CCTGCACCACCAACTGCTTA-**3'**	NM-017008.4	95	(210)
	5'-AGTGATGGCATGGACTGTGG-**3'**			

AT2R; Angiotensin II type 2 receptor, AT1Ra; Angiotensin II type 1 receptor a, ACE2; Angiotensin type converting enzyme 2, ACE; Angiotensin type converting enzyme, GAPDH; Glyceraldehyde-3-phosphate dehydrogenase, AN; Accession number, AS; Amplicon Size

4.9.9 Western Blot (WB) Analysis of the RAS Components

WB analysis was conducted on various rat tissues including heart, kidney, lung, and liver to study the protein expression of RAS components. The protocol used was published with some minor modifications. The frozen tissue samples were first thawed at room temperature, followed by homogenization of 25 mg of tissue in 1500 µL of radioimmunoprecipitation assay (RIPA) buffer containing a protease inhibitor tablet (1 tablet per 10 mL) (P/N 11697498001, Sigma Aldrich, St. Louis, MO, USA). The supernatants were collected after centrifugation at 15000 ×g for 15 mins at 4 °C, and the total protein was quantified using the Qubit® Protein assay kit

(Invitrogen, Eugene, OR, USA). The protein concentration ranged between 3-7 ng/mL. From each sample, a volume containing the same amount of protein (128 µg) was mixed with 1X lithium dodecyl buffer (LDS) buffer (P/N NP0007, Thermo Fisher Scientific, Waltham, MA, USA) and incubated at 95 °C for 7 mins using a Master cycler Epgradient S (Eppendorf, USA). 35 µL of the sample containing G-protein was loaded into each lane of a Tris-Glycine (4-12%) electrophoretic gel (P/N LC26754, Thermo Fisher Scientific, Waltham, MA, USA) and separated at 100 mV for 15 mins, followed by an increase to 200 mV. The proteins were then transferred to a PVDF membrane (P/N 1704156, Bio-rad, Hercules, CA, USA), which was washed with 0.1% Tween-containing tris base saline (TBST). The membrane was blocked by shaking with 5% skimmed milk powder in TBST for 1 hr at room temperature. The membrane was then incubated overnight at 4 °C with a primary antibody: ACE (Rabbit mono-clonal EPR22971-247 to ACE1, ab25422, Abcam1:1000), ACE2 (Rabbit monoclonal EPR4435(2) to ACE2, ab108252, Abcam1:1000), AT1R (Rabbit monoclonal EPR3873 to AT1R, ab124734, Abcam1:1000), AT2R (Rabbit monoclonal EPR3876 to AT2R, ab92445, Abcam1:1000), and β-actin (Mouse monoclonal AC-15 to β-actin, ab6276, Abcam1:1000). After washing the membrane four times for 10 minutes in TBST; it was incubated with Rabbit anti-mouse IgG with HRP Secondary Ab (NBP1-73435, Novus 1:10,000) for 1 hr at room temperature. The membrane was rewashed, incubated with Radiance Q Chemiluminescent substrate (Azure Biosystems, AC2101, Dublin, CA, USA), and imaged by an Azure biosystems c600 (Dublin, CA, USA) for 5-60 secs. The density of a specific band was then quantified using ImageJ software.

4.9.10 Immunohistochemistry (IHC) for RAS components

All frozen tissue samples were thawed at room temperature, and 50 mg of each sample was collected, washed with PBS, and excess solution was removed by blotting lightly with a Kim wipe. Tissue Trek® Cryomold® Molds/ Adapters, Sakura ® Fine trek, Intermediate Cryomold ®, L × W × D = 15 mm × 15 mm × 5 mm (Sakura P/N 4566, Radnor, PA, USA) were prepared by adding Tissue -Tek® O.C.T compound, Sakura ® Fine trek O.C.T compound (Sakura, P/N 4583, Radnor, PA, USA) and was properly labeled. The samples were then transferred to the molds with O.C.T, and swirled around with a pipette tip to semi-equilibrate the outside of the samples with O.C.T. The molds were then transferred to a liquid nitrogen tray and later stored at -20 °C.

To prepare for analysis, the molds containing the samples were sectioned to 5 µm by a Cryostat (Leica 3050 S Cryostat) and the resulting sections were placed in Fisher adhesive Microscope Slide (Fisher Scientific P/N 72204-40, Hampton, NH, USA). The sections were washed with phosphate-buffered saline with 0.1% tween (PBT) three times and peroxidase inactivation was done by applying 1% Hydrogen peroxide (H_2O_2) of H_2O_2 35% (w/w) in an aqueous solution (Alfa Aesar, P/N L14000-AP, Tewksbury, MA, USA) in 10 mL of PBT. The slides were then washed three times with PBT in a Coplin jar. Next, the slides were transferred to a humidified chamber, and 300 µL of Ultra Cruz blocking reagent (Santa Cruz Biotechnology P/N, SC-516214, Dallas, TX, USA) was added and incubated at room temperature for 2 hrs. After incubation, the pre-blocking solution was removed and replaced with primary antibody diluted in blocking solution, 300-400 µL per slide, and incubated overnight at 4 °C. The primary antibody used were ACE (Rabbit mono-clonal EPR22971-247 to ACE1, ab25422, Abcam1:100), ACE2 (Rabbit monoclonal EPR4435(2) to ACE2, ab108252, Abcam1:100), AT1R (Rabbit monoclonal

EPR3873 to AT1R, ab124734, Abcam1:100) and AT2R (Rabbit monoclonal EPR3876 to AT2R, ab92445, Abcam1:100).

After washing, the slides were returned to the horizontal rack and overlaid with a biotinylated secondary antibody (Goat anti-Rabbit IgG (H+L) Secondary Antibody horseradish peroxidase (HRP) (P/N NB7160, Novus biologicals, Centennials, CO, USA) for the species of the primary antibody diluted 1:250 in blocking solution with about ~300 µL and incubated at room temperature. The secondary antibody was then removed, and the slides were washed with PBT three times in a Coplin jar.

For detection, a 3,3'-diaminobenzidine (DAB) Enhanced substrate system tetrahydrochloride (Sigma-Aldrich, P/N D3939-1SET, St Louis, MO, USA) was prepared by mixing 2 drops of buffer solution and 4 drops of DAB solution with 5 mL of distilled water. After use, the substrate was disposed of in a bleach waste bottle since the DAB solution is considered toxic waste, and the slides were rinsed with water. DAB incubation could be repeated to achieve a more intense signal, followed by another rinse with water. Harris' hematoxylin (Electron Microscopy Sciences, P/N 26041-05, Hatfield, USA) was then washed with running water to counterstain the slides for 3 secs. The slides were dehydrated twice in 200-proof ethyl alcohol (Electron Microscopy Sciences, P/N 15058, Hatfield, USA), cleared three times with SafeClear II Xylene Substitutes (Thermo Fisher Scientific P/N AC302825000, Waltham, MA, USA) and mounted with Fluoromount-G® (Southern Biotech, P/N 0100-01, Birmingham, AL, USA) and covered with a 22 × 50 mm Microscopic Slide Cover glass (Electron Microscopy Sciences, P/N 26041-05, Hatfield, USA). The slides were then air-dried overnight and imaged using a Leica DM6B Upright Brightfield microscope at 20X magnification. After the immunohistochemical staining, images were scored semi-quantitatively for intensity by 3 graduate student researchers blinded.

A score of 0 represented minimal expression, 1 represented mild expression, 2 represented moderated expression, and 3 represented abundant expression (211).

4.9.11 Sample Preparation, Extraction, and LC-MS/MS Analysis of Ang Peptides

4.9.11.1 Chemicals

Ang 1-7 (Anaspec, AS-61039) and Ang II (Anaspec, AS-20633) were purchased from Anaspec Inc. (Fremont, CA, USA). Correspondingly, [asn^{1}, Val^{5}]-Angiotensin II) used as Internal Standard (IS) (Sigma-Aldrich A6402-1MG) was bought from Sigma Aldrich. C18 column (SepPak WAT020805) was bought from Waters (Milford, MA, USA). LC-MS grade water, acetonitrile, and formic acid were purchased from Fisher Scientific (Fair Lawn, NJ, USA).

4.9.11.2 Instrumentation

All LC-MS/MS experiments were carried out in an AB SCIEXQTRAP® 5500 mass spectrometer (Foster City, CA, USA) in tandem with a Nexera HPLC system from Shimadzu Corporation (Columbia, MD, USA). The HPLC system consists of a Sil-30AC autosampler, LC-30AD pumps, a CBM -30 A controller, a DGU-20A5R degasser, and a CTO-20A column oven. Analyst and Multiquanta software were used for data acquisition and quantitation.

4.9.11.3 Chromatographic and Mass Spectrometric Condition

Rat plasma samples were taken and analyzed for Ang 1-7 and Ang II levels by the published LC-MS/MS method (212). The method was applied for plasma sample analysis after minor modification and validation. Briefly, Ang peptides were separated by Synergi RP (2 mm×100 mm) column with a 2.5 µm particle size (Phenomenex, CA, USA) at ambient temperature. The mobile phase comprised of 0.1% formic acid in water (A) and ACN (B). The gradient time program started from 5% ACN to 30% ACN over 4 mins, and composition was kept constant for 4 to 8 mins, lowered to 5% ACN to 9 mins, and ran for 10 mins. The flow rate was 0.3 mL/min,

and the injection volume was 30 µL. Electrospray ionization was used, and analytes were detected using multiple reaction monitoring (MRM) in the positive mode. The optimized source/gas parameters were as follows: curtain gas, 30; collision gas, medium; ion spray voltage, 5500 V; temperature, 300 °C; ion source gas 1 (nebulizer gas), 20 psi; and ion source gas 2 (turbo gas), 25 psi. LC-MS analysis was performed with the single ion recording (SIR) mode, in which the *m/z* 300.5, 349.6, 516.6 were used for Ang 1-7, Ang II, and IS, respectively. LC-MS/MS has performed with MRM transitions of *m/z* 300.6→136 (Ang 1-7), *m/z* 349.6→136 (Ang II), and *m/z* 516→769.4 (IS).

4.9.11.4 Plasma Sample Preparation

An aliquot of 200 µL plasma, 100 µl of IS (100 ng/mL), and formic acid were added to the final concentration of 0.5% and mixed well. Solid-phase extraction (SPE) was done in Agilent positive pressure (PPE) manifold 48 processors. The sample solutions were applied to the C18 SPE cartridges (WAT020805, Milford, MA, USA) that had been preconditioned with 2 mL of ethanol and 2 mL of deionized water, respectively. After loading the sample, the cartridge was washed with 2 mL of deionized water. The water was let dry for 3 mins by turning on a high nitrogen gas flow. Then, Ang peptides were eluted from the cartridge using 2 mL methanol containing 5% formic acid, collected, and dried under the stream of nitrogen. Finally, the dried sample was reconstituted in water and transferred to a sample vial for LC-MS/MS analysis.

4.9.12 Sample Preparation, Extraction, and LC-MS/MS Analysis of ArA Metabolites

4.9.12.1 Chemicals

The reference standards were purchased from Cayman Chemical Company (Ann Arbor, MI, USA): 19-(R)-hydroxyeicosatetraenoic acid (19-HETE) (P/N, 10007767), 20-hydroxyeicosatetraenoic acid (20-HETE) (P/N, 90030), (±) 5,6-epoxyeicosatrienoic acid (5,6-

EET)(P/N, 50211), (±) 8,9-epoxyeicosatrienoic acid (8,9-EET) (P/N, 50351), (±)11,12-epoxyeicosatrienoic acid (11,12-EET) (P/N, 50511), (±)14,15-epoxyeicosatrienoic acid (14,15-EET)(P/N, 50651), (±) 5,6-dihydroxyeicosatrienoic acid (5,6-DiHT)(P/N, 51211), (±) 8,9-dihydroxyeicosatrienoic acid (8,9-DiHT)(P/N, 51351), (±) 11,12-dihydroxyeicosatrienoic acid (11,12-DiHT)(P/N, 51511), and (±) 14,15-dihydroxyeicosatrienoic acid (14,15-DiHT)(P/N, 51651). Additionally, the following deuterated internal standards (IS) were also obtained from Cayman: 8,9-EET-d11 (deuterium atoms at the 16, 16, 17, 17, 18, 18, 19, 19, 20, 20, and 20 positions; isotopic purity of ≥ 99%).

4.9.12.2 Instrumentation

Similar instrumentation to Ang peptide analysis was used for the ArA metaboliteS assay.

4.9.12.3 Chromatographic and Mass Spectrometric Conditions

The experimental protocol and assay condition were followed with slight optimization to analyze ArA metabolites as previously described (213). Briefly, eicosanoids were separated using a Synergi Reverse Phase (RP) (2 mm × 100 mm) column with a 2.5 µm particle size (Phenomenex, CA, USA) at ambient temperature. The mobile phase consisted of 0.1% formic acid in water (A) and ACN (B). The mobile phase gradient time program started from 5% ACN to 20% ACN over 2 mins, then increased to 55% ACN, kept constant for 2.5 to 6 mins, and increased to 100% ACN to 8 mins and ran until 9 mins. Then, it was subsequently reduced to 5% of ACN over a 10.5 mins total run. The flow rate was 0.3 mL/min, and the injection volume was 10 µL. The mass spectrometric condition consists of a triple quadrupole that is used to monitor their *m/z* transition by Analyst software. Electrospray ionization was used, and analytes were detected using MRM in the negative mode. The optimized source/gas parameters were as follows: curtain gas, 20 psi; collision gas, medium; ion spray voltage, −4500 V; temperature, 400

˚C; ion source gas 1 (nebulizer gas), 20 psi; and ion source gas 2 (turbo gas), 25 psi. LC-MS/MS analysis has been performed with MRM transitions for ArA metabolites according to the parameters listed in Table 4.

Table 4. Compound parameters for ArA metabolites and the deuterated IS with MRM in negative electrospray ionization mode.

Analyte	Q1 *m/z*	Q3 *m/z*	DPV	CE	CXP	EP
5,6-EET	319	191	-30	-14	-11	-10
8,9-EET	319	155	-30	-14	-11	-10
11,12-EET	319	208	-120	-18	-11	-10
11,12-EET	319	167	-120	-18	-11	-10
14,15-EET	319	219	-105	-16	-13	-10
5,6-DiHT	337	145	-115	-22	-11	-10
5,6-DiHT	337	145	-115	-22	-11	-10
8,9-DiHT	337	127	-105	-26	-11	-10
11,12-DiHT	337	167	-115	-24	-19	-10
14,15-DiHT	337	207	-40	-24	-13	-10
19-HETE	319	231	-125	-20	-12	-10
20-HETE	319	245	-95	-22	-15	-10

EET; epoxyeicosatrienoic acid, HETE; hydroxyeicosatetraenoic acid, DiHT; dihydroxyeicosatrienoic acid, DP; declustering potential, CE; collision energy, CXP; collision cell exit potential, EP; entrance potential.

4.9.12.4 Plasma Sample Preparation

An aliquot of 300 µL plasma sample was mixed with 100 µL of 8,9-EET d11 (IS, 100ng/mL), and 2 µL of FA was added. Then samples were vortex mixed and extracted with 500 µL of ethyl acetate twice. Each time samples were centrifuged at 15000 × g, 4 °C for 10 mins. 300 µL of the supernatant layer was taken after the first addition of ethyl acetate, and 500 µL of the supernatant layer was taken after the second addition of ethyl acetate. After mixing the separated organic phases, it was dried under nitrogen gas and reconstituted in methanol for LC-MS/MS analysis. The calibration curves were constructed over the range of 0.625 to 160 ng/mL for each ArA metabolite. The concentrations of each metabolite in the plasma samples were determined using the corresponding calibration curve.

4.9.13 Statistical Analysis

Data were analyzed by a standard computer program, GraphPad Prism Software PC software, version 9.3.1, Statistical Package for Social Sciences (SPSS) version 26 for Windows (SPSS Inc., Chicago, IL, USA) or Minitab software version 20 (Minitab LLC, Chicago, IL, USA) and are expressed as mean ± standard deviation (Mean ± SD) of at least three independent experiments. Data were analyzed for normal distribution and homogeneity of variance before proceeding with the parametric statistical tests. One-way analysis of variance (ANOVA) analyzed differences between mean values of multiple groups with Tukey's test for post hoc comparisons. To compare the % weight gain over time between treatment groups, a two-way ANOVA with post hoc Tukey's test was used. AI overtime between treatment groups was tested by the non-parametric Kruskal-Wallis's analysis of variance. The Mann-Whitney U-test was used to compare the significant difference between groups by SPSS. The linear correlation of ArA metabolites and RAS components was analyzed using GraphPad Prism software. The

orthogonal regression analysis was conducted to account for errors in observations on both the x- and the y- axis and find a line of best fit using Minitab software. *P*-values of less than 0.05 were considered statistically significant. The data labeled with different letters (a, b, c, or d) in tables or figures indicate a statistical difference between groups where $p < 0.05$.

4.10 Results

4.10.1 Effect of Novokinin and Novo Conj on Body Weight Gain and Clinical Symptoms of Adjuvant-Induced Arthritis

The appearance of adjuvant-induced arthritis (AIA) occurred 10-12 days after the injection. The initial signs were redness and inflammation of the paws and ankle joints, which then spread to the metatarsophalangeal and interphalangeal joints. The symptoms gradually extended to other areas of the hind and forepaws as time passed. Weight, paw size, and joint size measurements were taken three times per week. The percentage changes in paw and joint diameters on day 24 compared to day 0 are calculated.

The induction of arthritis caused a significant reduction in body weight gain, but treatment with novokinin and Novo Conj restored body weight over time. The percentage weight gain in the control rats was the highest at 54.8%, while arthritic rats without any treatment had the lowest weight gain at 8.8%. This suggests that arthritis induction disrupts the normal physiology of rats, leading to a significant drop in their percentage weight gain over time. However, drug treatment in arthritic rats caused an improvement in percentage weight gain. Arthritic rats treated with novokinin had a percentage weight gain of 34.8%, while arthritic rats treated with Novo Conj had a percentage weight gain of 42.7% over time. At the end of the treatment period, Novo Conj showed significant improvements in percentage body weight gain compared to its counterpart, then novokinin-treated rats.

The severity of signs and symptoms of arthritis were assessed using arthritis index (AI) scores. Arthritic rats had a higher AI score, which was calculated based on the number of paws and joints involved and their redness and swelling. However, at the end of the regimen, the score of Novo Conj treated rats was 2.2, and novokinin-treated rats was 3 thus showing a marked reduction in AI scores, significantly different from the arthritic group 5.2. Although therapeutic efficacy was observed after three consecutive doses, drug-treated rats showed marked differences at the end of the regimen, with Novo Conj-treated rats showing superior effects.

Table 5 shows that healthy rats have a standard percentage increase in paw and joint diameter due to their growth in body weight compared to day 0. Control rats had a 4.6 ± 3.6% increase in the left hind paw, 4.6 ± 3.6% increase in the right hind paw, 3.6 ± 3.7% increase in the left hind joint, and a 5.8 ± 3.2% increase in the right hind joint diameter. However, in arthritic rats, swelling due to inflammation resulted in a significant percent increase in diameter of 21.7 ± 4.9% and 23.7 ± 4.9% in the left and right hind paws, as well as a 25.7 ± 24.9% and 24.9 ± 5.7% increase in the left and right joint, respectively, compared to day 0. With novokinin treatment, there was a reduction in the percent increase by 16.9 ± 4.9% and 15.8 ± 3.9% in the left and right hind paws diameter, as well as an 18.7 ± 3.4% and 18.1 ± 6.3% reduction in the left and right joint diameter, respectively, in arthritic rats compared to day 0. Similarly, with Novo Conj treatment, the swelling rate was diminished by 13.9 ± 5.9% and 11.8 ± 4.9% in the left and right hind paws diameter, as well as a 10.4 ± 3.5% and 12.49 ± 2.7% reduction in the left and right joint diameter, respectively, in arthritic rats compared to day 0. These results indicate that both treatments reduced swelling, but Novo Conj treatment resulted in a better resolution of inflammation and reduced swelling.

Table 5. **Percent change in paw and joints diameter in different treatment groups on day 24 compared to day 0.**

	% increase in Paw Diameter		% increase in Joint Diameter	
Group	**L. Hind**	**R. Hind**	**L. Hind**	R. Hind
Control	4.6(3.6) [a]	4.3(2.6) [a]	3.6(3.7) [a]	5.8(3.2) [a]
Arthritic	21.7(4.9) [b]	23.7(4.9) [b]	25.7(4.8) [b]	24.9(5.7) [b]
Arthritic+ Novokinin	16.9(4.9) [b]	15.8(3.9) [b]	18.7(3.4) [c]	18.1(6.3) [b]
Arthritic+ Novo Conj	13.8(5.9) [c]	11.8(4.9) [c]	10.4(3.5) [d]	12.49(2.7) [c]

Novo Conj; Novokinin Conjugate, L. Hind; Left hind, R. Hind; Right hind. Mean ± SD (n = 5 or 6). Data labeled with different letters (a, b, c, or d) indicate a statistical difference between groups where $p < 0.05$.

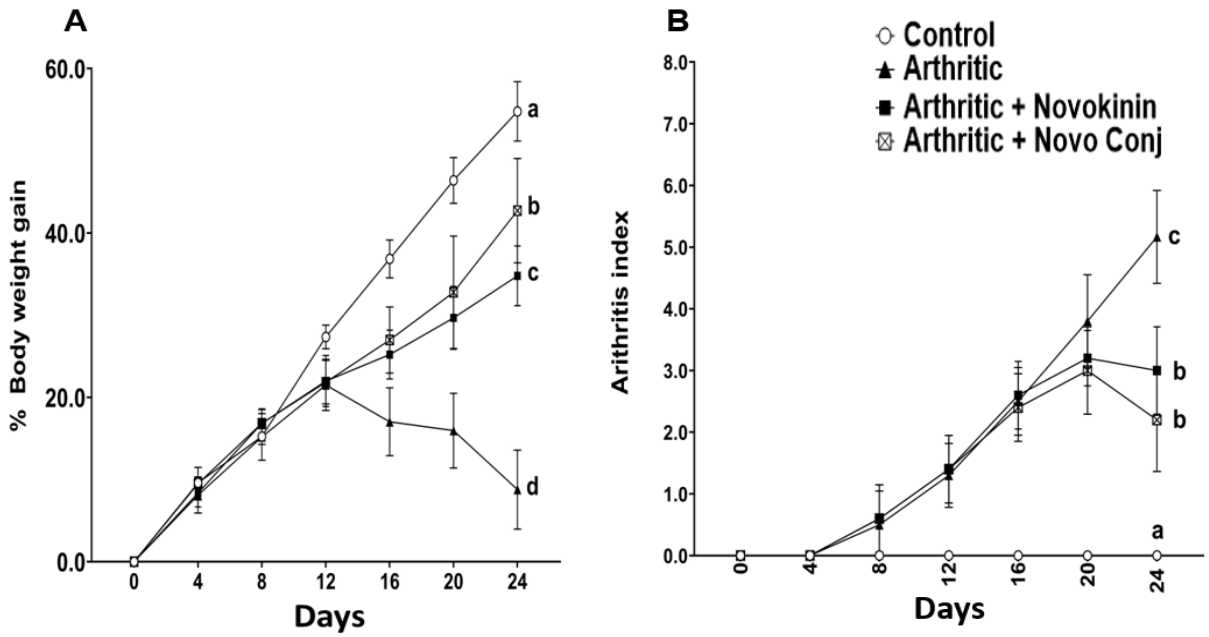

Figure 24.Treatment with Novokinin Conjugate (Novo Conj) restored (A) Body weight and decreased (B) Arthritis index (AI) score. Mean ± Standard deviation (SD) (n = 5 or 6 rats per group). Data labeled with different letters (a, b, or c) indicate a statistical difference between groups where p <0.05.

4.10.2 Novokinin and Novo Conj Reduce the Elevated Level of NO

Several studies have reported that NO is a marker of nitrosative stress and is directly involved in the pathogenesis of RA. Therefore, we used serum total NO as an indicator of inflammation resolution by Novo Conj treatment. In arthritic rats, inflammation drives up the NO level to 5.2 ng/µL. However, treatment with novokinin reduces the total NO level to 2.4 ng/µL, and Novo Conj further decreases it to 1.1 ng/µL. The total NO level in Novo Conj is almost comparable to control rats at 0.3 ng/µL. Figure 25 shows a significant improvement in the conjugate-treated arthritic rats.

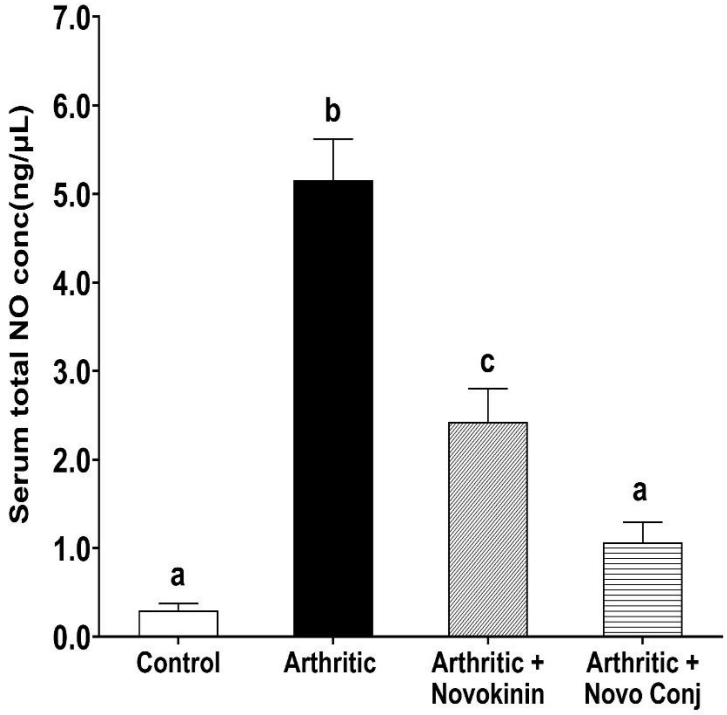

Figure 25. Treatment with Novokinin Conjugate (Novo Conj) reduced arthritis (AIA) induced elevated serum level of nitric oxide (NO). Mean ± Standard deviation (SD) (n = 5 or 6 rats per group). Data labeled with different letters (a, b, or c) indicate a statistical difference between groups where p <0.05.

4.10.3 Effect of Novokinin and Novo Conj on mRNA Expression of RAS Components

The mRNA expression of primary RAS components was analyzed in various tissues of rats in different treatment groups. The mRNA expression of ACE2 has been downregulated while that of ACE and AT1R is upregulated in inflamed rats compared to control and other treatment groups. This effect was reversed after novokinin or Novo Conj treatment, and there was an enhancement in ACE2 expression and a decline in elevated ACE and AT1R (data not shown). Figure 26A shows the ACE2/ACE fold increase ratio, normalized, and compared to control in the cardiac tissues. The treatment with Novo Conj improved the ACE2/ACE gene expression ratio significantly better than its parent compound. There was a trend in the increase of mRNA

expression of AT2R in the arthritic rats compared to the control group, and with the treatment, it was further increased (data not shown). However, as shown in Figure 26B, the AT2R/AT1R ratio fold was lower in the arthritic group compared to the control group. The treatment with Novo Conj upregulated the AT2R/AT1R ratio fold significantly higher than the control, arthritic, and arthritic + Novokinin-treated groups.

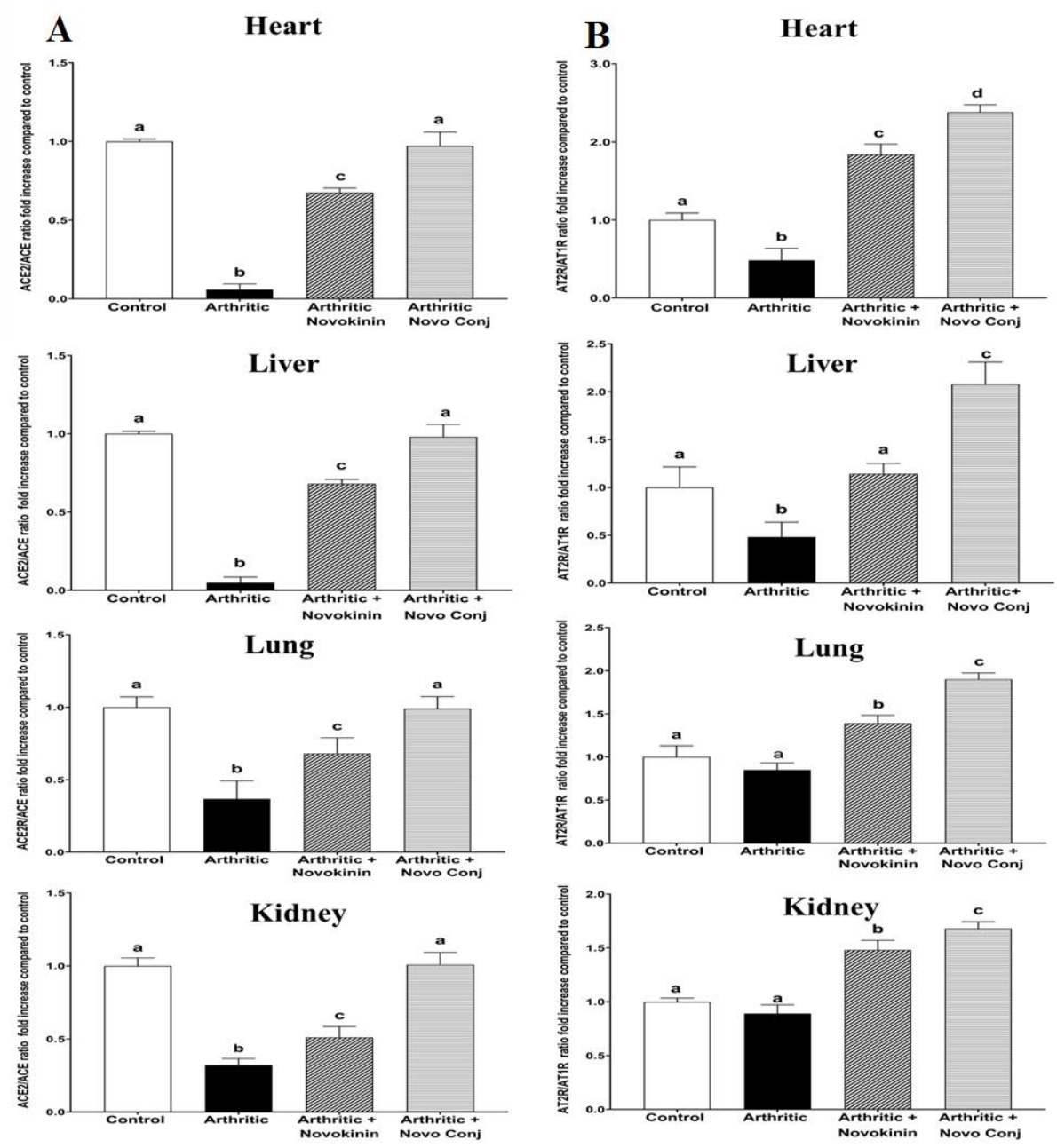

Figure 26. Novokinin Conjugate (Novo Conj) increases mRNA expression of (A) Angiotensin converting enzyme 2/ angiotensin converting enzyme (ACE2/ACE1) and (B) Angiotensin II type 2 receptor/ angiotensin II type 1 receptor (AT2R/AT1R) ratio fold compared to control in various tissues. Mean ± standard deviation (SD) of the mean (n = 5 or 6). Triplicates samples were run. Different letters represent statistical difference between groups where $p < 0.05$.

4.10.4 Effect of Novokinin and Novo Conj on Protein Expression of RAS Components by Western Blot (WB)

The protein expression of RAS components belonging to 2 opposite axes was investigated in various tissues like the heart, lung, liver, and kidney. The enzyme and receptor associated with the inflammatory axis ACE and AT1R were upregulated in arthritic rats. The drug treatment lowered their expression with a significant change seen in Novo Conj-treated rats than in the novokinin-treated group (Figure. 27A). In addition, a reverse effect was seen in the expression of an enzyme belonging to the anti-inflammatory axis ACE2 such that the ACE2/ACE ratio was higher in the Novo Conj group and comparable to the control. Like its gene expression, the protein expression of AT2R was upregulated in arthritic rats, and the treatment with drugs further increased their expression (data not shown). However, as shown in Figure 27B, the AT2R/AT1R protein expression ratio was significantly lower in the arthritic rats than in the control group. The treatment with novokinin restores it to a comparable level as the control group, while Novo Conj-treatment increases significantly compared to other treatment groups. Although there was not the same intensity of upregulation of beneficial RAS components over various tissues, similar trends were seen over all the tissues.

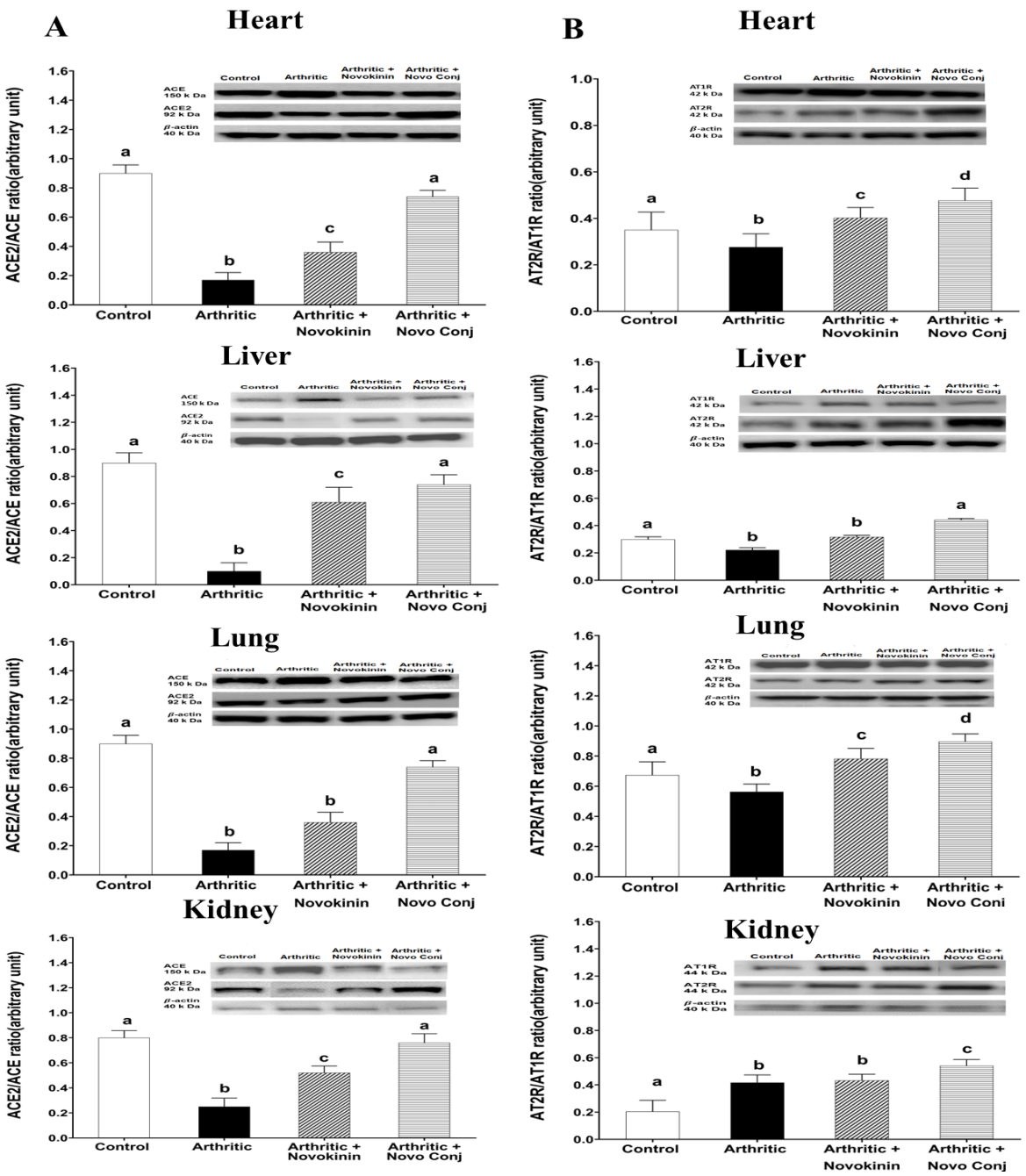

Figure 27. Novokinin Conjugate (Novo Conj) increases protein expression of (A)Angiotensin converting enzyme 2/ angiotensin converting enzyme (ACE2/ACE1) and (B) Angiotensin II type 2 receptor/ angiotensin II type 1 receptor (AT2R/AT1R) ratio in various tissues. Mean ± standard deviation (SD) of the mean (n = 5 or 6). Triplicates samples were run. Different letters represent statistical difference between groups where $p < 0.05$.

4.10.5 Effect of Novokinin and Novo Conj on protein expression of RAS components by Immunohistochemistry (IHC)

IHC was used to examine the expression of various components of the RAS, such as ACE, ACE2, AT1R, and AT2R, in tissues such as the heart, liver, lung, and kidney. In arthritic rats, the RAS axis was severely dysregulated, as evidenced by upregulation of ACE, AT1R, and AT2R and downregulation of ACE2 expression, compared to control rats. However, treatment with drugs led to a restoration of RAS balance, as observed in the tissues of rats treated with Novo Conj, which showed higher levels of ACE2 and AT2R and lower levels of ACE and AT1R compared to rats treated with novokinin as demonstrated in Figure 28 , 29, 30, 31. Furthermore, semi-quantitative results using a score ratio confirmed the shift towards a protective RAS axis as part of the resolution of inflammation following Novo Conj administration.

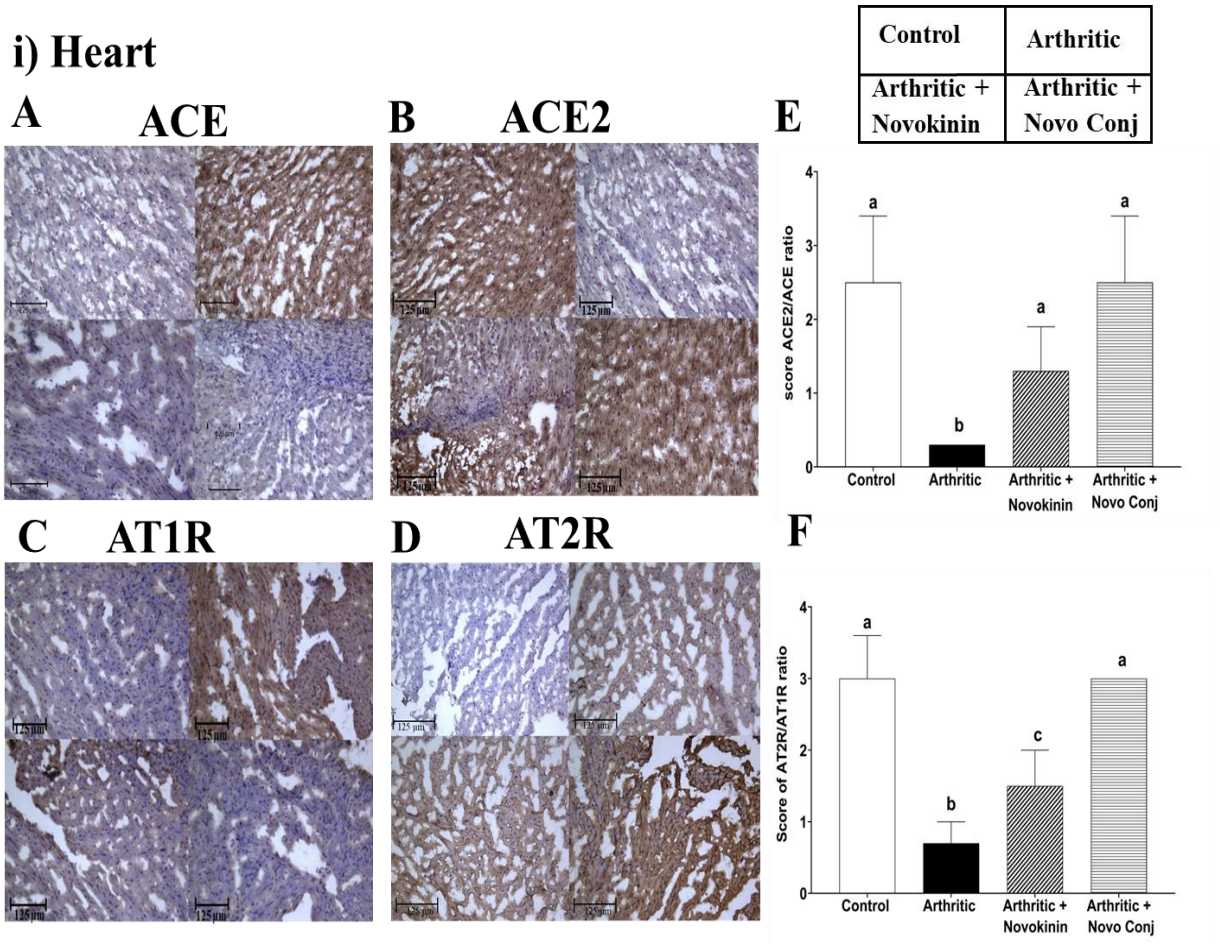

Figure 28. Effect of Novokinin Conjugate (Novo Conj) on protein expression in heart tissues. Representative images with scale bar 125 µM stained by various renin-angiotensin components (RAS) components by (A) Angiotensin converting enzyme (ACE) (B) Angiotensin converting enzyme 2 (ACE2) (C) Angiotensin II type 1 receptor (AT1R) and (D) Angiotensin II type 2 receptor (AT2R) (E) Intensity score ACE2/ACE and (F) AT2R/AT1R was graded in a blinded manner as described in material and methods.

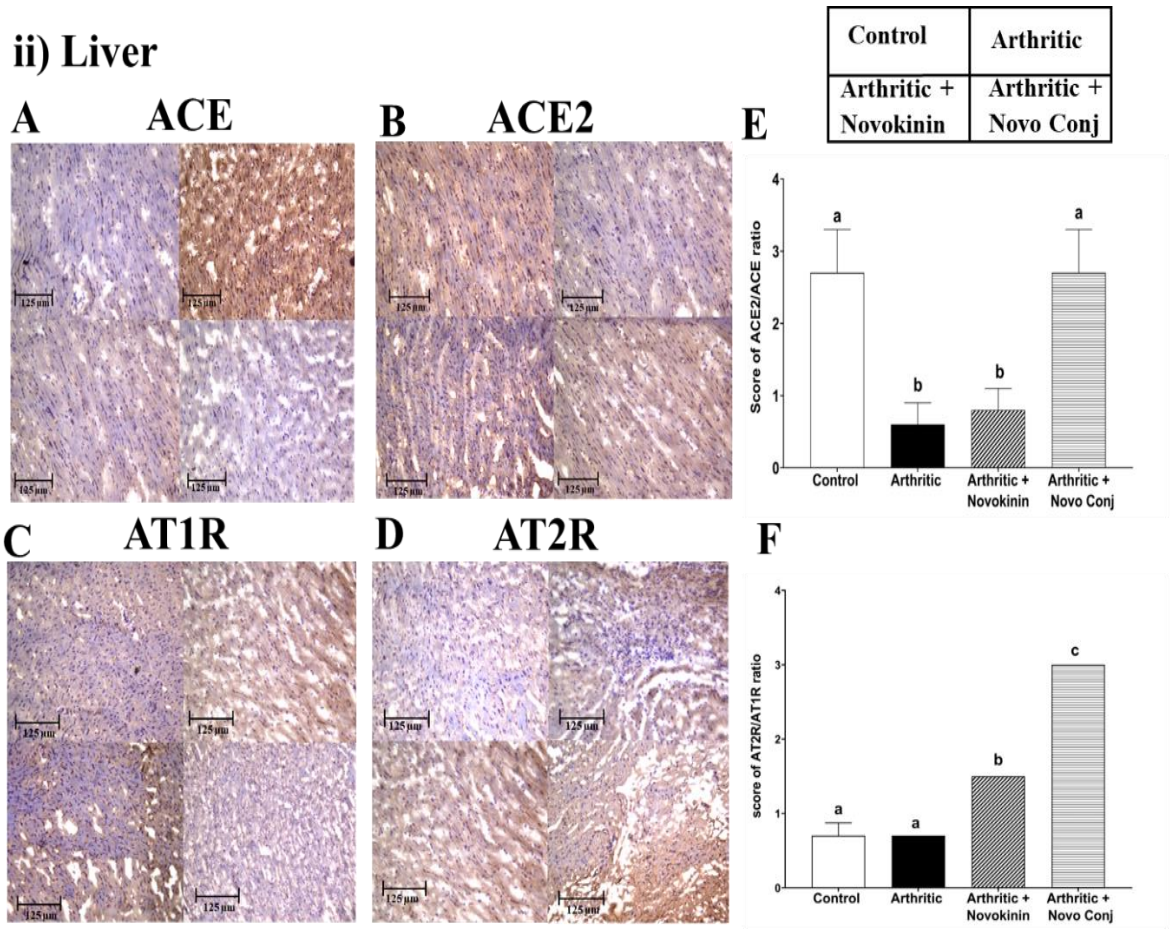

Figure 29. Effect of Novokinin Conjugate (Novo Conj) on protein expression in liver tissues. Representative images with scale bar 125 µM stained by various renin-angiotensin components (RAS) components by (A) Angiotensin converting enzyme (ACE) (B) Angiotensin converting enzyme 2 (ACE2) (C) Angiotensin II type 1 receptor (AT1R) and (D) Angiotensin II type 2 receptor (AT2R) (E) Intensity score of ACE2/ACE and F) AT2R/AT1R was graded in a blinded manner as described in material and methods.

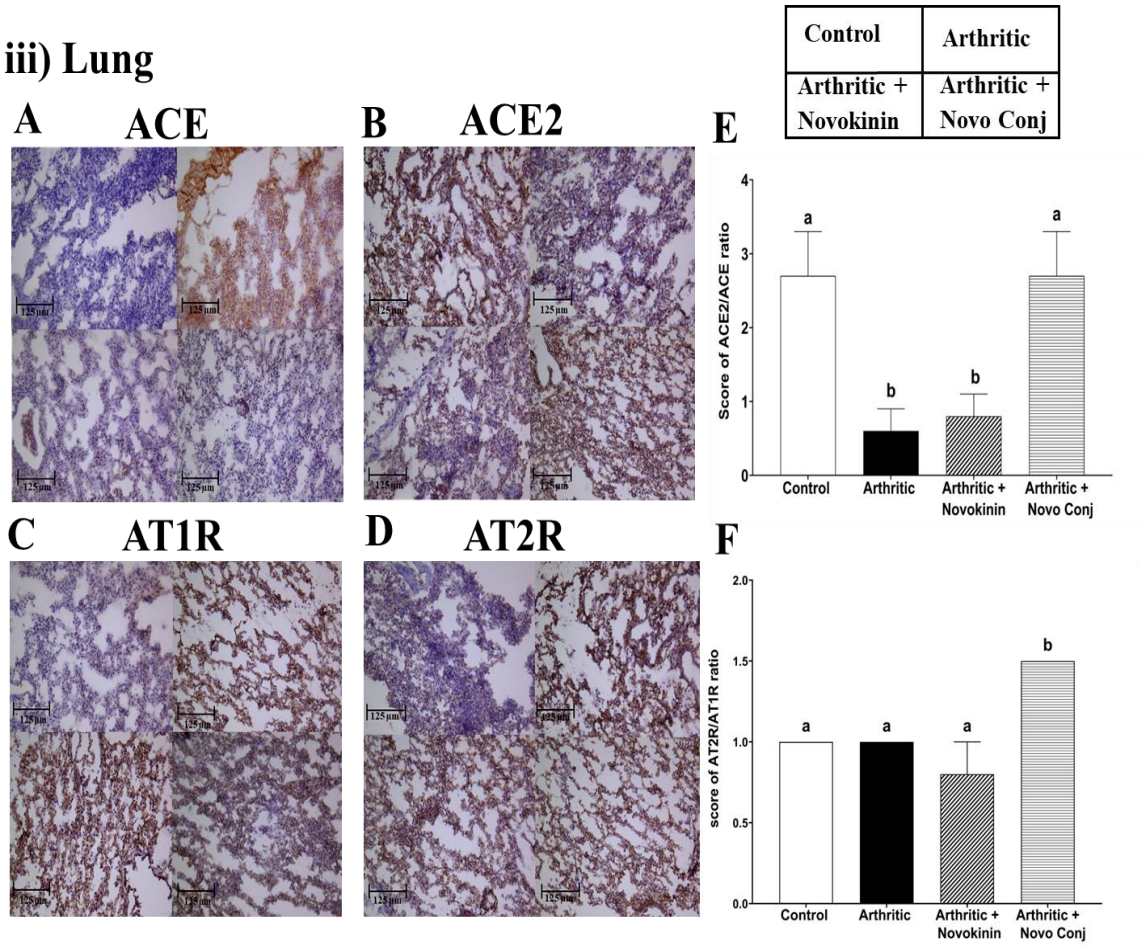

Figure 30. Effect of Novokinin Conjugate (Novo Conj) on protein expression in lung tissues. Representative images with scale bar 125 µM stained by various renin-angiotensin components (RAS) components by (A) Angiotensin converting enzyme (ACE) (B) Angiotensin converting enzyme 2 (ACE2) (C) Angiotensin II type 1 receptor (AT1R) and D) Angiotensin II type 2 receptor (AT2R) (E) Intensity score of ACE2/ACE and (F) AT2R/AT1R was graded in a blinded manner as described in material and methods.

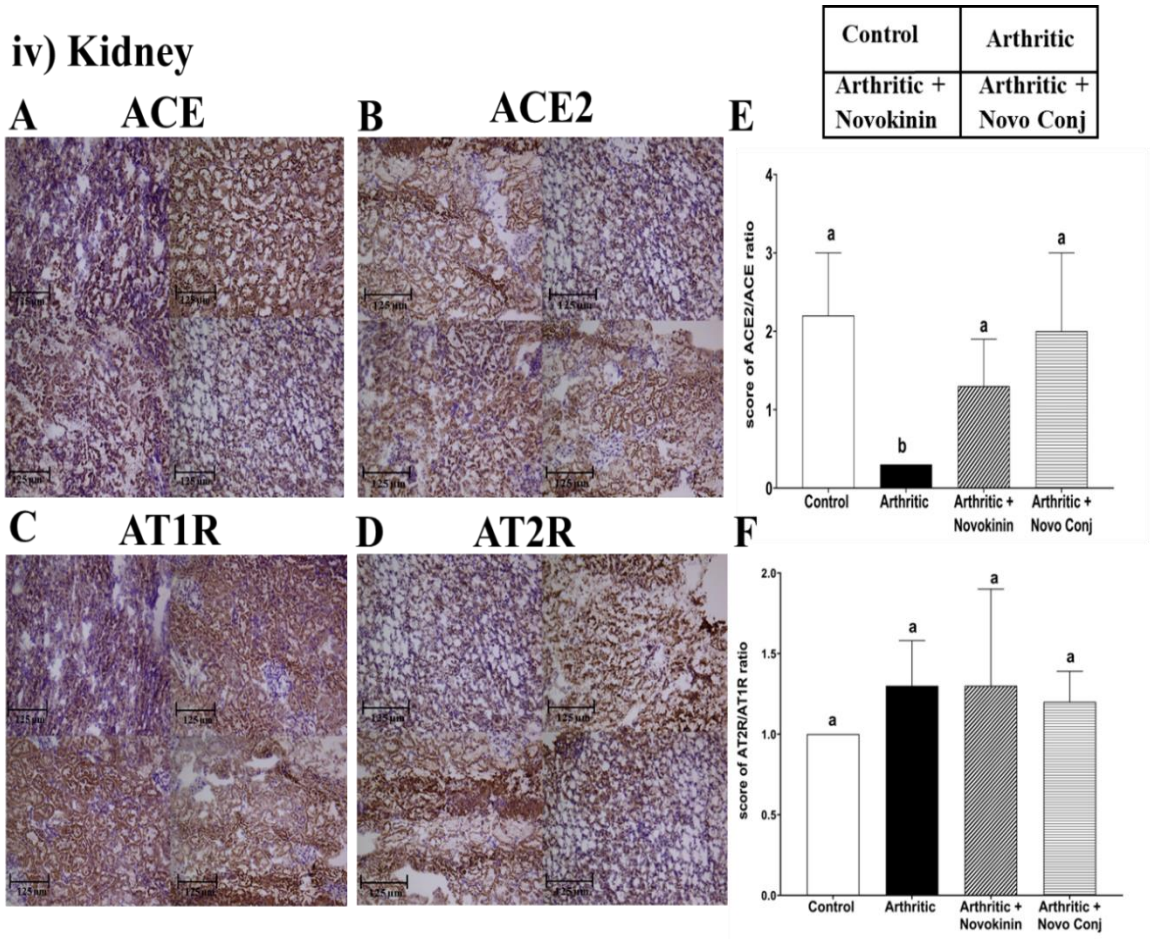

Figure 31. Effect of Novokinin Conjugate (Novo Conj) on protein expression in kidney tissues. Representative images with scale bar 125 µM stained by various renin-angiotensin components (RAS) components by (A) Angiotensin converting enzyme (ACE) B) Angiotensin converting enzyme 2 (ACE2) C) Angiotensin II type 1 receptor (AT1R) and (D) Angiotensin II type 2 receptor (AT2R) (E) Intensity score of ACE2/ACE and (F) AT2R/AT1R was graded in a blinded manner as described in material and methods.

4.10.6 Effect of Novokinin and Novo Conj in Ang 1-7 and Ang II Plasma Levels

The calibration curves were constructed over the range of 0.31 ng/mL to 5 ng/mL for Ang 1-7 and 200 pg/mL to 3200 pg/mL for Ang II for LC-MS/MS injection. Based on the chromatograph, it was determined that Ang 1-7 was observed at 4.14 mins at 300.6 →136 transitions, Ang II was observed at 4.94 mins at 349.6 →136 transitions and IS at 4.41 mins at 516 →769 transitions. The representative chromatograph is given on Figure 32. The Ang peptides concentrations were determined by comparing using the calibration curves. The precision and accuracy were evaluated by analyzing spiked plasma samples in triplicate at the following concentrations presented in Table 6. Accuracy was calculated using the following equation: Accuracy (%) = [(Mean observed measured concentrations/spiked concentrations)] ×100. The LLOQ was 0.15 ng/mL and 100 pg/mL for Ang 1-7 and Ang II, respectively. The coefficient of variance CV and accuracy percentage of Ang peptide are within the accepted range of less than 20% and between 80-120%, respectively.

Table 6. Inter- and intra-day precision and accuracy of angiotensin peptides.

Conc.	Intra-day		Inter-day	
	Precision (CV%)	Accuracy (%)	Precision (CV%)	Accuracy (%)
Ang 1-7 (ng/mL)				
0.31	9.39	105.61	6.64	102.74
1.25	3.42	95.11	1.29	108.09
5	1.34	100.78	2.17	98.95
Ang II (pg/mL)				
200	5.05	102.94	8.45	96.81
800	2.39	102.52	5.69	100.95
3200	1.076	99.12	0.95	101.03

Concentration; Conc., Ang 1-7; Angiotensin 1-7, Ang II; Angiotensin II, CV; Coefficient of Variance

The treatment with novokinin and Novo Conj affected the RAS enzymes, receptor, and the RAS peptides. AIA led to a decrease in the Ang 1-7 plasma level in the arthritic group (0.21 ± 0.051 ng/mL), but the treatment helped to restore its level. As presented in Figure 33A, Novo Conj had a significantly better effect (0.91 ± 0.03 ng/mL) than novokinin (0.49 ± 0.057 ng/mL) in restoring depleted Ang 1-7 levels in arthritic rats. Furthermore, the plasma level of Ang II increased (1214.85 ± 325.89 pg/mL), resulting in a remarkable reduction of the Ang II level in the novokinin (263.043 ± 53.88 pg/mL) and Novo Conj (215.71 ± 48.01 pg/mL) treated arthritic rats (Figure 30B&C), which were almost comparable to control rats (197.42 ± 39.28 pg/mL). The Ang 1-7/Ang II ratio in Figure 33C demonstrates that the administration of novokinin and Novo Conj restored the peptide ratio by decreasing Ang II and increasing Ang 1-7 levels to values comparable to those of the control group, mainly in the case of Novo Conj (Figure 30).

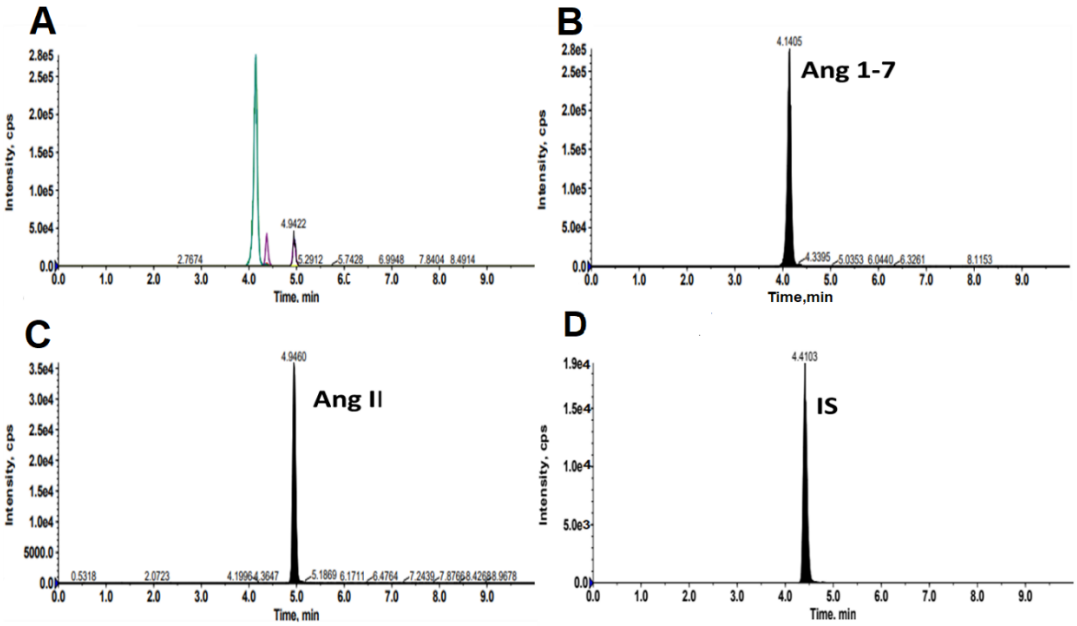

Figure 32. Representative chromatograph from LC-MS/MS analysis of angiotensin (Ang) peptides (A) Total ion chromatograph (TIC), extracted ion chromatograph (XIC) (B) Angiotensin 1-7 (Ang 1-7) (C) Angiotensin II (Ang II) (D) Internal Standard (IS).

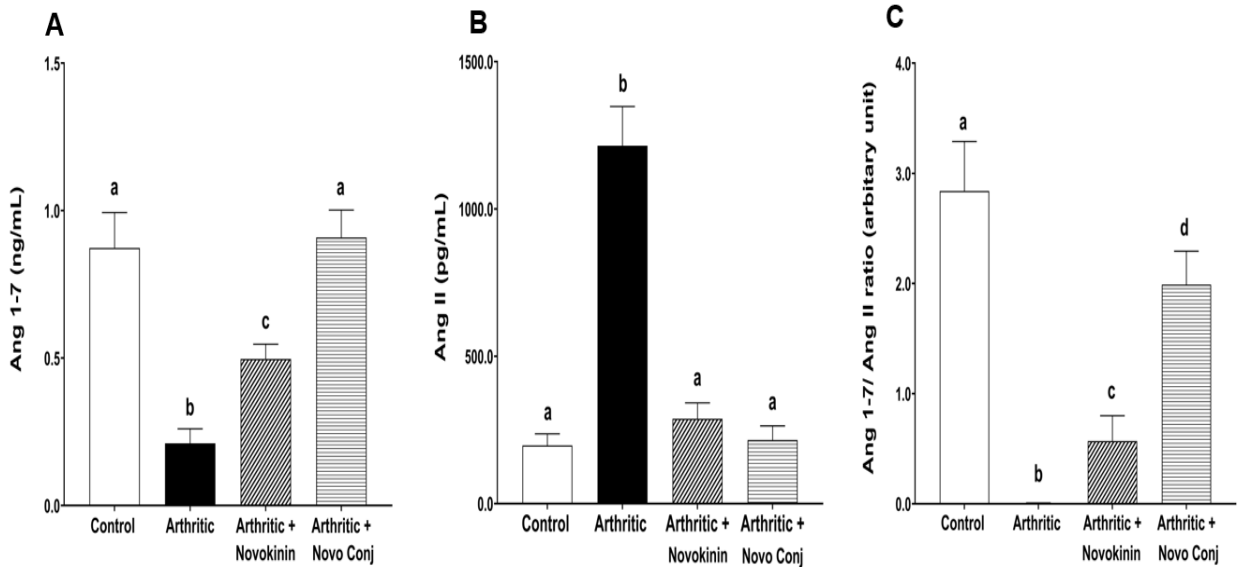

Figure 33. Novokinin and Novokinin Conjugate (Novo Conj) significantly (A) Increased angiotensin 1-7 (Ang 1-7), (B) Decreased angiotensin II (Ang II) levels, and (C) Increased the Ang 1-7/Ang II ratio in plasma of adjuvant-induced arthritis (AIA) rats. Mean ± Standard deviation (SD) (n = 5 or 6). Triplicates samples were run. Data labeled with different letters (a, b, c, or d) indicate a statistical difference between groups where p <0.05.

4.10.7 Effect of Novokinin and Novo Conj on ArA Metabolites Levels and Their Correlation with RAS Components

Calibration curves were created for each ArA metabolite across the 0.625 to 160 ng/mL range. Upon analysis of the chromatogram, the following observations were made: 5,6-EET was detected at 8.89 mins with 319→191 transitions, 8,9-EET was detected at 8.86 mins with 319→155 transitions, 11,12-EET was detected at 8.84 mins with 319→208 transitions, 14,15-EET was detected at 8.67 mins with 319→219 transitions, 19-HETE was detected at 7.09 minutes with 319→231 transitions, 20-HETE was detected at 7.29 mins with 319→245 transitions, 5,6-DiHT was detected at 7.02 mins with 337→145 transitions, 8,9-DiHT was detected at 6.67 mins with 337→127 transitions, 11,12-DiHT was detected at 6.39 mins with 337→167 transitions, 14,15-DiHT was detected at 6.12 mins with 337→207 transitions and IS was detected at 8.77 mins with 330→167 transitions. The concentrations of each metabolite in the plasma samples were determined using the corresponding calibration curve. The LLOQ, precision, and accuracy were evaluated by analyzing spiked plasma samples in triplicate at the following concentrations listed in Table 7.

The induction of arthritis led to an imbalance in ArA metabolism and RAS. Control rats exhibited a low level of total-HETEs (T-HETEs) at 16.39 ± 2.18 ng/mL, whereas arthritic rats had significantly higher levels at 116.6 ± 4.27 ng/mL. However, treatment with Novokinin and Novo Conj reduced the upregulated T-HETEs levels in AIA rats to 31.79 ± 8.66 ng/mL and 14.04 ± 1.83 ng/mL, respectively, as shown in Figure 35A. Conversely, control rats had high total-DiHTs (T-DiHTs) levels at 13.26 ± 1.63 ng/mL compared to arthritic rats without treatment who had only 3.11 ± 1.25 ng/mL. Novokinin-treated rats had 5.44 ± 1.61 ng/mL, and Novo Conj-treated rats had 8.19 ± 1.39 ng/mL. The total-EETs, which is the primary antioxidant

metabolite in CYP-derived ArA metabolism, exhibited the highest concentration in control rats at 98.23 ± 7.91 ng/mL. In comparison, the lowest concentration was observed in arthritic rats without treatment at 12.54 ± 2.91 ng/mL. Novokinin-administered rats had an intermediate level of 49.11 ± 11.61 ng/mL, and Novo Conj-administered rats had an even higher level of 72.11 ± 4.36 ng/mL. As reported in Figures 35B and 35C, drug treatment positively impacted on increasing T-EETs and T-DiHTs in plasma, bringing their levels closer to those of control rats. Consequently, the ratio of T-EETs/T-HETEs was significantly upregulated in the plasma of Novo Conj-treated rats compared to novokinin-treated rats, indicating that the former was a better treatment option when comparing ArA metabolite ratios across treatment groups (Figure 35D).

We also observed significant linear correlations between different ArA metabolites and RAS peptide levels in the plasma (Table 8). Strong and positive correlations existed between some individual EETs, DiHTs, T-EETs, T-DiHTs, T-EETs/T-HETEs, and T-DiHTs/T-HETEs with Ang 1-7 plasma levels. At the same time, those metabolites were inversely correlated with Ang II plasma levels. Accordingly, we observed a strong positive correlation between individual HETEs and T-HETEs with Ang II levels. In contrast, the sign of correlations was inversed in the case of Ang 1-7.

We conducted an orthogonal regression analysis to account for errors in observations on the x- and the y-axis (RAS peptides and ArA metabolites) and find a line of the best fit. The analysis outputs are presented in Table 9,10, Figure 36 and 37. The results shown in Figure 36, column 1, suggest that the best-fitted least-square and orthogonal regression lines, which were used to analyze the relationship between the RAS components and ArA metabolites of Total-EETs, Total-HETEs, and Total-DiHTs, indicate that the regression lines are identical in the case of Ang

1-7. Additionally, the graph shows that the regression lines are well-aligned with each other in the case of Ang II. The normal probability plots in the column of both figures display that the data sets are approximately normally distributed, and no outliers were identified in the data sets. The residuals of calculated values of RAS components are plotted against the experimental values in column 3 in Figure 36 and 37. As illustrated, the propagation of the residuals on both sides of the zero line indicates that no symmetric error exists in the development of the regression models.

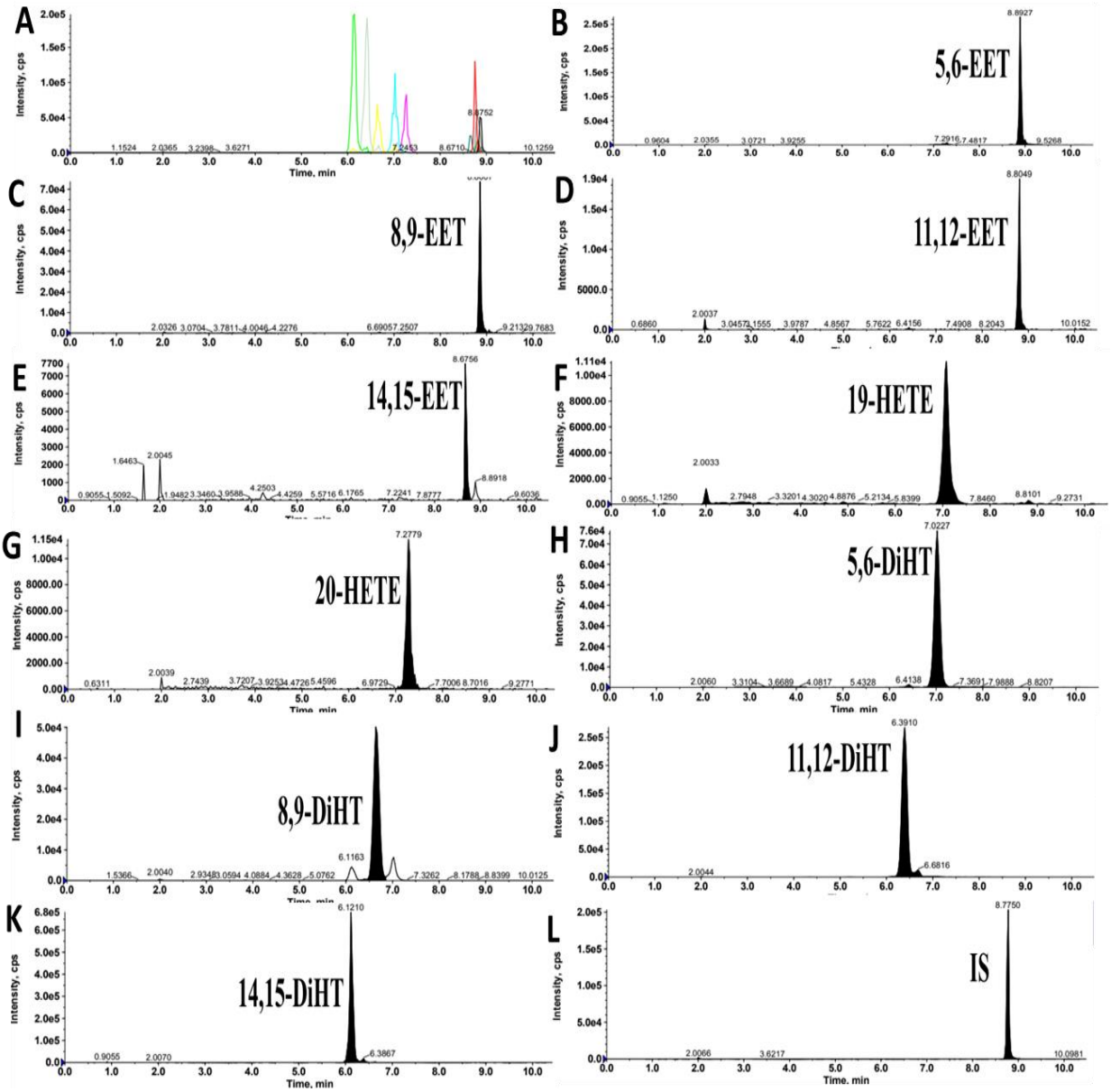

Figure 34. Representative chromatograph from LC-MS/MS analysis of Archidonic acid (ArA) metabolites (A) Total ion chromatograph (TIC) Extracted ion chromatograph (XIC) (B) 5,6-epoxyeicosatrienoic acid (5,6-EET), (C) 8,9-epoxyeicosatrienoic acid (8,9-EET), (D) 11,12-epoxyeicosatrienoic acid (11,12-EET), (E) 14,15-epoxyeicosatrienoic acid (14,15-EET), (F) 19-hydrooxyeicosatetraenoic acid (19-HETE), (G) 20-hydrooxyeicosatetraenoic acid (20-HETE), (H) 5,6-dihydroxyeicosatrienoic acids (5,6-DiHT), (I) 8,9-dihydroxyeicosatrienoic acids (8,9-DiHT), (J) 11,12-dihydroxyeicosatrienoic acids (11,12-DiHT), (K) 14,15-dihydroxyeicosatrienoic acids (14,15-DiHT) and (L) Internal Standard (IS).

Table 7. Inter-day and intra-day precision and accuracy of ArA metabolites

Conc.	Intra-day		Inter-day		
	Precision (CV%)	Accuracy (%)	Precision (CV%)	Accuracy (%)	LLOQ
5,6-EET (ng/mL)					0.07 ng/mL
0.62	8.76	101.883	4.53	107.73	
5	2.12	101.46	3.76	103.41	
40	7.23	98.27	6.36	99.30	
160	0.73	100.26	0.68	100.06	
8,9-EET (ng/mL)					0.28 ng/mL
0.62	3.13	106.12	7.74	101.86	
5	6.51	99.96	6.84	100.53	
40	4.89	100.66	4.32	99.86	
160	0.34	100.22	0.22	100.56	
11,12-EET (ng/mL)					0.45 ng/mL
0.62	3.57	103.76	7.62	97.68	
5	0.41	102.64	9.76	98.04	
40	1.92	98.91	2.31	96.67	
160	0.17	100.45	1.71	101.78	
14,15-EET (ng/mL)					0.31 ng/mL
0.62	7.54	100.26	6.69	96.53	
5	6.89	96.53	7.58	103.06	
40	6.55	99.525	5.74	101.35	
160	2.28	101.64	1.12	102.61	
5,6-DiHT (ng/mL)					0.14 ng/mL
0.62	5.97	101.33	9.37	97.06	
5	5.11	107.86	9.55	99.60	
40	2.95	103.15	5.85	104.37	
160	0.62	102.29	1.34	101.81	
8,9-DiHT (ng/mL)					0.01 ng/mL
0.62	9.74	101.33	9.35	100.26	
5	9.06	105.33	5.18	102.01	
40	3.06	102.28	3.11	100.23	
160	1.06	101.60	1.81	101.37	
11,12-DiHT(ng/mL)					0.20 ng/mL
0.62	5.00	104.80	7.92	101.54	
5	3.22	110.26	2.25	105.86	
40	2.73	106.32	2.43	103.44	
160	2.00	100.30	1.81	101.21	
14,15-DiHT (ng/mL)					0.12 ng/mL
0.62	4.76	99.62	3.91	103.78	
5	3.19	105.33	2.45	102.2	
40	2.17	103.44	4.46	101.95	
160	0.31	101.73	1.69	102.13	

19-HETE (ng/mL)					0.18 ng/mL
0.62	4.33	96.48	9.61	102.4	
5	5.49	110.40	4.23	114.6	
40	1.82	105.29	3.67	107.14	
160	2.81	102.69	2.26	102.27	
20-HETE (ng/mL)					0.25 ng/mL
0.62	4.87	105.51	3.38	106.56	
5	5.04	113.07	3.06	109.73	
40	2.91	106.89	1.87	106.87	
160	1.10	101.64	1.46	102.83	

Concentration; Conc., EET; epoxyeicosatrienoic acid, HETE; hydroxyeicosatetraenoic acid, DiHT; dihydroxyeicosatrienoic acid, LLOQ; Lower Limit of Quantification

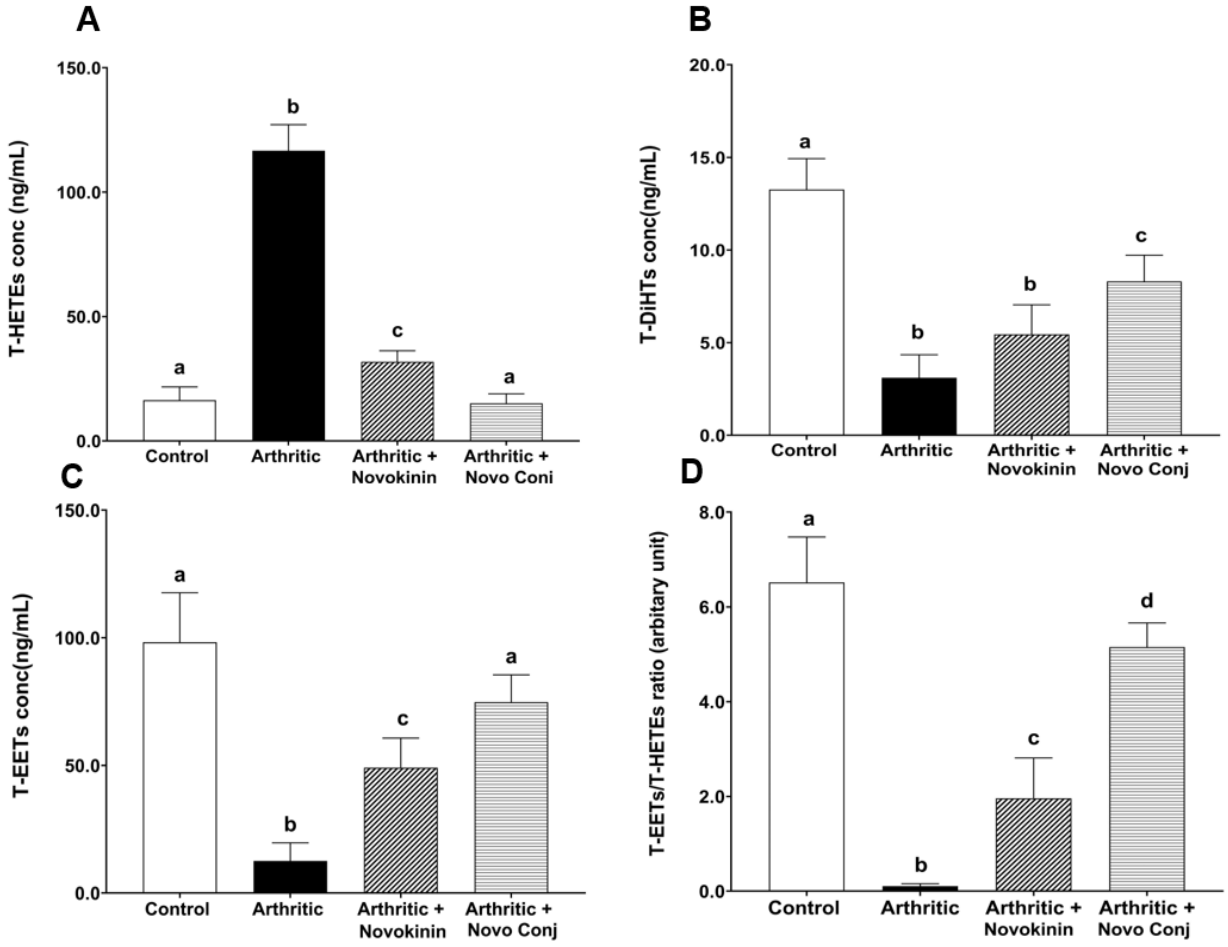

Figure 35. Impact of novokinin and Novokinin Conjugate (Novo Conj) treatment on (A) Total-hydroxyeicosatetraenoic acids (T-HETEs), (B) Total-dihydroxyeicosatrienoic acids (T-DiHTs), (C) Total-epoxyeicosatrienoic acids (T-EETs), and (D) the ratio of T-EETs/T-HETEs arthritic rats' plasma. Mean ± SD (n = 5 or 6). Data labeled with different letters (a, b, c, or d) indicate a statistical difference between groups where p <0.05.

Table 8. Significant linear correlations between RAS peptides and ArA metabolites

	Ang 1-7		Ang II	
Plasma ArA metabolites	**r**	***P* value**	**r**	***P* value**
11,12- EET	0.7188	**0.0002**	-0.5613	**0.0066**
14,15-EET	0.7245	**0.0001**	-0.6809	**0.0005**
T-EETs	0.7110	**0.0002**	-0.5887	**0.0039**
19-HETE	-0.7001	**0.0003**	0.6209	**0.0021**
20-HETE	-0.7379	**<0.0001**	0.7518	**<0.0001**
T-HETEs	-0.7381	**<0.0001**	0.7474	**<0.0001**
T-EETs/T-HETEs	0.6505	**0.0010**	-0.5382	**0.0098**
5,6-DiHT	0.5525	**0.0077**	-0.4943	**0.0194**
8,9-DiHT	0.6846	**0.0004**	-0.5679	**0.0058**
11,12-DiHT	0.4643	**0.0295**	-0.5157	**0.0140**
T-DiHTs	0.4674	**0.0283**	-0.5619	**0.0065**
T-DiHTs/T-HETEs	0.4693	**0.0276**	-0.4631	**0.0301**

EET; epoxyeicosatrienoic acid, T-EETs; Total-EETs, HETE; hydroxyeicosatetraenoic acid, T-HETEs; Total-HETE, DiHT; dihydroxyeicosatrienoic acid, T-DiHTs; Total-DiHTs

Table 9. Orthogonal regression analysis result of Ang 1-7

Predictor	Coef.	SE of Coef.	Z value	*P* value	Constant Coef.	Error in X-axis	Error in Y-axis
11,12-EET	0.012	0.003	4.600	0.000	0.246	0.068	0.061
14,15-EET	0.019	0.004	4.830	0.000	0.252	0.064	0.058
Total EETs	0.007	0.001	4.580	0.000	0.220	0.068	0.061
19-HETE	-0.110	0.025	-4.338	0.000	0.850	0.071	0.064
20-HETE	-0.006	0.001	-4.853	0.000	0.883	0.064	0.058
Total-HETE	-0.006	0.001	-4.854	0.000	0.882	0.064	0.058
T-EETs/T-HETEs	0.075	0.020	3.756	0.000	0.355	0.081	0.073
5,6-DiHT	0.247	0.083	2.966	0.003	0.361	0.091	0.082
8,9-DiHT	1.183	0.281	4.208	0.000	-0.006	0.037	0.033
11,12-DiHT	0.070	0.030	2.336	0.020	0.392	0.109	0.098
Total DiHT	0.032	0.014	2.366	0.018	0.371	0.109	0.098

EET; epoxyeicosatrienoic acid, T-EETs; Total-EETs, HETE; hydroxyeicosatetraenoic acid, T-HETEs; Total-HETE, DiHT; dihydroxyeicosatrienoic acid, T-DiHTs; Total-DiHTs

Table 10. Orthogonal regression analysis result of Ang II

Predictor	Coef.	SE of Coef.	Z value	*P* value	Constant Coef.	Error in X-axis	Error in Y-axis
11,12-EET	-52.876	18.723	-2.824	0.005	2076.738	291.826	262.643
14,15-EET	-63.560	15.490	-4.103	0.000	1724.281	100.672	90.605
Total EETs	-27.711	8.968	-3.090	0.002	2100.215	897.738	807.964
19-HETE	426.846	124.759	3.421	0.001	-407.324	3.147	2.833
20-HETE	18.379	3.673	5.004	0.000	-319.640	817.982	736.184
Total HETEs	17.615	3.569	4.935	0.000	-322.993	914.167	822.750
T-EETs/T-HETEs	-362.518	133.396	-2.718	0.007	1760.554	6.668	6.001
5,6-DiHT	-1372.640	586.893	-2.339	0.019	1913.940	0.609	0.548
8,9-DiHT	-3301.788	1122.04	-2.943	0.003	2232.545	0.070	0.063
11,12-DiHT	-496.300	201.883	-2.458	0.014	2087.269	4.260	3.834
14,15-DiHT	-569.245	254.774	-2.234	0.025	2099.332	3.835	3.451
Total DiHTs	-208.195	72.326	-2.879	0.004	2074.492	18.206	16.385

EET; epoxyeicosatrienoic acid, T-EETs; Total-EETs, HETE; hydroxyeicosatetraenoic acid, T-HETEs; Total-HETE, DiHT; dihydroxyeicosatrienoic acid, T-DiHTs; Total-DiHTs

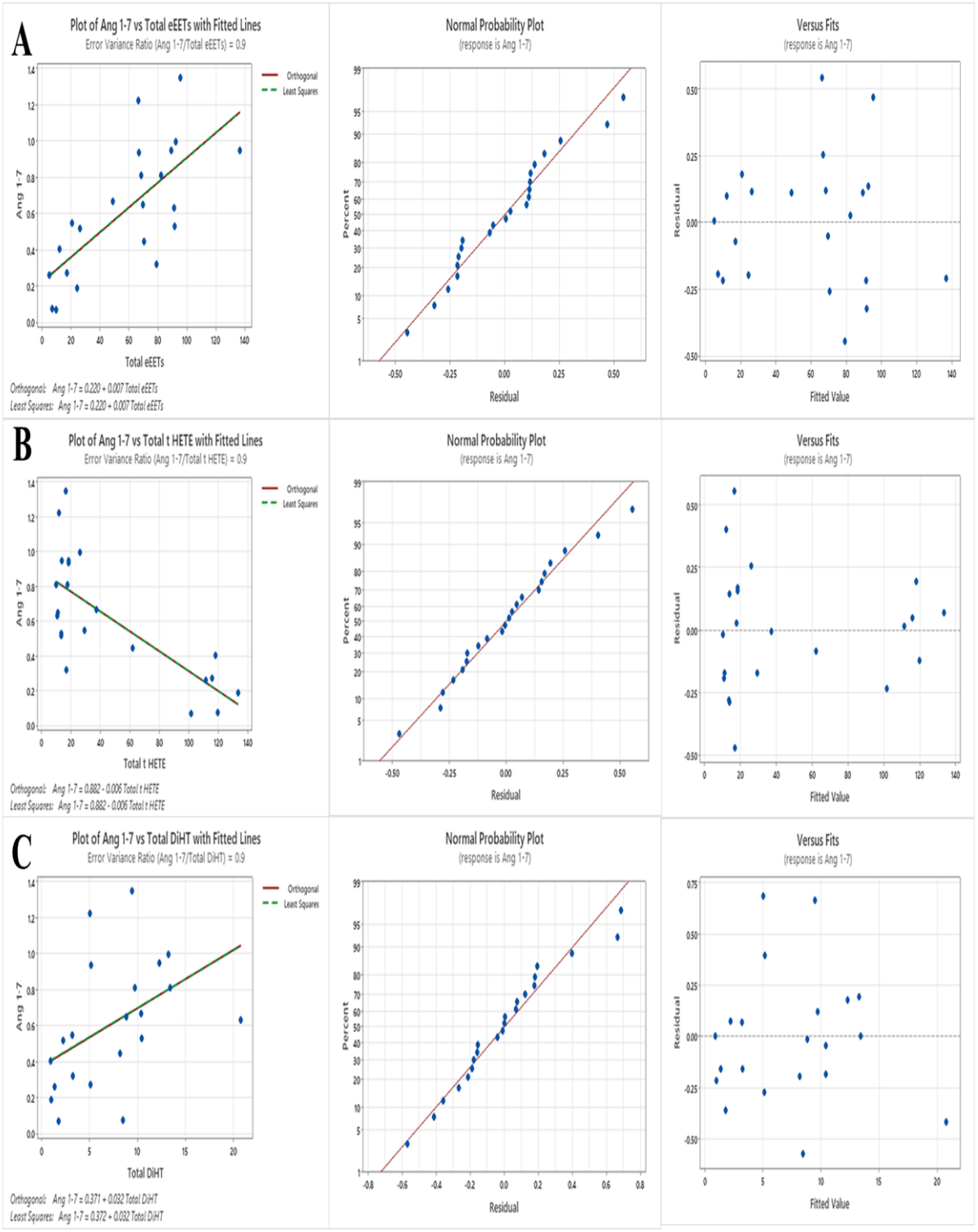

Figure 36 .The orthogonal regression graphs with line best fit of (A) Angiotensin 1-7 (Ang 1-7) vs total-epoxyeicosatrienoic acids (T-EETs) (B) Ang 1-7 vs total hydroxyeicosatetraenoic acids (T-HETEs) and (C) Ang 1-7 vs total dihyroxyeicosatrienoic acid (T-DiHTs).

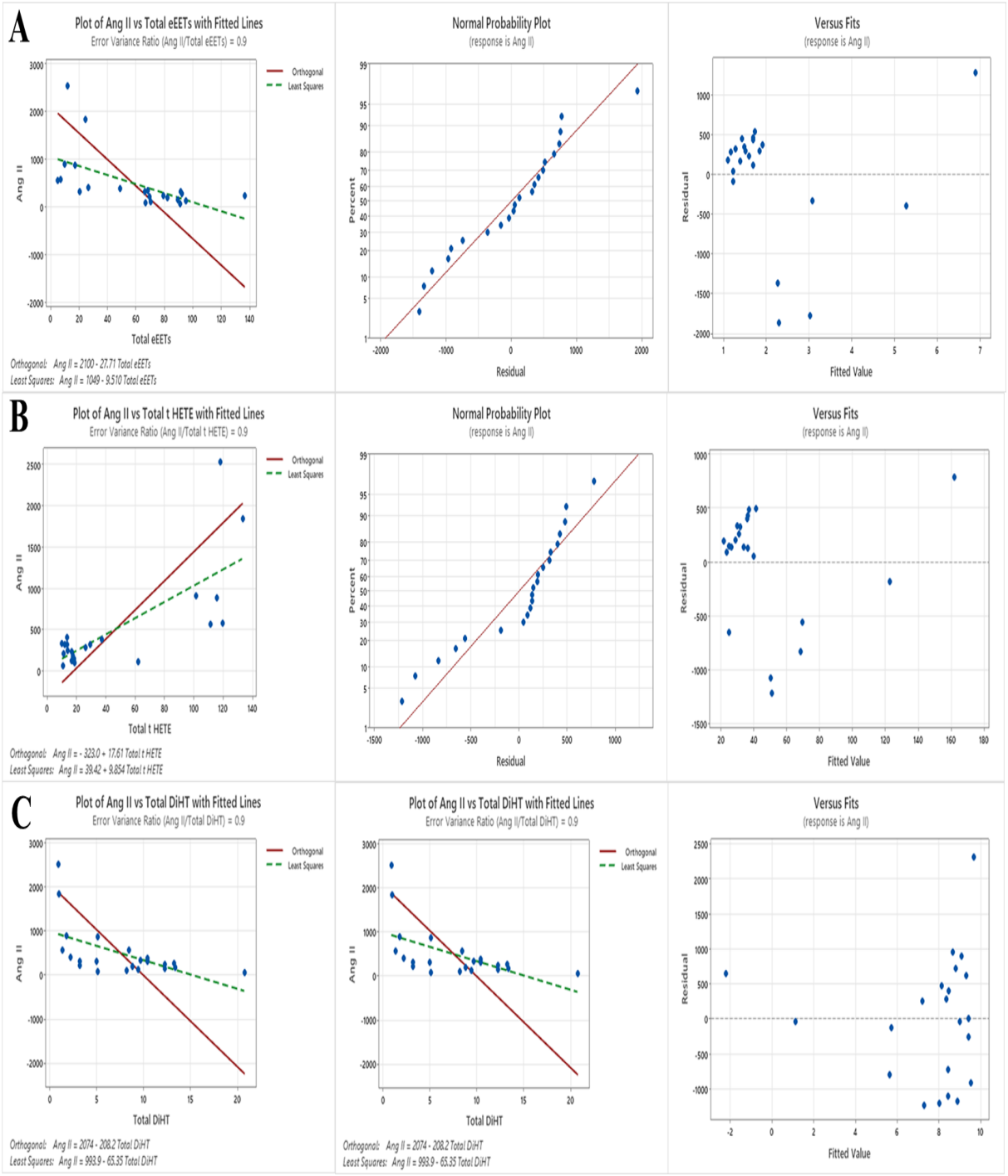

Figure 37. The orthogonal regression graphs with line best fit of (A) Angiotensin II (Ang II) vs total-epoxyeicosatrienoic acids (T-EETs) (B) Ang II vs total hydroxyeicosatetraenoic acids (T-HETEs) and (C) Ang II vs total dihyroxyeicosatrienoic acid (T-DiHTs).

4.11 Discussion

Novokinin is a six-amino-acid synthetic peptide that acts as an AT2R agonist and has been shown to have a variety of biological effects, including anti-hypertensive, vasorelaxant, anorexigenic, gastroprotective, anti-inflammatory, and cyclooxygenase-inhibiting effects (74). In this study, we report the novel anti-inflammatory effects of novokinin in a rat model of AIA. Despite its numerous therapeutic benefits, peptide drugs like novokinin face significant challenges in drug development due to their instability. We administered a stable version of novokinin known as Novo Conj to enhance its anti-inflammatory effect.

Although collagen-induced arthritis is the most relevant model, the literature indicates that AIA is appropriate for studying cardiovascular and other complications associated with human RA (214, 215). As we were interested in investigating the cardiovascular protection of Novo Conj through RAS and ArA pathways, we chose the AIA model for our study. In the present work, we observed almost 100% incidence of AIA through a single administration of *Mycobacterium butyricum*, as reported previously (216). The role of the AT2R in the resolution of inflammation in the RA rat model has also been studied by AT2R agonists like CGP42112A (186). To explore the anti-inflammatory spectrum of AT2R, we tested the effect of novokinin, a synthetic peptide AT2R agonist, and its conjugate, Novo Conj, modulating the experimental AIA. The dose of novokinin was selected based on previous studies to test its other biological activities. It has been reported that novokinin was used in a wide range of 0.1 mg/kg intravenously to 30–100 mg/kg orally (75, 217). In this pilot study, we chose a 0.4 mg/kg dose to be delivered subcutaneously every other day (thrice weekly for two weeks) to test its anti-inflammatory effect. The animals tolerated both novokinin and Novo Conj administered dose well.

In concert with the earlier reports, weight loss and swelling of joints and paws were major hallmarks of successful induction of AIA (186, 216). Without any treatment, these symptoms tend to worsen in AIA rats, but the intervention with drugs helps recover by restoring weight loss and decreasing swelling of joints and paws. The subsequent reduction in AI score was realized in Novo Conj-treated rats with significant improvement in the resolution of inflammation, as shown in Figure 24. Similarly, NO has been found to play an essential role in the pathogenesis of inflammation, as demonstrated by extensive studies (218, 219). The administration of Novo Conj prevents the rise in the serum nitrite concentration, the stable form of NO metabolite, further validating its anti-inflammatory role shown in Figure 25.

Similarly, the therapeutic efficacy of novokinin and Novo Conj on reducing AI was not significantly noticeable until the end. This observation could be attributed to the time required for novokinin plasma concentration to release from the conjugate and to reach an adequate steady-state concentration. The two weeks treatment period with this dose of novokinin or Novo Conj in this pilot study presents an attractive alternative option that can be used as enhanced by increasing dose, duration or as an additive therapy with ARBs.

Apart from the physical symptoms, here in our study, we analyzed the molecular mechanism of RA through the lens of RAS. It is a known fact that an interplay between RAS and the inflammatory axis controls the outcome of RA (220). The overactivation of the classical arm of RAS, i.e., ACE/Ang II/AT1R, is known to stimulate the pro-inflammatory cytokines, exacerbate angiogenesis, and promote osteopenia, thus leading to the gradual destruction of the joints and increased deformation and dysfunction (179, 221). In contrast, stimulation of the alternative arm of RAS, i.e., AT2R and ACE2/Ang 1-7/MasR axis, can lead to inhibition of oxidation, promotion of osteogenesis, and downregulation of pro-inflammatory mediators (186, 222). In

this study, we demonstrated that novokinin and Novo Conj utilize the activation of an alternative RAS axis to resolve inflammation. We saw an increase in ACE2/ACE ratio and AT2R/AT1R ratio in the mRNA and protein expression in various tissues obtained from treated AIA rats, as shown in Figures 26, 27 and 28. We observed that the results of Novo Conj treatment were more significant than novokinin-treated rats. With the change in mRNA and protein expression in cardiac tissue in arthritic rats, we could show RA is involved in the pathogenesis of cardiovascular disease and our Novo Conj plays a therapeutic role in restoring imbalance RAS (223). Histological studies on various intact tissues confirmed the protein expression measured in the WB. These studies showed an increase in the protective axis ACE2 and AT2R and a decrease in the classical axis ACE and AT1R in the treatment group. In contrast, the arthritic group with no treatment showed the opposite effect, with a reduction in the protective axis and an increase in the classical axis.

Our data suggests that AT2R stimulation is associated with ACE2 activation. This event is in agreement with the outcome of several studies that reported the activation of AT2R increases ACE2 activity which was seen in diabetic nephropathy (224), obesity-related hypertension (225), and inflammation (226). In our study, we found a significant increase in the Ang 1-7/Ang II ratio as Ang 1-7 and Ang II levels were increased and decreased, respectively, in the plasma of novokinin or Novo Conj-treated AIA rats. As ACE protein levels did not change by drug treatments, the rise in Ang 1-7 can be attributed to two factors i) direct conversion of Ang II to Ang 1-7 through the enhanced ACE2 expression and ii) indirect conversion by ACE2 by the promotion of Ang I metabolism to Ang 1-9, which in turn yields Ang 1-7 (227). This fact led to the rationale that ACE2 activation shifted the power balance between Ang 1-7 and Ang II in

favor of the RAS protective arm. Thus, novokinin and, more efficiently, the Novo Conj reduce inflammation by promoting alternative RAS axis and restoring balance.

Besides creating an imbalance in the RAS, inflammation also causes alterations in CYP expression, which controls one of the critical pathways for the metabolism of ArA (8). For instance, there is increased ω-hydroxylase expression, encoded predominately by the CYP4A and CYP4F, which gives rise to HETE metabolites from ArA. The 20-HETE enhances the production of inflammatory cytokines/chemokines (IL-8, IL-13, IL-4, and prostaglandin E2 and exacerbates RA (228). At the same time, there is decreased epoxygenase encoded by CYP2C and CYP2J, leading to a lower level of EETs and DiHTs, suppressing their anti-inflammatory activity (229). Our study also found an association between inflammation and CYP-derived eicosanoids, as arthritic rats have higher T-HETEs but lower T-EETs and T-DiHTs concentrations.

Nevertheless, we saw an increase in T-EETs and T-DiHTs and a decrease in T-HETEs concentration in drug-treated rats with Novo Conj treatment able to bring to the control level (Figure 35). The rise in EETs and its comparatively low potent product DiHTs, counteract inflammation by reducing cytokines like TNF-α and inhibiting the transcription of the NF-κB translocation, thereby blocking leukocyte adhesion. In addition, their rise also downregulates different enzymes, such as LOX-5 and COX-2, as well as the iNOS, that are responsible for the aggravation of inflammation (202).

Our findings show a strong correlation (with opposite signs) between some individual EETs, HETEs, T-EETs, and T-HETEs with Ang 1-7 or Ang II levels (Table 8). These correlations were confirmed by orthogonal regression analysis data and the line best-fit graphs (Table 9,10 and Figures 36 and 37. This interconnection hints that the modulators of both RAS and CYP-derived

eicosanoids work in tandem to resolve or worsen inflammation. We also found a mild positive correlation between DiHTs and Ang 1-7 and an inverse negative correlation between DiHTs and Ang II levels, affirming that they are low potent anti-inflammatory mediators (Table 8). The AT2R stimulation through Novo Conj increases EETs and Ang 1-7 levels, thus promoting recovery and healing in AIA rats. Agonist novokinin falls short of adequately resolving inflammation due to its instability. But the conjugation of novokinin with PEG and BP helped to improve stability and sustain its anti-inflammatory action. The upregulation of ACE2/ACE, Ang 1-7/Ang II, and AT2R/AT1R ratios by Novo Conj in arthritic rats confirms its role in maintaining the physiological balance of RAS components for the resolution of inflammation. In addition, the enhanced production of anti-inflammatory ArA metabolites, EETs, and DiHTs was due to prolonged AT2R activation by Novo Conj, which further promotes its anti-inflammatory effects. Thus, bone-targeted delivery of Novo Conj supported by HA binding affinity data (Figure 11) and bone tissue distribution of similar conjugate (Ang 1-7 Conjugate) (27) offers efficacious alternative therapy for the management of RA and could be utilized for various RAS disorders.

4.12 Conclusion

In summary, AT2R stands out as an attractive receptor-targeting approach for managing RA due to its influence on the RAS and ArA pathways. However, the AT2R peptide agonist, novokinin, falls short of efficiently resolving inflammation due to instability. But the conjugation of novokinin with PEG and BP helps to improve stability and sustain its anti-inflammatory action. The upregulation of ACE2/ACE, Ang 1-7/Ang II, and AT2R/AT1R ratios by Novo Conj in arthritic rats confirmed its role in maintaining the physiological balance of RAS components for the resolution of inflammation. Similar effects of Novo Conj on restoring the balance between anti- and pro-inflammatory metabolites of ArA are in concert with the RAS. The dynamic crosstalk between these two pathways and the Novo Conj effect on restoring their physiological homeostasis is very significant and indicative of its feasibility in controlling inflammatory conditions. Hence, the bone-targeted delivery of novokinin offers an effective alternative therapy for the modulation of RA and could be further utilized for various RAS disorders.

Chapter V: Development and Validation of Novokinin LC-MS/MS in Rat Plasma and its Application to Pharmacokinetics Study

5.1 Introduction of Novokinin

Novokinin, a synthetic peptide derived from chymotrypsin digest, ovokinin (2-7) (Arg-Ala-Asp-His-Pro-Phe), of egg albumin. The ovokinin (2-7) elicited vasorelaxation mediated by AT2R with a binding affinity of 210 μM. It evoked a hypotensive effect in SHR at the dose of 10 mg/kg after oral administration (*p.o*). Later this was modified to the (Pro^2, Phe^3) -ovokinin (2-7), which evoked anti-hypertensive effects at a dose of 0.3 mg/kg corresponding to more than 30-fold times less amount compared to ovokinin (2-7) after oral administration (72).

In the quest to design more potent bioactive peptides, the alanine scan was performed, which aided in determining suitable amino acid residues for each individual position. Like, Arg^1 residue at N-terminal is crucial for anti-hypertensive effects. Similarly, Pro at the 2nd and 5th positions conferred resistance to gastrointestinal degradation by protecting it from the action of enzymes like aminopeptidase and carboxypeptidase without affecting vasorelaxant activity. The aromatic Phe^3 is replaced with aliphatic Leu to escape degradation by chymotrypsin-type protease. They also established that aromatic amino acid residue with high hydrophobicity is required at the carboxyl-terminal, and Trp gives them the best results in terms of anti-hypertensive activity. Replacing 4 amino acids from the original 6 [ovokinin (2-7)] gives them a more potent peptide called novokinin. This peptide (Arg-Pro-Leu-Lys-Pro-Trp) has superior binding affinity at 7×10^{-6} M, and its bioactivity is seen at a lesser dose than its parent peptide (73, 74).

Novokinin induced relaxation in the mesenteric artery pre-constricted by phenylephrine at the concentration of 10^{-5} M. They also showed encouraging anti-hypertensive effect in the SHR at a dose of 0.03 mg/kg (saline) intravenous (*i.v*) and 0.1 mg/kg (emulsified in 30% egg yolk) after

(*p.o*) but no effect in normal hypotensive Wister Kyoto rat. This hypotensive effect was blocked by AT2R antagonist, COX inhibitor and prostaglandin I2 receptor antagonist but also insignificantly by NOS inhibitor. This proved the observed biological action was majorly mediated through the IP receptor downstream of the AT2R, but the contribution of NO cannot be ruled out completely. Similarly, it did not induce hypotension in normal and AT2R-deficient mice (74). The study by Mutlu et al. (75) tried to shed light on the role of the NO pathway for novokinin. In this study, novokinin was administered intraperitoneally (*i.p*) at a 0.1 mg/kg dose for two weeks to the salt-fed and L-NAME-induced hypertensive rats. Novokinin showed a decline in the enzymes responsible for end-organ damage like asymmetric dimethylarginine (ADMA), nicotinamide adenine dinucleotide phosphate (NADPH) oxidase and Rho kinase level induced in the hypertension; however, these changes did not reach statistical significance.

Beside the vasorelaxant and anti-hypertensive effects, novokinin was also found to affect the central nervous system. In the study done by Ohinata et al. (76) novokinin presented with anorexigenic effects at 100 mg/kg/mice (*p.o*) and 30 nmol/mouse intracerebroventricular (*i.c.v*) administration. This effect was mediated by the prostaglandin E receptor 4 (EP4) system via AT2R as it was reversed by AT2R antagonist, cyclooxygenase (COX) inhibitor and EP4 antagonist. Similarly, another central nervous effect of novokinin was reported by, which exerted an anti-opioid effect. Here, centrally administrated novokinin (30 nmol/mouse) inhibits the antinociceptive effect of morphine (μ agonist) in mice, as evaluated by the tail-pinch test. The EP3 system mediated this effect via AT2R as this was reversed by AT2R antagonist, COX inhibitor and EP3 antagonist (77).

In addition, novokinin also exerted gastroprotective effects via AT2R-PGs pathway (78). Here, it inhibited basal gastric acid secretion and protected gastric mucosa from alcohol-induced injury in

a dose-related manner in rats after (*i.c.v.*) administration at the dose of 50 and 100 nmol/rat, respectively. AT2R antagonist and COX inhibitor occluded this effect. Further exploration of the multitude of therapeutic effects of novokinin revealed that it also had a beneficial role in asthma (79). Novokinin was found to lower lung inflammation and airway reactivity at the dose of 0.3 mg/kg, (*i.p*) in allergen-sensitized mice mediated via AT2R.

Despite the multitude of therapeutic effects of novokinin, there is no reported quantitative method in the scientific domain that explains the gap of knowledge in the analytical spectrum. The quantitative method of any drug in solution and the biological matrix is a foundational requirement for further drug development and research. Chromatographic methods like LC coupled with UV-Vis fluorescence, MS, and GC emerged as a common approach to analyzing drug compounds (230). However, the ability of LC-MS/MS to provide certainty, clarity and confidence based on mass, charge and retention gives it an edge over other techniques, making it a popular assay for higher sensitivity, selectivity and higher throughput without affecting the compound's volatility (231). Apart from this, sample clean-up procedure in biological samples is considered mandatory, and SPE emerges as a viable option as it significantly reduces interference from the matrix and concentrates analytes. This method also prevents clogging in the instruments, thus ensuring the smooth running of instruments and giving better recovery of samples than its counterparts, like protein precipitation and liquid extraction techniques (232). This study aimed to develop a simple, selective, and sensitive method that employs highly reliable SPE for sample preparation and liquid chromatography with electrospray ionization- MS for its quantitation in rat plasma. In our current study, we have reported the selectivity, calibration curves, stability, accuracy and precision and limits of quantification (LOQ) and limit

of detection (LOD) to ensure method reproducibility. The method was fully validated and applied to rat samples for a PK study**.**

5.2 Experimental materials and methods

5.2.1 Chemicals reagents

[asn^{1}, Val^{5}]-angiotensin II used as Internal Standard (IS) (Sigma-Aldrich A6402-1MG) was bought from Sigma Aldrich (St. Louis, MO, USA). C18 column (SepPak WAT020805) was bought from Waters (Milford, MA, USA). LC-MS grade water, acetonitrile, and formic acid were purchased from Fisher Scientific (Fair Lawn, NJ, USA). Blank rat plasma (IRTSDPLAK2E100ML) was purchased from Innovative Research (Novi, MI, USA). Heparin Sodium Injection (NDC 25021-400-40) was purchased from Sagent Pharmaceuticals (Schaumburg, IL, USA).

5.2.2 Instrumentation

See section 4.9.11.2

5.2.3 Chromatographic and Mass Condition

Novokinin was analyzed in Synergii RP (2 × 100 mm) column with a 2.5 µm particle size (Phenomenex, CA, USA) at ambient temperature. The mobile phase comprised of 0.1% formic acid in water (A) and ACN (B). The gradient time program started from 5% ACN to 30% ACN over 4 mins, and composition was kept constant for 4 to 6 mins and increased up to 90% till 8 mins and kept constant till 10 mins and lowered to 5% ACN to 10.5 mins and ran till 12 mins. The flow rate was 0.3 mL/min, and the injection volume was 30 µL. Electrospray ionization was used, and analytes were detected using MRM in the positive mode. The optimized source/gas parameters were as follows: curtain gas, 30; collision gas, medium; ion spray voltage, 5500 V; temperature, 300 °C; ion source gas 1 (nebulizer gas), 20 psi; and ion source gas 2 (turbo gas), 25

psi. LC-MS analysis was performed with the single ion recording (SIR) mode, in which the *m/z* 398 and 516.6 were used for novokinin and IS, respectively. LC-MS/MS was performed with MRM transitions of *m/z* 398→495 novokinin and *m/z* 516→769.4 (IS).

5.2.4 Preparation of Standard and Quality Control

A stock solution of novokinin (1 mg/mL) was prepared by dissolving the 1 mg of novokinin in 1 mL of water. Working solutions were prepared by diluting the stock solution to 10 µg/mL, 1 µg/mL, 800 ng/mL, 400 ng/mL, 100 ng/mL, 25 ng/mL, 6.25 ng/mL, 1.56 ng/mL with water. The final effective concentrations for the analyte in constructing standard curves were 800, 400, 100, 25, 6.25, 1.56 and 0.78 ng/mL. The stock solution was stable for 3 months at -20 °C. A stock solution of IS was prepared by dissolving IS in water at a 1 mg/mL concentration. The stock solution was stable for 3 months at -20 °C. The working solutions for Quality control (QC) samples were independently prepared at the attention of 7.8, 15.6, 250, and 4000 ng/mL, which were ten times that of the effective concentrations: 0.78 (LLOQ), 1.56 (LQC), 25 (MQC), and 400 ng/mL (HQC).

5.2.5 Plasma Sample Preparation

An aliquot of 200 µL plasma, 100 µL of IS (250 ng/mL), and formic acid was added to the final concentration of 0.5% and mixed well. SPE has been carried out in Agilent PPE manifold 48 processors. The sample solutions were applied to the C18 column preconditioned with 2 mL of ethanol and 2 mL of deionized water, respectively. After loading the sample, the cartridge was washed with 2 mL of deionized water. The water was left to dry for 3 mins by turning on a high nitrogen gas flow. Then, novokinin was eluted from the cartridge using 2 mL methanol containing 5% formic acid and 2 mL of 70:30 ACN: Water in 0.1% Trifluoroacetic acid (TFA)

collected and dried under the stream of nitrogen. Finally, the dried sample was reconstituted in water and transferred to a sample vial for LC-MS/MS analysis.

5.2.6 Validation of LC-MS/MS method

5.2.6.1 Linearity

Calibration curves were prepared in rat plasma at seven concentrations (final concentration of Novokinin at 800, 400, 100, 25, 6.12, 1.56 and 0.78 ng/mL. A standard curve of y = Ax+B was determined by plotting the peak area ratio of the known standard concentration of novokinin to IS. The slope, intercept, and coefficient of determination were calculated using the linear regression method with a weighting of 1/x.

5.2.6.2 Specificity

Six different batches of rat plasma were analyzed for the investigation of the specificity of the assay. This ensured the exclusion of any endogenous co-eluting interference at the peak region of novokinin and IS.

5.2.6.3 Accuracy and Precision

Quality control (QC) samples (1.56, 25, and 400 ng/mL) were prepared and analyzed three times in the same run (intra-run precision) and three separate runs (inter-run precision). Accuracy was calculated as follows: $\frac{measured\ concentration}{nominal\ concentration} \times 100\%$. And CV% was used to estimate the precision

5.2.6.4 LLOQ

QC samples at 0.78 ng/mL of novokinin were processed and analyzed three times in the same run. The accuracy and precision were calculated from the data of three measurements.

5.2.6.5 Matrix effect and Percentage Recovery

The matrix effect and extraction recovery were determined at three levels (LQC, MQC, and HQC) in three replicates.

Matrix effects were calculated as follows:

$$\frac{Peak\ area\ ratio\ of\ \ post\ extracted\ QC\ samples\ \ (novokinin/IS)}{Peak\ area\ ratio\ of\ QC\ sample\ in\ the\ neat\ solution\ (novokinin/IS)} - 1 \times 100\%$$

Recoveries were calculated as follows:

$$\frac{Peak\ area\ ratio\ of\ \ spiked\ \ QC\ samples\ \ (novokinin/IS)\ in\ plasma}{Peak\ area\ ratio\ of\ \ post\ extracted\ QC\ samples\ \ (novokinin/IS)} \times 100\%$$

5.2.7 Stability

The QC samples of all three levels were prepared and subjected to autosampler, bench top, freeze-thaw, and long-term stability tests. The autosampler stability of Novokinin was investigated by keeping three replicates of QC samples at 10 °C for 12 hrs in the auto-sampler tray. Similarly, benchtop stability was analyzed by subjecting QC samples at room temperature for 2 hrs. Likewise, QC samples were put through 3 freeze and thaw cycles to determine freeze-thaw stability, and long-term stability was measured by keeping pieces at -80 °C for 30 days. All the stability tests were determined and compared by running fresh calibration and QC samples. For all the stability study samples, the criteria for acceptance of accuracy and precision are to be within ± 15%.

5.2.8 Animal and Treatment

Adult male SpD rats weighing 200-250 g were obtained from Charles River (Wilmington, MA, USA) and were housed under ambient temperature and ventilation with a 12 hrs day and night cycles. Rats were kept in standard cages with free access to drinking water and regular rat chow

ad libitum. After two weeks of the washout period, rats were grouped for Novokinin (*i.v.*) (n = 4); the animal study protocol was reviewed and approved Animal Care Facility Committee of Idaho State University (Protocol #772, 22 September 2021).

Rats were cannulated via jugular vein a day before dosing. For (*i.v.*) grouped rats, a single 1 mg/kg dose was administered via a jugular vein. Blood samples were collected into heparin-added tubes before and after dosing at various time intervals i.e., 3 mins, 5 mins, 15 mins, 30 mins, 1 hr, 2 hrs, 4 hrs, 6 hrs, 8 hrs, 10 hrs and 24 hrs. Plasma samples were separated immediately by centrifugation of the blood samples at 13,000 rpm for 15 mins and kept at −80 ℃ until analysis. For each time point, three replicates were analyzed, and results were reported as mean values with SD for each time point. Non-compartmental analysis was used to determine the pharmacokinetic parameters of novokinin. The PK parameters, including the area under the plasma concentration-time curve during the period of measurable observation $AUC_{(0–t)}$, the area under the plasma concentration-time curve extrapolated to infinity $AUC_{(0–\infty)}$, the apparent clearance (CL), the total body mean residence time (MRT), and the terminal elimination half-life ($t_{1/2}$) were estimated.

5.3 Results and Discussion

5.3.1 Physiochemical Properties of Novokinin.

Novokinin is a six-amino acid hydrophilic peptide. It consists of 2 basic polar positively charged amino acids (1 Arg and 1 Lys), 1 aromatic amino acid (1 Trp) and 3 hydrophobic nonpolar uncharged amino acids (2 Pro and 1 Leu). The charge and isoelectric point of the peptide are primarily affected by 2 basic amino acids in the novokinin peptide sequence. The isoelectric end point of the novokinin was observed as 11.39. The charge of the novokinin peptide at pH 7 was found to be 2 with a positive charge.

5.3.2 LC-MS/MS Method Optimization

The tuning of novokinin and IS was conducted through the continuous, direct infusion of neat standard solutions at a 10 µL/min flow rate into the ESI source in positive mode. The mass parameters of novokinin and IS were optimized for producing reproducible results. The mass parameters such as ion source temperature, ion source voltage, curtain gas, collision gas, turbo ion gas, and nebular gas were optimized at 300 °C, 5500 eV, 30 psi, high, 40 psi and 40 psi, respectively. The precursor ions of Q1 of charge states with *m/z* values of novokinin observed at 796.4 ($[M+1]^{1+}$) and 398.5 ($[M+2]^{2+}$) and for IS were 1031.2 ($[M+1]^{1+}$) and 516.42 ($[M+2]^{2+}$). The ($[M+2]^{2+}$) was prominent among Q1 ions for both Novokinin and IS, and their product ions (Q3) were further evaluated. For quantitative analysis, the predominant Q1/Q3 transitions were selected in MRM mode as 398.5/495 and 516/769, respectively, using positive ESI potential Figures 38A and 38B. The compound parameters viz dwell time, EP, DP, CE and CXP for novokinin and IS were 500 msec, 10 eV,100 eV and 90 eV, 23 eV and 25 eV, 20 eV, respectively. After the mass parameters optimization, LC conditions were selected, including column selection, mobile phase composition, and flow rate (10-30 µL/min). The optimum condition was observed in Synergii RP (2 × 100 mm) column using flow rate 30 µL/min with a mobile phase consisting of water and ACN-0.1% formic acid for novokinin and IS. The total chromatographic run time was 12 mins.

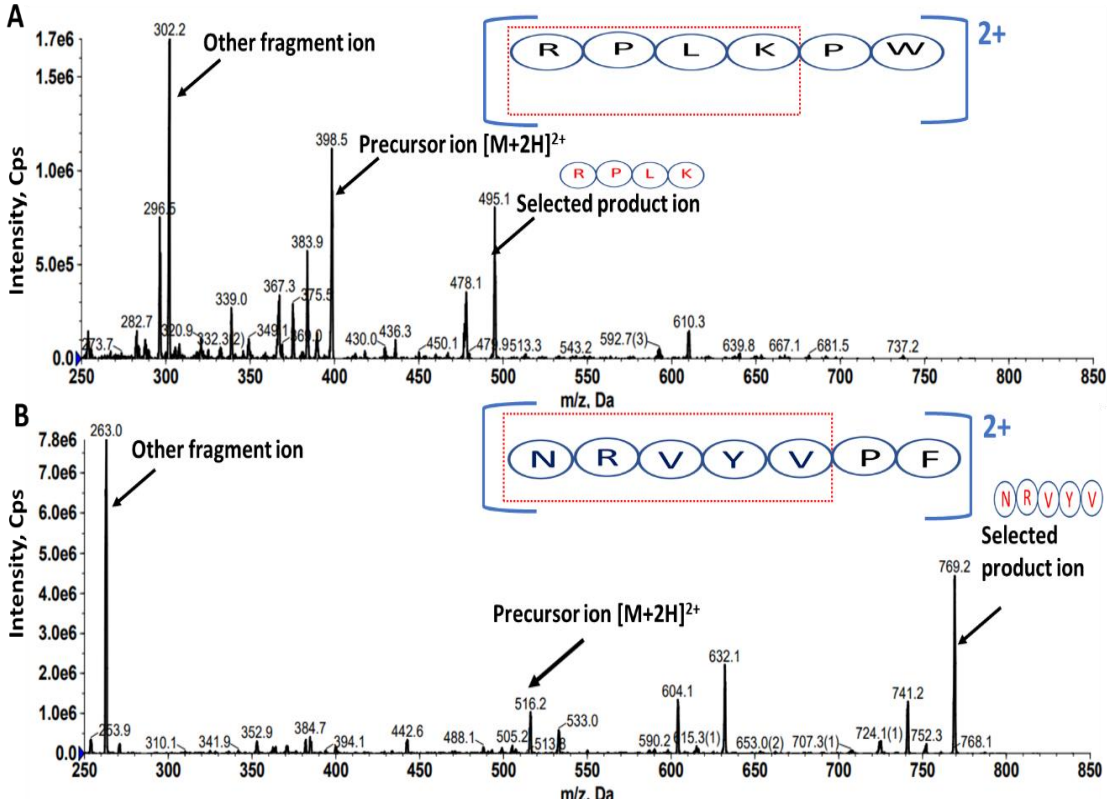

Figure 38. Mass ion spectra of ([M+H] +) of (A) Novokinin and (B) Internal Standard (IS)

5.3.3 Extraction Optimization and Recovery

The preliminary experiments were performed with protein precipitation for plasma extraction with different organic solvents. The plasma precipitation showed poor recovery and extensive background noise, which can be attributed to its suppression of ions and non-selective removal of small molecules and endogenous peptide interference (233). As SPE is attributed to more excellent selectivity, low interference, higher sensitivity, and longer column life, an SPE method was developed. Different types of SPE cartridges (anionic, cationic, C18 reverse) columns were tested for investigation. The pH of novokinin was changed from 3 to 10, and samples were eluted

from both acidic and basic organic solvents. We observed the best results in C18 column with an acidic sample and acidic elution. The matrix effects were investigated using the post-extraction spike method, and recoveries were calculated by comparing peak areas in QC samples to those of post-extracted QC samples. The absolute mean extraction for Novokinin was more than 80% for 3 QC levels and the % matrix effect was listed in Table 11 for 3 QC levels.

Table 11. Recovery and matrix effects of Novokinin and Internal standard (IS)

	Nominal Conc. (ng/mL)	**Matrix effect (%) (n = 3)**	**Recovery (%) (n = 3)**
Novokinin	1.56	-19.91 ± 1.77	86.62 ± 4.43
	25	-22.37 ± 0.72	85.12 ± 4.68
	400	-18.56 ± 1.01	84.05 ± 2.74
IS	250	-19.89 ± 3.64	80.11 ± 3.65

Conc; Concentration, IS; internal standard

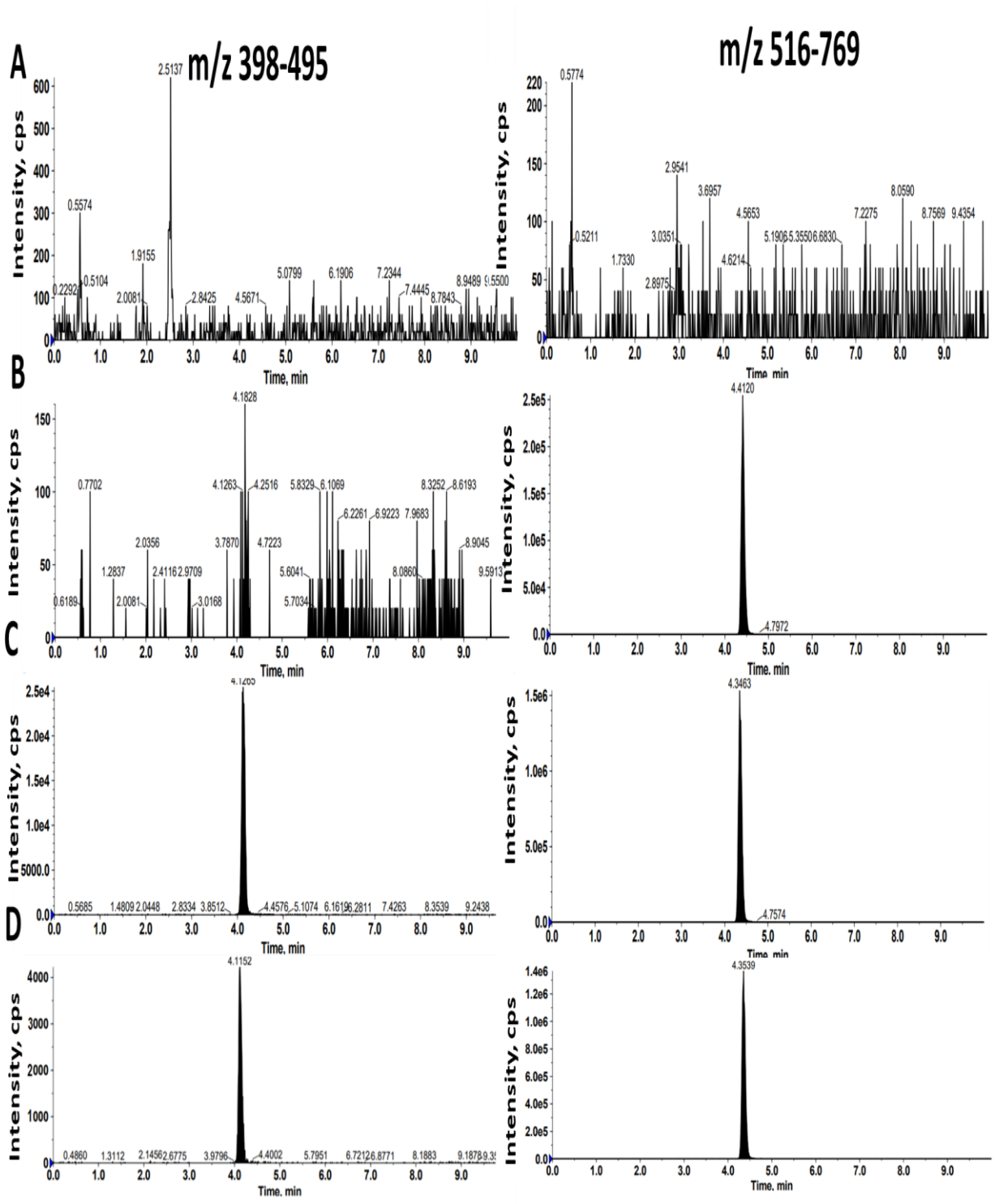

Figure 39. Representative MRM chromatograms in (A) Double blank plasma (B) Blank Plasma with internal standard (IS) (C) Plasma with Novokinin and IS (D) Rat novokinin plasma at 5 minutes.

5.3.4 Bioanalytical Assay Validation

The plasma matrix interferences were not detected at 4.11 mins and 4.35 mins retention time for novokinin and IS, respectively. The SPE sample extraction procedure was found to be selective and specific. Figure 39 shows the MRM chromatogram for the blank rat plasma (39A), blank rat plasma and IS (39B), rat plasma spiked with novokinin and IS (39C) and rat plasma sample with novokinin at 5 mins and IS (39D). The LOD and LLOQ for novokinin were observed at 0.12 ng/mL and 0.78 ng/mL, respectively. The signal/noise ratio was observed as 3.3 and 11 for LOD and LLOQ, respectively. The linearity of novokinin in rat plasma was achieved and reproduced across the concentration range of 0.78-800 ng/mL with r^2 of 0.998 (n = 3). The linear regression with the mean calibration curve equation was determined as $y = 0.0177x + 0.0615$. The accuracy and precision data of the QC shown in Table 12 are within the range of acceptable limits with reproducibility over a well-established concentration range. The accuracy was 3.33%, and the precision was 5.38%, suggesting proper dilution falls within acceptable criteria.

Table 12. Intra-day and inter-day accuracy and precision of novokinin in rat plasma

	Intra-day (n = 3)			Inter-day (n = 3)		
Nominal conc. (ng/mL)	**Observed conc. (Mean ± SD)**	**Precision (CV%)**	**Accuracy (%)**	**Observed conc. (Mean ± SD)**	**Precision (CV%)**	**Accuracy (%)**
0.78 (LLOQ)	0.86 ± 0.02	2.46	109.79	0.76 ± 0.09	11.49	98.07
1.56 (LQC)	1.73 ± 0.11	6.39	110.76	1.64 ± 0.23	13.91	104.99
25 (MQC)	26.61 ± 0.82	3.07	106.43	25.93 ± 2.66	10.25	103.73
400 (HQC)	396 ± 2.46	0.62	99.20	397 ± 9.32	2.35	99.36

Conc.; concentration, LLOQ; lower limit of quantification, LQC; lower-quality control, MQC; middle-quality control, HQC; high-quality control

5.3.5 Stability Studies

To evaluate the stability of the drug in different storage conditions during processing, we subjected novokinin to various stability conditions in rat plasma. The accuracy and precision of varying stability conditions were found to be within the range of acceptable criteria, as shown in Table 13. However, the benchtop stability of novokinin at 4 hrs exceeded accepted criteria (-17.84%) which suggested that it should be processed while at the ice.

Table 13.**Stability data of novokinin in rat plasma**

		Calculated conc. (ng/mL) (n = 3)		
	Nominal conc. (ng/mL)	**Observed conc. (Mean ± SD)**	**Accuracy (%)**	**Precision (CV%)**
Auto Sampler	1.56	1.41 ± 0.03	90.45	2.30
(10 °C, 24 hr)	25	23.46 ± 3.17	93.84	3.17
	400	387.31 ± 0.29	96.83	0.29
Bench Top (25 °C, 2 hr)	1.56	1.43 ± 0.04	92.01	2.85
	25	23.92 ± 0.70	95.69	2.94
	400	391.06 ± 2.42	97.77	0.62
Freeze and thaw	1.56	1.33 ± 0.03	85.34	2.72
(-80 °C to 4 °C, 3	25	21.64 ± 1.71	86.58	7.88
cycles)	400	348.74 ± 7.6	87.19	2.18
Long-term	1.56	1.46 ± 0.05	94.11	3.75
(-80 °C, 30 days)	25	24.07 ± 0.73	96.31	3.04
	400	390.73 ± 7.98	97.68	2.04

Conc.; concentration

5.3.6 PK studies of Novokinin in rat

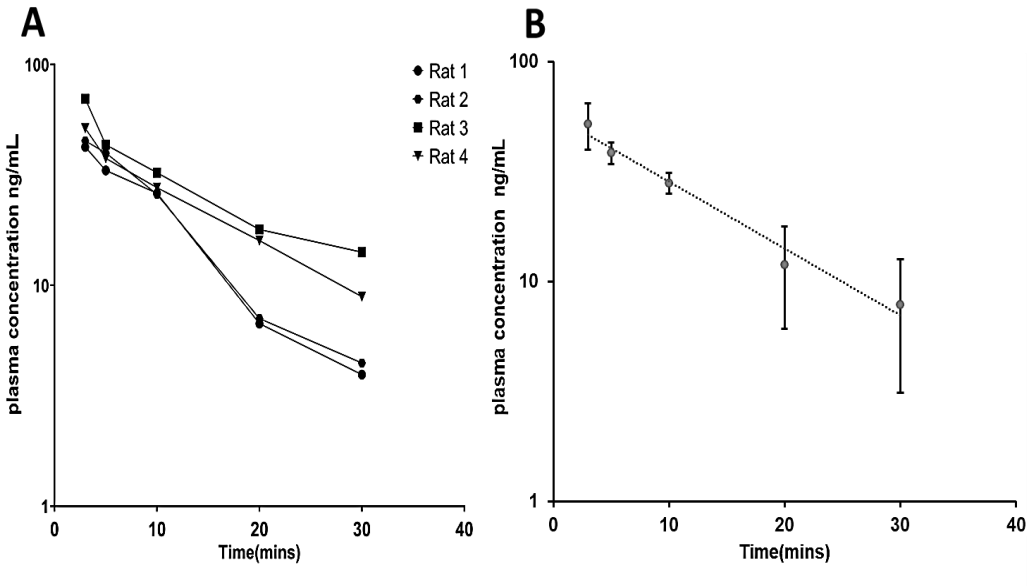

Figure 40. Plasma pharmacokinetics (PK) profile of (A) Individual rats following a single intravenous bolus (*i.v.*) injection n and (B) Average plasma PK profile.

After the validation of novokinin, the same assay was utilized to exhibit the PK studies in rats. Four healthy male SpD rats were administered a single dose of 1 mg/kg (*i.v.*). The PK profiles of novokinin following (*i.v.*) non-compartmental model calculated administration and their results are shown in Figure 40 and Table 14. This suggested a rapid initial distribution phase followed by a rapid elimination phase.

Table 14. Pharmacokinetics parameters estimated by non-compartmental model followed by single *i.v.* bolus injection of novokinin to healthy rats (n = 4).

Pharmacokinetics parameters	***i.v.***
Dose (mg/kg)	1
Ke (min^{-1})	0.08 ± 0.001
$t_{1/2}$ (min)	9.17 ± 2.58
AUC_{0-t} (min.ng/mL)	88.45 ± 23.80
$AUC_{0-\infty}$ (min.ng/mL)	843.47 ± 247.20
V_d (L)	3.34 ± 0.57
Cl (L/min)	0.25 ± 0.14

Ke: elimination rate constant; $t_{1/2}$: half-life; AUC_{0-t} area under the plasma concentration-time curve during the period of measurable observation; $AUC_{0-\infty}$ area under the plasma concentration-time curve extrapolated to infinity; Vd: Volume of distribution; Cl; clearance.

5.4 Conclusion

In the present work, we have developed a sensitive, accurate, reproducible, and convenient LC-MS/MS method and validated it fully for quantifying novokinin in rat plasma. Sep-Pak Cartridges was selected for the extraction of novokinin from biological samples due to its excellent recovery. Novokinin was found to be stable in rat plasma in different stability conditions. It also exhibited good linearity across the 0.78-800 ng/mL calibration concentration range. We could show this method's importance due to low volume (100 µL) and high sensitivity 0.78 ng/mL. We successfully applied this method for its PK study in rats. As a pilot study, we had fewer rats and used a single dose to estimate PK, which gave us a rough idea of how novokinin behaves. But for a more detailed characterization of PK parameters, we plan to study in large groups of rats with varying doses of novokinin through various routes of administration.

Thus, our current study provided a crucial step for quantifying novokinin, a synthetic peptide with various therapeutic applications, and propelled it forward for drug development. In addition, our study would be useful as a reference for developing LC-MS/MS assays for similar peptides and small molecules.

Summary

6.1 General Conclusions

RAS is an intricate cascade of enzymes, peptides and receptors working in tandem to illicit regulatory cardiovascular and renal function. With the advent of local and circulating RAS, its implications have been found, from the maintenance of the vascular system to physiological balance in the nervous, metabolic, reproductive, and immune systems. The two opposing arms of RAS, i.e., the classical arm, consists of Ang II, ACE and AT1R, whose overactivation has been linked to vasoconstriction, inflammation, proliferation, hypertrophy, and fibrosis. At the same time, another arm called the alternative arm consists of AT2R and ACE2-Ang 1-7-MasR axis whose activation has been reported to counteract the classical arm.

AT2R, a unique subclass of ang receptor, is scarcer in the expression in the adulthood but reappears in the pathophysiological condition and provides functional antagonism to AT1R. This distinctive feature of AT2R makes it a potential target for new drug development. Several small molecules and peptide drugs targeting AT2R are currently in the research phase for various disorders. With peptide drugs offering better selectivity, less toxicity and easy modifiability, the demand for the exploration of peptide drugs has skyrocketed. Novokinin, a six amino acid synthetic peptide, is one of the AT2R agonists with multitude of therapeutic effects like vasodilation, anorexigenic, gastric protective, anti-inflammatory and cox inhibiting effects. However, peptide drugs like novokinin face major challenges in drug development as they are cleared rapidly from the body. Most of them suffer from poor bioavailability due to their easy degradation from gastrointestinal enzymes. They also have a short half-life and are unstable, so they have poor absorption, distribution, metabolism, and excretion. All of these contribute to the low permeability, metabolic instability, and short residence time of the peptide drugs in the body,

thus reducing their suitability in the therapeutic realms despite having potent activity and selectivity. In our own PK studies, we also observed that novokinin has a half-life of about 9 mins, reducing its efficacy as a therapeutic drug. Therefore, we employed a bone-targeted drug delivery approach as it offered a suitable target and protection from metabolic degradation compared to other peptide delivery methods. This approach increased the drug concentration at the desired site while reducing systemic toxicity. It targeted the bone, and a specific conjugation with a polyethylene spacer mediates such capability.

In our study, we successfully synthesized both novokinin and Novo Conj and determined their in-solution stability and bone-targeting capacity. Although we could not determine the PK parameters of Novo Conj, we demonstrated its superior pharmacodynamic effects compared to the unconjugated peptide. *In vitro* studies on neuroblastoma and breast cancer cell lines, we also confirmed its prolonged antiproliferative and neurite outgrowth effects mediated by AT2R activation.

The RA animal model selected for our study was induced through the AIA method with a 100% disease incidence in 10-12 days. It served as an excellent model for cardiovascular complications due to RAS imbalance which was the primary focus of our study. Our results indicated that treatment of drugs for arthritic rats restored RAS imbalance by stimulating the protective RAS and reducing activation of classical RAS by performing various molecular assays to analyze each RAS component. We also explored the correlation between RAS and the CYP-mediated ArA pathway in the pathogenesis of RA. Our findings indicated that AT2R activation by novokinin and Novo Conj positively impacted anti-inflammatory mediators, such as epoxidation producing EETs and their metabolites DiHTs while having a negative impact on pro-inflammatory mediators such as HETEs. Hence, we observed that Novo Conj-treated AIA rats demonstrated

better maintenance of dynamic ArA metabolites. Therefore, we were able to show Novo Conj modulated RAS and ArA pathways for the resolution of inflammation, leading to improved cardiovascular therapeutic outcomes.

Overall, the study's results gave a new perspective on the delivery of peptide drugs such that it can overcome their limitations for their maximum therapeutic benefits. This study design includes innovative tools and approaches. Our chemical conjugation of the peptide also applies to the different peptides and small molecules for improved delivery, thus establishing our conjugate model as a multipurpose solution for various drugs.

6.2 Future Directions

The lack of a sensitive and accurate method for quantifying Novo Conj in plasma has hindered delineating its PK parameters. Although conjugated peptides have shown extended half-lives of up to four hrs, a proper analytical method for Novo Conj using LC-MS/MS could aid in characterizing its PK profile. To address sensitivity and selectivity issues in the analytical method, a suitable column for large, PEGylated BP compounds could be used, and higher doses could be administered to animals.

Furthermore, Novo Conj's therapeutic spectrum could be explored by testing it in various *in vivo* animal models, such as hypertensive and cancer rats. As novokinin has been primarily used as an antihypertensive agent, its efficacy in hypertensive animal models could establish Novo Conj as a leading drug candidate for cardiovascular disorders. Moreover, an appropriate release study of novokinin from conjugation could also prove helpful in establishing Novo Conj as a viable drug candidate for further clinical development.

6.3 Strengths and Limitations

Our research study utilized a bone-targeted delivery of novokinin to exploit its maximum potential therapeutic benefits. One of the biggest strengths of our research relies on study design and techniques being innovative and reproducible simultaneously. We employed a RAS-targeting peptide, which has a multitude of therapeutic potential. We channeled AT2R, a lesser-known receptor in RAS that has emerged as a promising drug development target due to its ability to antagonize AT1R. Our simple chemical conjugation of the peptide has the potential to provide a reliable standalone or additive therapy option for various clinical RAS-related disorders.

Similarly, our study's strengths rely on our novel technical techniques. We developed HPLC-UV and LC-MS/MS methods for detecting novokinin in plasma, which had not been previously delineated despite the peptide's reported antihypertensive and gastroprotective effects. Using our analytical method, we determined the PK properties of the novokinin. Additionally, we demonstrated that novokinin had therapeutic benefits beyond its conventional anti-hypertensive effects. It promoted neurite outgrowth and exhibited antiproliferative activity in neuroblastoma and breast cancer cell lines. For the first time, we also showed the anti-inflammatory effect of novokinin via cardiovascular regulation in an adjuvant arthritis rat model. Thus, we were able to show that the bone drug delivery approach improves the pharmacodynamics effect of novokinin.

However, our limitation lies in the lack of proper characterization of PK parameters of Novo Conj. This missing link makes it challenging to determine how conjugation has helped novokinin prolong its biological effects. Additionally, the analysis of immune cytokines in various tissues, including joints, could have strengthened our study for its establishment of drug candidates for inflammatory disease apart from the measurement of RAS mediators.

References

1. Stroth U, Unger T. The renin-angiotensin system and its receptors. Journal of cardiovascular pharmacology. 1999;33:S21-S8.

2. Paul M, Poyan Mehr A, Kreutz R. Physiology of local renin-angiotensin systems. Physiological reviews. 2006;86(3):747-803.

3. Santos RA, Campagnole-Santos MJ, Andrade SlP. Angiotensin-(1–7): an update. Regulatory peptides. 2000;91(1-3):45-62.

4. Chiu AT, Herblin WF, McCall DE, Ardecky RJ, Carini DJ, Duncia JV, et al. Identification of angiotensin II receptor subtypes. Biochemical and biophysical research communications. 1989;165(1):196-203.

5. Gebre AK, Altaye BM, Atey TM, Tuem KB, Berhe DF. Targeting renin–angiotensin system against Alzheimer's disease. Frontiers in pharmacology. 2018;9:440.

6. Deshayes F, Nahmias C. Angiotensin receptors: a new role in cancer? Trends in Endocrinology & Metabolism. 2005;16(7):293-9.

7. Benigni A, Cassis P, Remuzzi G. Angiotensin II revisited: new roles in inflammation, immunology and aging. EMBO molecular medicine. 2010;2(7):247-57.

8. De Gasparo M, Siragy H. The AT2 receptor: fact, fancy and fantasy. Regulatory peptides. 1999;81(1-3):11-24.

9. De Gasparo M, Catt K, Inagami T, Wright J, Unger T. International union of pharmacology. XXIII. The angiotensin II receptors. Pharmacological reviews. 2000;52(3):415-72.

10. Nakajima M, Mukoyama M, Pratt RE, Horiuchi M, Dzau VJ. Cloning of cDNA and analysis of the gene for mouse angiotensin II type 2 receptor. Biochemical and biophysical research communications. 1993;197(2):393-9.

11. Kambayashi Y, Bardhan S, Takahashi K, Tsuzuki S, Inui H, Hamakubo T, et al. Molecular cloning of a novel angiotensin II receptor isoform involved in phosphotyrosine phosphatase inhibition. Journal of Biological Chemistry. 1993;268(33):24543-6.

12. Lazard D, Briend-Sutren M, Villageois P, Mattei M, Strosberg A, Nahmias C. Molecular characterization and chromosome localization of a human angiotensin II AT2 receptor gene highly expressed in fetal tissues. Receptors & channels. 1994;2(4):271-80.

13. Murasawa S, Matsubara H, Kijima K, Maruyama K, Ohkubo N, Mori Y, et al. Down-regulation by cAMP of angiotensin II type 2 receptor gene expression in PC12 cells. Hypertension Research. 1996;19(4):271-9.

14. Silva-Antonialli MM, Tostes RC, Fernandes L, Fior-Chadi DR, Akamine EH, Carvalho MHC, et al. A lower ratio of AT1/AT2 receptors of angiotensin II is found in female than in male spontaneously hypertensive rats. Cardiovascular Research. 2004;62(3):587-93.

15. Hayashida W, Horiuchi M, Dzau VJ. Intracellular Third Loop Domain of Angiotensin II Type-2 Receptor ROLE IN MEDIATING SIGNAL TRANSDUCTION AND CELLULAR FUNCTION. J Biol Chem. 1996;271(36):21985-92.

16. Heerding JN, Yee DK, Krichavsky MZ, Fluharty SJ. Mutational analysis of the angiotensin type 2 receptor: contribution of conserved amino acids in the region of the sixth transmembrane domain. Regulatory peptides. 1998;74(2-3):113-9.

17. Zhang H, Han GW, Batyuk A, Ishchenko A, White KL, Patel N, et al. Structural basis for selectivity and diversity in angiotensin II receptors. Nature. 2017;544(7650):327-32.

18. Connolly A, Holleran BJ, Simard É, Baillargeon J-P, Lavigne P, Leduc R. Interplay between intracellular loop 1 and helix VIII of the angiotensin II type 2 receptor controls its activation. Biochemical Pharmacology. 2019;168:330-8.

19. Asada H, Inoue A, Kadji FMN, Hirata K, Shiimura Y, Im D, et al. The crystal structure of angiotensin II type 2 receptor with endogenous peptide hormone. Structure. 2020;28(4):418-25. e4.

20. Miura Si, Karnik SS. Ligand-independent signals from angiotensin II type 2 receptor induce apoptosis. The EMBO journal. 2000;19(15):4026-35.

21. Miura S-i, Karnik SS, Saku K. Constitutively active homo-oligomeric angiotensin II type 2 receptor induces cell signaling independent of receptor conformation and ligand stimulation. Journal of Biological Chemistry. 2005;280(18):18237-44.

22. Pickel L, Matsuzuka T, Doi C, Ayuzawa R, Maurya DK, Xie S-X, et al. Over-expression of angiotensin II type 2 receptor gene induces cell death in lung adenocarcinoma cells. Cancer biology & therapy. 2010;9(4):277-85.

23. Liu M, Jing D, Wang Y, Liu Y, Yin S. Overexpression of angiotensin II type 2 receptor promotes apoptosis and impairs insulin secretion in rat insulinoma cells. Molecular and cellular biochemistry. 2015;400(1-2):233-44.

24. Pei N, Mao Y, Wan P, Chen X, Li A, Chen H, et al. Angiotensin II type 2 receptor promotes apoptosis and inhibits angiogenesis in bladder cancer. J Exp Clin Cancer Res. 2017;36(1):77.

25. Hein L, Meinel L, Pratt RE, Dzau VJ, Kobilka BK. Intracellular trafficking of angiotensin II and its AT1 and AT2 receptors: evidence for selective sorting of receptor and ligand. Molecular Endocrinology. 1997;11(9):1266-77.

26. Widdop RE, Matrougui K, Levy BI, Henrion D. AT2 receptor-mediated relaxation is preserved after long-term AT1 receptor blockade. Hypertension. 2002;40(4):516-20.

27. Singh KD, Karnik SS. Angiotensin receptors: structure, function, signaling and clinical applications. Journal of cell signaling. 2016;1(2).

28. Steckelings UM, Kaschina E, Unger T. The AT2 receptor—a matter of love and hate. Peptides. 2005;26(8):1401-9.

29. Ruiz-Ortega M, Esteban V, Suzuki Y, Ruperez M, Mezzano S, Ardiles L, et al. Renal expression of angiotensin type 2 (AT2) receptors during kidney damage. Kidney international. 2003;64:S21-S6.

30. Li J, Culman J, Hörtnagl H, Zhao Y, Gerova N, Timm M, et al. Angiotensin AT2 receptor protects against cerebral ischemia-induced neuronal injury. The FASEB Journal. 2005;19(6):1-25.

31. Busche S, Gallinat S, Bohle R-M, Reinecke A, Seebeck J, Franke F, et al. Expression of angiotensin AT1 and AT2 receptors in adult rat cardiomyocytes after myocardial infarction: a single-cell reverse transcriptase-polymerase chain reaction study. The American journal of pathology. 2000;157(2):605-11.

32. Namsolleck P, Recarti C, Foulquier S, Steckelings UM, Unger T. AT 2 receptor and tissue injury: therapeutic implications. Current hypertension reports. 2014;16:1-10.

33. Gallinat S, Busche S, Raizada MK, Sumners C. The angiotensin II type 2 receptor: an enigma with multiple variations. American Journal of Physiology-Endocrinology And Metabolism. 2000;278(3):E357-E74.

34. Hansen JL, Servant G, Baranski TJ, Fujita T, Iiri T, Sheikh SP. Functional reconstitution of the angiotensin II type 2 receptor and Gi activation. Circulation research. 2000;87(9):753-9.

35. Buisson B, Laflamme L, Bottari SP, de Gasparo M, Gallo-Payet N, Payet MD. AG Protein Is Involved in the Angiotensin AT2 Receptor Inhibition of the T-Type Calcium Current in Non-differentiated NG108-15 Cells (∗). Journal of Biological Chemistry. 1995;270(4):1670-4.

36. Nouet S, Nahmias C. Signal transduction from the angiotensin II AT2 receptor. Trends in Endocrinology & Metabolism. 2000;11(1):1-6.

37. BEDECS K, Elbaz N, Sutren M, Masson M, Susini C, Strosberg AD, et al. Angiotensin II type 2 receptors mediate inhibition of mitogen-activated protein kinase cascade and functional activation of SHP-1 tyrosine phosphatase. Biochemical Journal. 1997;325(2):449-54.

38. Feng Y-H, Sun Y, Douglas JG. Gβγ-independent constitutive association of Gαs with SHP-1 and angiotensin II receptor AT2 is essential in AT2-mediated ITIM-independent activation of SHP-1. Proceedings of the National Academy of Sciences. 2002;99(19):12049-54.

39. Shenoy UV, Richards EM, Huang X-C, Sumners C. Angiotensin II type 2 receptor-mediated apoptosis of cultured neurons from newborn rat brain. Endocrinology. 1999;140(1):500-9.

40. Horiuchi M, Hayashida W, Kambe T, Yamada T, Dzau VJ. Angiotensin type 2 receptor dephosphorylates Bcl-2 by activating mitogen-activated protein kinase phosphatase-1 and induces apoptosis. Journal of Biological Chemistry. 1997;272(30):19022-6.

41. Horiuchi M, Hayashida W, Akishita M, Tamura K, Daviet L, Lehtonen JY, et al. Stimulation of different subtypes of angiotensin II receptors, AT1 and AT2 receptors, regulates STAT activation by negative crosstalk. Circulation research. 1999;84(8):876-82.

42. Nahmias C, Boden C. Molecular aspects of AT 2 receptor. Angiotensin Vol I. 2004:375-97.

43. Miura S-i, Karnik SS. Ligand-independent signals from angiotensin II type 2 receptor induce apoptosis. The EMBO journal. 2000;19(15):4026-35.

44. Martínez-Meza S, Díaz J, Sandoval-Bórquez A, Valenzuela-Valderrama M, Díaz-Valdivia N, Rojas-Celis V, et al. AT2 receptor mediated activation of the tyrosine phosphatase PTP1B blocks caveolin-1 enhanced migration, invasion and metastasis of cancer cells. Cancers. 2019;11(9):1299.

45. Carey R, Jin X, Wang Z, Siragy H. Nitric oxide: a physiological mediator of the type 2 (AT2) angiotensin receptor. Acta physiologica scandinavica. 2000;168(1):65-71.

46. Tsai EJ, Kass DA. Cyclic GMP signaling in cardiovascular pathophysiology and therapeutics. Pharmacology & therapeutics. 2009;122(3):216-38.

47. Côté F, Laflamme L, Payet MD, Gallo-payet N. Nitric oxide, a new second messenger involved in the action of angiotensin II on neuronal differentiation of NG108-15 cells. Endocrine research. 1998;24(3-4):403-7.

48. Gendron L, Côté F, Payet MD, Gallo-Payet N. Nitric oxide and cyclic GMP are involved in angiotensin II AT2 receptor effects on neurite outgrowth in NG108-15 cells. Neuroendocrinology. 2002;75(1):70-81.

49. Zhao Y, Biermann T, Luther C, Unger T, Culman J, Gohlke P. Contribution of bradykinin and nitric oxide to AT2 receptor-mediated differentiation in PC12 W cells. Journal of neurochemistry. 2003;85(3):759-67.

50. Jin X-H, Wang Z-Q, Siragy HM, Guerrant RL, Carey RM. Regulation of jejunal sodium and water absorption by angiotensin subtype receptors. American Journal of Physiology-Regulatory, Integrative and Comparative Physiology. 1998;275(2):R515-R23.

51. Siragy HM, Jaffa AA, Margolius HS, Carey RM. Renin-angiotensin system modulates renal bradykinin production. American Journal of Physiology-Regulatory, Integrative and Comparative Physiology. 1996;271(4):R1090-R5.

52. Gohlke P, Pees C, Unger T. AT2 receptor stimulation increases aortic cyclic GMP in SHRSP by a kinin-dependent mechanism. Hypertension. 1998;31(1):349-55.

53. Tsutsumi Y, Matsubara H, Masaki H, Kurihara H, Murasawa S, Takai S, et al. Angiotensin II type 2 receptor overexpression activates the vascular kinin system and causes vasodilation. The Journal of clinical investigation. 1999;104(7):925-35.

54. Bergaya S, Hilgers RH, Meneton P, Dong Y, Bloch-Faure M, Inagami T, et al. Flow-dependent dilation mediated by endogenous kinins requires angiotensin AT2 receptors. Circulation research. 2004;94(12):1623-9.

55. Messadi-Laribi E, Griol-Charhbili V, Pizard A, Vincent M-P, Heudes D, Meneton P, et al. Tissue kallikrein is involved in the cardioprotective effect of AT1-receptor blockade in acute myocardial ischemia. Journal of Pharmacology and Experimental Therapeutics. 2007;323(1):210-6.

56. Su JB. Different cross-talk sites between the renin–angiotensin and the kallikrein–kinin systems. Journal of the Renin-Angiotensin-Aldosterone System. 2014;15(4):319-28.

57. Abadir PM, Periasamy A, Carey RM, Siragy HM. Angiotensin II type 2 receptor–bradykinin B2 receptor functional heterodimerization. Hypertension. 2006;48(2):316-22.

58. Zhu L, Carretero OA, Xu J, Wang L, Harding P, Rhaleb N-E, et al. Angiotensin II type 2 receptor-stimulated activation of plasma prekallikrein and bradykinin release: role of SHP-1. American Journal of Physiology-Heart and Circulatory Physiology. 2012;302(12):H2553-H9.

59. Hakam AC, Hussain T. Angiotensin II AT2 receptors inhibit proximal tubular Na+-K+-ATPase activity via a NO/cGMP-dependent pathway. American Journal of Physiology-Renal Physiology. 2006;290(6):F1430-F6.

60. Dulin NO, Alexander LD, Harwalkar S, Falck JR, Douglas JG. Phospholipase A2-mediated activation of mitogen-activated protein kinase by angiotensin II. Proceedings of the National Academy of Sciences. 1998;95(14):8098-102.

61. Jiao H, Cui X-L, Torti M, Chang C-H, Alexander LD, Lapetina EG, et al. Arachidonic acid mediates angiotensin II effects on p21ras in renal proximal tubular cells via the tyrosine kinase-Shc-Grb2-Sos pathway. Proceedings of the National Academy of Sciences. 1998;95(13):7417-21.

62. Miura S-i, Karnik SS. Angiotensin II type 1 and type 2 receptors bind angiotensin II through different types of epitope recognition. Journal of hypertension. 1999;17(3):397-404.

63. Rosenström U, Sköld C, Lindeberg G, Botros M, Nyberg F, Karlén A, et al. A Selective AT2 Receptor Ligand with a γ-Turn-like Mimetic Replacing the Amino Acid Residues 4− 5 of Angiotensin II. Journal of medicinal chemistry. 2004;47(4):859-70.

64. Schmidt B, Lindman S, Tong W, Lindeberg G, Gogoll A, Lai Z, et al. Design, synthesis, and biological activities of four angiotensin II receptor ligands with γ-turn mimetics replacing amino acid residues 3− 5. Journal of medicinal chemistry. 1997;40(6):903-19.

65. De Gasparo M, Whitebread S, Kamber B, Criscione L, Thomann H, Riniker B, et al. Effect of covalent dimer conjugates of angiotensin II on receptor affinity and activity in vitro. Journal of receptor research. 1991;11(1-4):247-57.

66. Georgsson J, Rosenström U, Wallinder C, Beaudry H, Plouffe B, Lindeberg G, et al. Short pseudopeptides containing turn scaffolds with high AT2 receptor affinity. Bioorganic & medicinal chemistry. 2006;14(17):5963-72.

67. Georgsson J, Sköld C, Botros M, Lindeberg G, Nyberg F, Karlén A, et al. Synthesis of a new class of druglike angiotensin II C-terminal mimics with affinity for the AT2 receptor. Journal of medicinal chemistry. 2007;50(7):1711-5.

68. Hallberg A, Hallberg M, Sävmarker J. Angiotensin peptides as AT2 receptor agonists. Current Protein and Peptide Science. 2017;18(8):809-18.

69. Vasile S, Hallberg A, Sallander J, Hallberg M, Åqvist J, Gutiérrez-de-Terán H. Evolution of angiotensin peptides and peptidomimetics as angiotensin II receptor type 2 (AT2) receptor agonists. Biomolecules. 2020;10(4):649.

70. Wan Y, Wallinder C, Plouffe B, Beaudry H, Mahalingam A, Wu X, et al. Design, synthesis, and biological evaluation of the first selective nonpeptide AT2 receptor agonist. Journal of medicinal chemistry. 2004;47(24):5995-6008.

71. Hallberg M, Sumners C, Steckelings UM, Hallberg A. Small-molecule AT2 receptor agonists. Medicinal Research Reviews. 2018;38(2):602-24.

72. MAToBA N, Yamada Y, UsUI H, Nakagiri R, Yoshikawa M. Designing potent derivatives of ovokinin (2-7), an anti-hypertensive peptide derived from ovalbumin. Bioscience, biotechnology, and biochemistry. 2001;65(3):736-9.

73. Yamada Y, Matoba N, Usui H, Onishi K, Yoshikawa M. Design of a highly potent anti-hypertensive peptide based on ovokinin (2-7). Bioscience, biotechnology, and biochemistry. 2002;66(6):1213-7.

74. Yoshikawa M, Ohinata K, Yamada Y. The Pharmacological Effects of Novokinin; a Designed Peptide Agonist of the Angiotensin AT⊂ 2 Receptor. Current pharmaceutical design. 2013;19(17):3009-12.

75. Yamada Y, Yamauchi D, Usui H, Zhao H, Yokoo M, Ohinata K, et al. Hypotensive activity of novokinin, a potent analogue of ovokinin (2–7), is mediated by angiotensin AT2 receptor and prostaglandin IP receptor. Peptides. 2008;29(3):412-8.

76. Ohinata K, Fujiwata Y, Shingo F, Masaru I, Masatsugu H, Yoshikawa M. Orally administered novokinin, an angiotensin AT2 receptor agonist, suppresses food intake via prostaglandin E2-dependent mechanism in mice. Peptides. 2009;30(6):1105-8.

77. Yamada Y, Ohinata K, Lipkowski AW, Yoshikawa M. Angiotensin AT2 receptor agonists act as anti-opioids via EP3 receptor in mice. Peptides. 2009;30(4):735-9.

78. Zhang Y, Xiu M, Jiang J, He J, Li D, Liang S, et al. Novokinin inhibits gastric acid secretion and protects against alcohol-induced gastric injury in rats. Alcohol. 2016;56:1-8.

79. Patel M, Kurade M, Rajalingam S, Bhavsar R, Mustafa SJ, Ponnoth DS. Role of angiotensin II type 1 (AT1) and type 2 (AT2) receptors in airway reactivity and inflammation in an allergic mouse model of asthma. Immunopharmacology and immunotoxicology. 2019;41(3):428-37.

80. Craik DJ, Kan M-W. How can we improve peptide drug discovery? Learning from the past. Expert Opinion on Drug Discovery. 2021;16(12):1399-402.

81. Ayoub M, Scheidegger D. Peptide drugs, overcoming the challenges, a growing business. Chimica oggi. 2006;24(4):46.

82. Anand U, Bandyopadhyay A, Jha NK, Pérez de la Lastra JM, Dey A. Translational aspect in peptide drug discovery and development: An emerging therapeutic candidate. BioFactors. 2022.

83. Craik DJ, Fairlie DP, Liras S, Price D. The future of peptide-based drugs. Chemical biology & drug design. 2013;81(1):136-47.

84. Lamers C. Overcoming the shortcomings of peptide-based therapeutics. Future Drug Discovery. 2022;4(2):FDD75.

85. Otvos Jr L, Wade JD. Current challenges in peptide-based drug discovery. Frontiers Media SA; 2014. p. 62.

86. Hamman JH, Enslin GM, Kotzé AF. Oral delivery of peptide drugs: barriers and developments. BioDrugs. 2005;19:165-77.

87. Werle M, Bernkop-Schnürch A. Strategies to improve plasma half life time of peptide and protein drugs. Amino acids. 2006;30:351-67.

88. Henninot A, Collins JC, Nuss JM. The current state of peptide drug discovery: back to the future? Journal of medicinal chemistry. 2018;61(4):1382-414.

89. Philippe GJ, Craik DJ, Henriques ST. Converting peptides into drugs targeting intracellular protein–protein interactions. Drug Discovery Today. 2021;26(6):1521-31.

90. Lee ES, Youn YS. Albumin-based potential drugs: focus on half-life extension and nanoparticle preparation. Journal of Pharmaceutical Investigation. 2016;46:305-15.

91. Veronese FM. Peptide and protein PEGylation: a review of problems and solutions. Biomaterials. 2001;22(5):405-17.

92. Fahmy TM, Samstein RM, Harness CC, Saltzman WM. Surface modification of biodegradable polyesters with fatty acid conjugates for improved drug targeting. Biomaterials. 2005;26(28):5727-36.

93. Wijesinghe A, Kumari S, Booth V. Conjugates for use in peptide therapeutics: A systematic review and meta-analysis. Plos one. 2022;17(3):e0255753.

94. Anarjan FS. Active targeting drug delivery nanocarriers: Ligands. Nano-Structures & Nano-Objects. 2019;19:100370.

95. Hirabayashi H, Fujisaki J. Bone-specific drug delivery systems: approaches via chemical modification of bone-seeking agents. Clinical pharmacokinetics. 2003;42:1319-30.

96. Chen Y, Wu X, Li J, Jiang Y, Xu K, Su J. Bone-targeted nanoparticle drug delivery system: an emerging strategy for bone-related disease. Frontiers in Pharmacology. 2022;13.

97. Sun S, Tao J, Sedghizadeh PP, Cherian P, Junka AF, Sodagar E, et al. Bisphosphonates for delivering drugs to bone. British journal of pharmacology. 2021;178(9):2008-25.

98. Van Beek E, Löwik C, Ebetino F, Papapoulos S. Binding and antiresorptive properties of heterocycle-containing bisphosphonate analogs: structure-activity relationships. Bone. 1998;23(5):437-42.

99. Kuźnik A, Październiok-Holewa A, Jewula P, Kuźnik N. Bisphosphonates—much more than only drugs for bone diseases. European Journal of Pharmacology. 2020;866:172773.

100. Drake MT, Clarke BL, Khosla S, editors. Bisphosphonates: mechanism of action and role in clinical practice. Mayo Clinic Proceedings; 2008: Elsevier.

101. Rodan GA, Fleisch HA. Bisphosphonates: mechanisms of action. The Journal of clinical investigation. 1996;97(12):2692-6.

102. Giger EV, Castagner B, Leroux J-C. Biomedical applications of bisphosphonates. Journal of Controlled Release. 2013;167(2):175-88.

103. Fazil M, Baboota S, Sahni JK, Ameeduzzafar, Ali J. Bisphosphonates: therapeutics potential and recent advances in drug delivery. Drug delivery. 2015;22(1):1-9.

104. Farrell KB, Karpeisky A, Thamm DH, Zinnen S. Bisphosphonate conjugation for bone specific drug targeting. Bone reports. 2018;9:47-60.

105. Uludag H. Bisphosphonates as a foundation of drug delivery to bone. Current pharmaceutical design. 2002;8(21):1929-44.

106. Fujisaki J, Tokunaga Y, Takahashi T, Shimojo F, Kimura S, Hata T. Osteotropic drug delivery system (ODDS) based on bisphosphonic prodrug. Iv effects of osteotropic estradiol on bone mineral density and uterine weight in ovariectomized rats. Journal of drug targeting. 1998;5(2):129-38.

107. Yang Y, Bhandari KH, Panahifar A, Doschak MR. Synthesis, characterization and biodistribution studies of 125 I-radioiodinated di-PEGylated bone targeting salmon calcitonin analogue in healthy rats. Pharmaceutical research. 2014;31:1146-57.

108. Bhandari KH, Newa M, Chapman J, Doschak MR. Synthesis, characterization and evaluation of bone targeting salmon calcitonin analogs in normal and osteoporotic rats. Journal of controlled release. 2012;158(1):44-52.

109. Khajeh pour S, Ranjit A, Summerill EL, Aghazadeh-Habashi A. Anti-Inflammatory Effects of Ang-(1-7) Bone-Targeting Conjugate in an Adjuvant-Induced Arthritis Rat Model. Pharmaceuticals. 2022;15(9):1157.

110. Yee DK, Kisley LR, Heerding JN, Fluharty SJ. Mutation of a conserved fifth transmembrane domain lysine residue (Lys215) attenuates ligand binding in the angiotensin II type 2 receptor. Molecular brain research. 1997;51(1-2):238-41.

111. Amblard M, Fehrentz J-A, Martinez J, Subra G. Methods and protocols of modern solid phase peptide synthesis. Molecular biotechnology. 2006;33:239-54.

112. Palomo JM. Solid-phase peptide synthesis: an overview focused on the preparation of biologically relevant peptides. Rsc Advances. 2014;4(62):32658-72.

113. Aghazadeh-Habashi A, Khajehpour S. Improved pharmacokinetics and bone tissue accumulation of Angiotensin-(1–7) peptide through bisphosphonate conjugation. Amino Acids. 2021;53(5):653-64.

114. Yewle JN, Puleo DA, Bachas LG. Bifunctional bisphosphonates for delivering PTH (1-34) to bone mineral with enhanced bioactivity. Biomaterials. 2013;34(12):3141-9.

115. Veronese FM, Mero A. The impact of PEGylation on biological therapies. BioDrugs. 2008;22:315-29.

116. Chakrabarty B, Ghoshal A, Purkait M. Effect of molecular weight of PEG on membrane morphology and transport properties. Journal of membrane science. 2008;309(1-2):209-21.

117. Caliceti P, Veronese FM. Pharmacokinetic and biodistribution properties of poly (ethylene glycol)–protein conjugates. Advanced drug delivery reviews. 2003;55(10):1261-77.

118. Lin J. Bisphosphonates: a review of their pharmacokinetic properties. Bone. 1996;18(2):75-85.

119. Laflamme L, de Gasparo M, Gallo J-M, Payet MD, Gallo-Payet N. Angiotensin II induction of neurite outgrowth by AT2 receptors in NG108-15 cells: Effect counteracted by the AT1 receptors. Journal of Biological Chemistry. 1996;271(37):22729-35.

120. Jedhe GS, Kotmale AS, Rajamohanan PR, Pasha S, Sanjayan GJ. Angiotensin II analogs comprised of Pro-Amb (γ-turn scaffold) as angiotensin II type 2 (AT 2) receptor agonists. Chemical Communications. 2016;52(8):1645-8.

121. Rosenström U, Sköld C, Lindeberg G, Botros M, Nyberg F, Hallberg A, et al. Synthesis and AT2 receptor-binding properties of angiotensin II analogues. The Journal of peptide research. 2004;64(5):194-201.

122. Rosenström U, Sköld C, Plouffe B, Beaudry H, Lindeberg G, Botros M, et al. New Selective AT2 Receptor Ligands Encompassing a γ-Turn Mimetic Replacing the Amino Acid Residues 4− 5 of Angiotensin II Act as Agonists. Journal of medicinal chemistry. 2005;48(12):4009-24.

123. Yamada T, Horiuchi M, Dzau VJ. Angiotensin II type 2 receptor mediates programmed cell death. Proceedings of the National Academy of Sciences. 1996;93(1):156-60.

124. de Miranda FS, Guimarães JPT, Menikdiwela KR, Mabry B, Dhakal R, layeequr Rahman R, et al. Breast cancer and the renin-angiotensin system (RAS): Therapeutic approaches and related metabolic diseases. Molecular and Cellular Endocrinology. 2021;528:111245.

125. Rasha F, Ramalingam L, Gollahon L, Rahman RL, Rahman SM, Menikdiwela K, et al. Mechanisms linking the renin-angiotensin system, obesity, and breast cancer. Endocrine-related cancer. 2019;26(12):R653-R72.

126. Shum M, Pinard S, Guimond M-O, Labbé SM, Roberge C, Baillargeon J-P, et al. Angiotensin II type 2 receptor promotes adipocyte differentiation and restores adipocyte size in high-fat/high-fructose diet-induced insulin resistance in rats. American Journal of Physiology-Endocrinology and Metabolism. 2013;304(2):E197-E210.

127. Exner EC, Geurts AM, Hoffmann BR, Casati M, Stodola T, Dsouza NR, et al. Interaction between Mas1 and AT1RA contributes to enhancement of skeletal muscle angiogenesis by angiotensin-(1-7) in Dahl salt-sensitive rats. PLoS One. 2020;15(4):e0232067.

128. Li H, Qi Y, Li C, Braseth LN, Gao Y, Shabashvili AE, et al. Angiotensin type 2 receptor–mediated apoptosis of human prostate cancer cellsAT2R-Induced Apoptosis of Prostate Cancer Cells. Molecular cancer therapeutics. 2009;8(12):3255-65.

129. Barber RD, Harmer DW, Coleman RA, Clark BJ. GAPDH as a housekeeping gene: analysis of GAPDH mRNA expression in a panel of 72 human tissues. Physiological genomics. 2005;21(3):389-95.

130. Gendron∗ L, Laflamme∗ L, Rivard N, Asselin C, Payet MD, Gallo-Payet N. Signals from the AT2 (angiotensin type 2) receptor of angiotensin II inhibit p21ras and activate MAPK (mitogen-activated protein kinase) to induce morphological neuronal differentiation in NG108–15 cells. Molecular endocrinology. 1999;13(9):1615-26.

131. Vinson GP, Barker S, Puddefoot JR. The renin–angiotensin system in the breast and breast cancer. Endocrine-related cancer. 2012;19(1):R1-R19.

132. George AJ, Thomas WG, Hannan RD. The renin–angiotensin system and cancer: old dog, new tricks. Nature Reviews Cancer. 2010;10(11):745-59.

133. Benndorf R, Böger RH, Ergün Sl, Steenpass A, Wieland T. Angiotensin II type 2 receptor inhibits vascular endothelial growth factor–induced migration and in vitro tube formation of human endothelial cells. Circulation research. 2003;93(5):438-47.

134. Horwitz K, Costlow M, McGuire WL. MCF-7: a human breast cancer cell line with estrogen, androgen, progesterone, and glucocorticoid receptors. Steroids. 1975;26(6):785-95.

135. Herr D, Rodewald M, Fraser H, Hack G, Konrad R, Kreienberg R, et al. Potential role of renin–angiotensin-system for tumor angiogenesis in receptor negative breast cancer. Gynecologic oncology. 2008;109(3):418-25.

136. Chen L, Deng H, Cui H, Fang J, Zuo Z, Deng J, et al. Inflammatory responses and inflammation-associated diseases in organs. Oncotarget. 2018;9(6):7204.

137. Abbas AK, Lichtman AH, Pillai S. Basic immunology e-book: functions and disorders of the immune system: Elsevier Health Sciences; 2019.

138. Serhan CN, Ward PA, Gilroy DW. Fundamentals of inflammation: Cambridge University Press; 2010.

139. Kumar R, Clermont G, Vodovotz Y, Chow CC. The dynamics of acute inflammation. Journal of theoretical biology. 2004;230(2):145-55.

140. Lawrence T, Gilroy DW. Chronic inflammation: a failure of resolution? International journal of experimental pathology. 2007;88(2):85-94.

141. Schmid-Schönbein GW. Analysis of inflammation. Annu Rev Biomed Eng. 2006;8:93-151.

142. Pahwa R, Goyal A, Jialal I. Chronic inflammation. StatPearls [Internet]. 2021.

143. Murakami M, Hirano T. The molecular mechanisms of chronic inflammation development. Frontiers Media SA; 2012. p. 323.

144. van den Brink W, van Bilsen J, Salic K, Hoevenaars FP, Verschuren L, Kleemann R, et al. Current and future nutritional strategies to modulate inflammatory dynamics in metabolic disorders. Frontiers in Nutrition. 2019;6:129.

145. Amor S, Puentes F, Baker D, Van Der Valk P. Inflammation in neurodegenerative diseases. Immunology. 2010;129(2):154-69.

146. Nakamura K, Smyth MJ. Targeting cancer-related inflammation in the era of immunotherapy. Immunology and cell biology. 2017;95(4):325-32.

147. Duan L, Rao X, Sigdel KR. Regulation of inflammation in autoimmune disease. Hindawi; 2019.

148. Firestein GS. Evolving concepts of rheumatoid arthritis. Nature. 2003;423(6937):356-61.

149. Demoruelle MK, Deane KD, Holers VM. When and where does inflammation begin in rheumatoid arthritis? Current opinion in rheumatology. 2014;26(1):64.

150. England BR, Mikuls TR. Epidemiology of, risk factors for, and possible causes of rheumatoid arthritis. URL: https://www uptod ate com/conte nts/epide miolo gy-of-risk-facto rs-for-and-possi ble-cause s-ofrheum atoid-arthr itis UpToDate. 2020.

151. Prakken B, Albani S, Martini A. Juvenile idiopathic arthritis. The Lancet. 2011;377(9783):2138-49.

152. Firestein GS, McInnes IB. Immunopathogenesis of rheumatoid arthritis. Immunity. 2017;46(2):183-96.

153. Sugiyama D, Nishimura K, Tamaki K, Tsuji G, Nakazawa T, Morinobu A, et al. Impact of smoking as a risk factor for developing rheumatoid arthritis: a meta-analysis of observational studies. Annals of the rheumatic diseases. 2010;69(01):70-81.

154. Ksir S, Akasbi N, Efemba K, El Aissaoui A, El Kinany K, Harzy T. Factors Associated with Extra Articular Manifestations in Rheumatoid Arthritis. Integrative Journal of Medical Sciences. 2019;6.

155. Majithia V, Geraci SA. Rheumatoid arthritis: diagnosis and management. The American journal of medicine. 2007;120(11):936-9.

156. Aletaha D, Smolen JS. Diagnosis and management of rheumatoid arthritis: a review. Jama. 2018;320(13):1360-72.

157. Marcucci E, Bartoloni E, Alunno A, Leone M, Cafaro G, Luccioli F, et al. Extra-articular rheumatoid arthritis. Reumatismo. 2018;70(4):212-24.

158. De Rycke L, Peene I, Hoffman I, Kruithof E, Union A, Meheus L, et al. Rheumatoid factor and anticitrullinated protein antibodies in rheumatoid arthritis: diagnostic value, associations with radiological progression rate, and extra-articular manifestations. Annals of the rheumatic diseases. 2004;63(12):1587-93.

159. Källberg H, Padyukov L, Plenge RM, Rönnelid J, Gregersen PK, van der Helm-van AH, et al. Gene-gene and gene-environment interactions involving HLA-DRB1, PTPN22, and smoking in two subsets of rheumatoid arthritis. The American Journal of Human Genetics. 2007;80(5):867-75.

160. McInnes IB, Schett G. The pathogenesis of rheumatoid arthritis. New England Journal of Medicine. 2011;365(23):2205-19.

161. Haringman JJ, Gerlag DM, Zwinderman AH, Smeets TJ, Kraan MC, Baeten D, et al. Synovial tissue macrophages: a sensitive biomarker for response to treatment in patients with rheumatoid arthritis. Annals of the rheumatic diseases. 2005;64(6):834-8.

162. Boldt AB, Goeldner I, de Messias-Reason IJ. Relevance of the lectin pathway of complement in rheumatic diseases. Advances in clinical chemistry. 2012;56(105-153):100.

163. McInnes IB, Leung BP, Liew FY. Cell-cell interactions in synovitis Interactions between T lymphocytes and synovial cells. Arthritis Research & Therapy. 2000;2(5):1-5.

164. Sweeney SE, Firestein GS. Rheumatoid arthritis: regulation of synovial inflammation. The international journal of biochemistry & cell biology. 2004;36(3):372-8.

165. Szekanecz Z, Pakozdi A, Szentpetery A, Besenyei T, Koch AE. Chemokines and angiogenesis in rheumatoid arthritis. Frontiers in bioscience (Elite edition). 2009;1:44.

166. Geusens P. The role of RANK ligand/osteoprotegerin in rheumatoid arthritis. Therapeutic advances in musculoskeletal disease. 2012;4(4):225-33.

167. Crowson CS, Liao KP, Davis III JM, Solomon DH, Matteson EL, Knutson KL, et al. Rheumatoid arthritis and cardiovascular disease. American heart journal. 2013;166(4):622-8. e1.

168. England BR, Thiele GM, Anderson DR, Mikuls TR. Increased cardiovascular risk in rheumatoid arthritis: mechanisms and implications. Bmj. 2018;361.

169. Bilgici A, Ulusoy H, Kuru O, Celenk C, Ünsal M, Danacı M. Pulmonary involvement in rheumatoid arthritis. Rheumatology international. 2005;25:429-35.

170. Antin-Ozerkis D, Evans J, Rubinowitz A, Homer RJ, Matthay RA. Pulmonary manifestations of rheumatoid arthritis. Clinics in chest medicine. 2010;31(3):451-78.

171. Shaw M, Collins BF, Ho LA, Raghu G. Rheumatoid arthritis-associated lung disease. European Respiratory Review. 2015;24(135):1-16.

172. Kapoor T, Bathon J. Renal manifestations of rheumatoid arthritis. Rheumatic Disease Clinics. 2018;44(4):571-84.

173. Kochi M, Kohagura K, Shiohira Y, Iseki K, Ohya Y. Inflammation as a risk of developing chronic kidney disease in rheumatoid arthritis. PLoS One. 2016;11(8):e0160225.

174. Hanaoka H, Kikuchi J, Hiramoto K, Saito S, Kondo Y, Kaneko Y. Decreased chronic kidney disease in rheumatoid arthritis in the era of biologic disease-modifying anti-rheumatic drugs. Clinical Kidney Journal. 2022;15(7):1373-8.

175. Gettings L. Psychological well-being in rheumatoid arthritis: a review of the literature. Musculoskeletal care. 2010;8(2):99-106.

176. Young LD. Psychological factors in rheumatoid arthritis. Journal of consulting and clinical psychology. 1992;60(4):619.

177. Braz NFT, Pinto MRC, Vieira ÉLM, Souza AJ, Teixeira AL, Simões-e-Silva AC, et al. Renin–angiotensin system molecules are associated with subclinical atherosclerosis and disease activity in rheumatoid arthritis. Modern Rheumatology. 2021;31(1):119-26.

178. Wang Y, Kou J, Zhang H, Wang C, Li H, Ren Y, et al. The renin-angiotensin system in the synovium promotes periarticular osteopenia in a rat model of collagen-induced arthritis. International immunopharmacology. 2018;65:550-8.

179. Chang Y, Wei W. Angiotensin II in inflammation, immunity and rheumatoid arthritis. Clinical & Experimental Immunology. 2015;179(2):137-45.

180. Cobankara V, Öztürk MA, Kiraz S, Ertenli I, Haznedaroglu IC, Pay S, et al. Renin and angiotensin-converting enzyme (ACE) as active components of the local synovial renin-angiotensin system in rheumatoid arthritis. Rheumatology international. 2005;25:285-91.

181. Wu Y, Li M, Zeng J, Feng Z, Yang J, Shen B, et al. Differential expression of renin-angiotensin system-related components in patients with rheumatoid arthritis and osteoarthritis. The American Journal of the Medical Sciences. 2020;359(1):17-26.

182. Sakuta T, Morita Y, Satoh M, Fox DA, Kashihara N. Involvement of the renin–angiotensin system in the development of vascular damage in a rat model of arthritis: effect of angiotensin receptor blockers. Arthritis & Rheumatism. 2010;62(5):1319-28.

183. Price A, Lockhart J, Ferrell W, Gsell W, McLean S, Sturrock R. Angiotensin II type 1 receptor as a novel therapeutic target in rheumatoid arthritis: in vivo analyses in rodent models of arthritis and ex vivo analyses in human inflammatory synovitis. Arthritis & Rheumatism: Official Journal of the American College of Rheumatology. 2007;56(2):441-7.

184. Moreira FRC, de Oliveira TA, Ramos NE, Abreu MAD, Simões e Silva AC. The role of renin angiotensin system in the pathophysiology of rheumatoid arthritis. Molecular Biology Reports. 2021;48(9):6619-29.

185. Peeters A, Netea M, Kullberg B, Thien T, Van Der Meer J. The effect of renin–angiotensin system inhibitors on pro-and anti-inflammatory cytokine production. Immunology. 1998;94(3):376-9.

186. Terenzi R, Manetti M, Rosa I, Romano E, Galluccio F, Guiducci S, et al. Angiotensin II type 2 receptor (AT2R) as a novel modulator of inflammation in rheumatoid arthritis synovium. Scientific Reports. 2017;7(1):1-11.

187. Wang X, Tu J, Jiang J, Zhang Q, Liu Q, Körner H, et al. Angiotensin II type 2 receptor modulates synovial macrophage polarization by inhibiting GRK2 membrane translocation in a rat model of collagen-induced arthritis. The Journal of Immunology. 2020;205(11):3141-53.

188. Gao W, Shen L, Long D-d, Pan T-t, Wang D, Chai X-q, et al. Angiotensin II type 2 receptor pharmacological agonist, C21, reduces the inflammation and pain hypersensitivity in mice with joint inflammatory pain. International Immunopharmacology. 2022;110:108921.

189. Verdonk K, Danser AJ, van Esch JH. Angiotensin II type 2 receptor agonists: where should they be applied? Expert opinion on investigational drugs. 2012;21(4):501-13.

190. Wang D, Hu S, Zhu J, Yuan J, Wu J, Zhou A, et al. Angiotensin II type 2 receptor correlates with therapeutic effects of losartan in rats with adjuvant-induced arthritis. Journal of cellular and molecular medicine. 2013;17(12):1577-87.

191. Tallima H, El Ridi R. Arachidonic acid: Physiological roles and potential health benefits–A review. Journal of advanced research. 2018;11:33-41.

192. Hanna VS, Hafez EAA. Synopsis of arachidonic acid metabolism: A review. Journal of advanced research. 2018;11:23-32.

193. Morteau O. Prostaglandins and inflammation: the cyclooxygenase controversy. Inflammation. 2001:67-81.

194. Vishnupriya P, Aparna A, Viswanadha VP. Lipoxygenase (LOX) pathway: a promising target to combat cancer. Current Pharmaceutical Design. 2021;27(31):3349-69.

195. Hoxha M. A systematic review on the role of eicosanoid pathways in rheumatoid arthritis. Advances in medical sciences. 2018;63(1):22-9.

196. Spector AA, Fang X, Snyder GD, Weintraub NL. Epoxyeicosatrienoic acids (EETs): metabolism and biochemical function. Progress in lipid research. 2004;43(1):55-90.

197. Guan H, Zhao L, Cao H, Chen A, Xiao J. Epoxyeicosanoids suppress osteoclastogenesis and prevent ovariectomy-induced bone loss. The FASEB Journal. 2015;29(3):1092-101.

198. Zordoky BN, El-Kadi AO. Effect of cytochrome P450 polymorphism on arachidonic acid metabolism and their impact on cardiovascular diseases. Pharmacology & therapeutics. 2010;125(3):446-63.

199. Liu Y, Zhang Y, Schmelzer K, Lee T-S, Fang X, Zhu Y, et al. The antiinflammatory effect of laminar flow: the role of PPARγ, epoxyeicosatrienoic acids, and soluble epoxide hydrolase. Proceedings of the National Academy of Sciences. 2005;102(46):16747-52.

200. Falck JR, Krishna UM, Reddy YK, Kumar PS, Reddy KM, Hittner SB, et al. Comparison of vasodilatory properties of 14, 15-EET analogs: structural requirements for dilation. American Journal of Physiology-Heart and Circulatory Physiology. 2003;284(1):H337-H49.

201. Boyce BF, Xiu Y, Li J, Xing L, Yao Z. NF-κB-mediated regulation of osteoclastogenesis. Endocrinology and metabolism. 2015;30(1):35-44.

202. Hoxha M, Zappacosta B. CYP-derived eicosanoids: Implications for rheumatoid arthritis. Prostaglandins & Other Lipid Mediators. 2020;146:106405.

203. Garcia V, Shkolnik B, Milhau L, Falck JR, Schwartzman ML. 20-HETE activates the transcription of angiotensin-converting enzyme via nuclear factor-κB translocation and promoter binding. Journal of Pharmacology and Experimental Therapeutics. 2016;356(3):525-33.

204. Alonso-Galicia M, Maier KG, Greene AS, Cowley Jr AW, Roman RJ. Role of 20-hydroxyeicosatetraenoic acid in the renal and vasoconstrictor actions of angiotensin II. American Journal of Physiology-Regulatory, Integrative and Comparative Physiology. 2002;283(1):R60-R8.

205. Jung O, Brandes RP, Kim I-H, Schweda F, Schmidt R, Hammock BD, et al. Soluble epoxide hydrolase is a main effector of angiotensin II–induced hypertension. Hypertension. 2005;45(4):759-65.

206. Rompe F, Artuc M, Hallberg A, Alterman M, Ströder K, Thöne-Reineke C, et al. Direct angiotensin II type 2 receptor stimulation acts anti-inflammatory through epoxyeicosatrienoic acid and inhibition of nuclear factor κB. Hypertension. 2010;55(4):924-31.

207. Wang B, Wu L, Chen J, Dong L, Chen C, Wen Z, et al. Metabolism pathways of arachidonic acids: Mechanisms and potential therapeutic targets. Signal transduction and targeted therapy. 2021;6(1):94.

208. Liu CX, Hu Q, Wang Y, Zhang W, Ma ZY, Feng JB, et al. Angiotensin-converting enzyme (ACE) 2 overexpression ameliorates glomerular injury in a rat model of diabetic nephropathy: a comparison with ACE inhibition. Molecular Medicine. 2011;17(1):59-69.

209. Dai S-Y, Peng W, Zhang Y-P, Li J-D, Shen Y, Sun X-F. Brain endogenous angiotensin II receptor type 2 (AT2-R) protects against DOCA/salt-induced hypertension in female rats. Journal of neuroinflammation. 2015;12(1):1-11.

210. Wang T, Lian G, Cai X, Lin Z, Xie L. Effect of prehypertensive losartan therapy on AT1R and ATRAP methylation of adipose tissue in the later life of high-fat-fed spontaneously hypertensive rats. Molecular Medicine Reports. 2018;17(1):1753-61.

211. Tao Y, Wang Z, Wang L, Shi J, Guo X, Zhou W, et al. Downregulation of miR-106b attenuates inflammatory responses and joint damage in collagen-induced arthritis. Rheumatology. 2017;56(10):1804-13.

212. Cui L, Nithipatikom K, Campbell WB. Simultaneous analysis of angiotensin peptides by LC–MS and LC–MS/MS: metabolism by bovine adrenal endothelial cells. Analytical biochemistry. 2007;369(1):27-33.

213. Edpuganti V, Mehvar R. UHPLC–MS/MS analysis of arachidonic acid and 10 of its major cytochrome P450 metabolites as free acids in rat livers: effects of hepatic ischemia. Journal of Chromatography B. 2014;964:153-63.

214. Bordy R, Moretto J, Devaux S, Wendling D, Moretto-Riedweg K, Demougeot C, et al. Adjuvant-induced arthritis is a relevant model to mimic coronary and myocardial impairments in rheumatoid arthritis. Joint Bone Spine. 2021;88(1):105069.

215. Bendele A. Animal models of rheumatoid arthritis. J Musculoskelet Neuronal Interact. 2001;1(4):377-85.

216. Aghazadeh-Habashi A, Kohan MG, Asghar W, Jamali F. Glucosamine dose/concentration-effect correlation in the rat with adjuvant arthritis. Journal of pharmaceutical sciences. 2014;103(2).

217. Mutlu E, Ilhan N, Ilhan N, Ilhan S, Susam S. Comparative Effectıveness of Novokinin, Perindopril and Losartan on Blood Pressure, Adma, Nadph Oxidase and Rho Kinase at Renal Tissue in L-Name and Salt Induced Hypertension. Clin Exp Pharmacol 5: 197. doi: 10.4172/2161-1459.1000197 Page 2 of 6 Volume 5• Issue 6• 1000197 Clin Exp Pharmacol ISSN: 2161-1459 CPECR, an open access journal phenylephrine were purchased from Sigma Aldrich (Inc. St. Louis, MO. USA). All drugs were dissolved in saline. vivo studies: Systolic blood pressure (SBP) was measured. 2015.

218. Nagy G, Koncz A, Telarico T, Fernandez D, Érsek B, Buzás E, et al. Central role of nitric oxide in the pathogenesis of rheumatoid arthritis and sysemic lupus erythematosus. Arthritis research & therapy. 2010;12(3):1-6.

219. Conforti A, Lussignoli S, Bertani S, Ortolani R, Cuzzolin L, Benoni G, et al. Cytokine and nitric oxide levels in a rat model of immunologic protection from adjuvant-induced arthritis. International Journal of Immunopathology and Pharmacology. 2001;14(3):153-60.

220. Moreira FRC, de Oliveira TA, Ramos NE, Abreu MAD, Simoes ESAC. The role of renin angiotensin system in the pathophysiology of rheumatoid arthritis. Mol Biol Rep. 2021;48(9):6619-29.

221. Cobankara V, Öztürk MA, Kiraz S, Ertenli I, Haznedaroglu IC, Pay S, et al. Renin and angiotensin-converting enzyme (ACE) as active components of the local synovial renin-angiotensin system in rheumatoid arthritis. Rheumatology international. 2005;25(4):285-91.

222. Rodrigues Prestes TR, Rocha NP, Miranda AS, Teixeira AL, Simoes-e-Silva AC. The anti-inflammatory potential of ACE2/angiotensin-(1-7)/Mas receptor axis: evidence from basic and clinical research. Current Drug Targets. 2017;18(11):1301-13.

223. Urman A, Taklalsingh N, Sorrento C, McFarlane IM. Inflammation beyond the joints: rheumatoid arthritis and cardiovascular disease. SciFed journal of cardiology. 2018;2(3).

224. Chang S-Y, Chen Y-W, Chenier I, Tran SLM, Zhang S-L. Angiotensin II type II receptor deficiency accelerates the development of nephropathy in type I diabetes via oxidative stress and ACE2. Experimental diabetes research. 2011;2011.

225. Ali Q, Wu Y, Hussain T. Chronic AT2 receptor activation increases renal ACE2 activity, attenuates AT1 receptor function and blood pressure in obese Zucker rats. Kidney international. 2013;84(5):931-9.

226. Zhu L, Carretero OA, Xu J, Harding P, Ramadurai N, Gu X, et al. Activation of angiotensin II type 2 receptor suppresses TNF-α-induced ICAM-1 via NF-κB: possible role of ACE2. American Journal of Physiology-Heart and Circulatory Physiology. 2015;309(5):H827-H34.

227. Barzegar M, Stokes KY, Chernyshev O, Kelley RE, Alexander JS. The Role of the ACE2/MasR axis in ischemic stroke: new insights for therapy. Biomedicines. 2021;9(11):1667.

228. Ishizuka T, Cheng J, Singh H, Vitto MD, Manthati VL, Falck JR, et al. 20-Hydroxyeicosatetraenoic acid stimulates nuclear factor-κB activation and the production of inflammatory cytokines in human endothelial cells. Journal of Pharmacology and Experimental Therapeutics. 2008;324(1):103-10.

229. Xu X, Zhang XA, Wang DW. The roles of CYP450 epoxygenases and metabolites, epoxyeicosatrienoic acids, in cardiovascular and malignant diseases. Advanced drug delivery reviews. 2011;63(8):597-609.

230. Mattrey FT, Makarov AA, Regalado EL, Bernardoni F, Figus M, Hicks MB, et al. Current challenges and future prospects in chromatographic method development for pharmaceutical research. TrAC Trends in Analytical Chemistry. 2017;95:36-46.

231. Langman LJ, Snozek CL. LC-MS in Drug Analysis: Springer; 2019.

232. Buszewski B, Szultka M. Past, present, and future of solid phase extraction: a review. Critical Reviews in Analytical Chemistry. 2012;42(3):198-213.

233. Valicherla GR, Riyazuddin M, Shahi S, Gupta AP, Syed AA, Husain A, et al. LC-ESI-MS/MS assay development and validation of a novel antidiabetic peptide PSTi8 in mice plasma using SPE: An application to pharmacokinetics. Journal of Pharmaceutical and Biomedical Analysis. 2020;180:113074.